CRUSTAL STRUCTURE AND TECTONOSTRATIGRAPHIC EVOLUTION OF THE EASTERN GULF OF MEXICO BASIN

A Dissertation Presented to

the Faculty of the Department of Earth and Atmospheric Sciences

University of Houston

In Partial Fulfillment

of the Requirements for the Degree

Doctor of Philosophy

By

Pin Lin

August 2018

CRUSTAL STRUCTURE AND TECTONOSTRATIGRAPHIC EVOLUTION OF THE EASTERN GULF OF MEXICO BASIN

Pin Lin

APPROVED:

Dr. Paul Mann, Chairman

Dr. Julia Wellner

Dr. Dale Bird

Dr. Gyorgy Marton
Total E&P USA

Dean, College of Natural Sciences and Mathematics

DEDICATION

To my beloved family

ACKNOWLEDGEMENTS

I would like to thank Dr. Paul Mann for serving as my primary dissertation supervisor, proposing this topic for my Ph.D. study, helping to arrange data access through seismic data providers, and providing my financial support as a graduate research assistant. I also thank the other members of the dissertation committee for their many contributions to the thesis study: Dr. Dale Bird in the area of gravity and magnetics modeling and interpretation; Dr. Julia Wellner in the area of sequence stratigraphic interpretation; and Dr. Gyorgy Marton, my external committee member from Total Exploration and Production Americas, whose mentorship and previous dissertation results from his study in the 1990's helped to better define the goals of this study.

I thank the industry sponsors of the CBTH project whose continued financial support was the source of my graduate research assistantship and travel support that allowed me to present my results at several conferences over the past 3.5 years. I thank the American Association of Petroleum Geologists Foundation for providing me a student grant-in-aid that also helped financially support my study.

Access to industry seismic and well data formed the observational basis for this study. I thank Mike Saunders, Laurie Geiger, Jackie Samford, and Denny Leung at Spectrum Geo, Inc. for their efforts in making these data sets available for my study and providing the permissions for me to use these data in this dissertation. I also thank Lisa

Gahagan of the Marine Seismic Data Center at the University of Texas at Austin for her help in locating and providing me vintage seismic lines from the study area.

I thank fellow students of the CBTH project for their technical assistance and friendship over the past three and one half years: Patrick Loureiro, Naila Dowla, Shenelle Gomez, Luis Carlos Carvajal, Lucia Torrado, Luan Nguyen, Andrew Steier, and Nawaz Bugti. I also thank EAS grad students Jing Hua, and Simin Gao for their support.

Finally, I would like to thank my beloved family in China for their continuous support and encouragement.

CRUSTAL STRUCTURE AND TECTONOSTRATIGRAPHIC EVOLUTION OF THE EASTERN GULF OF MEXICO BASIN

An Abstract of a Dissertation

Presented to

the Faculty of the Department of Earth and Atmospheric Sciences

University of Houston

In Partial Fulfillment

of the Requirements for the Degree

Doctor of Philosophy

By

Pin Lin

August 2018

ABSTRACT

The crustal structure and tectonostratigraphy of the eastern Gulf of Mexico record five major tectonic events that include: 1) Late Paleozoic collision of the Florida block and its northwestward indentation along northwest-striking, right-lateral, strike-slip faults; 2) late Triassic to middle Jurassic, northwest-to-southeast, Phase 1 rifting of the Gulf of Mexico; 3) seawater filling and evaporite formation (Callovian Louann salt) within a large sag basin that overlies this area of crustal extension; 4) late Jurassic, southwest-to-northeast rifting and oceanic crust formation (Phase 2) of the eastern Gulf of Mexico related to the counterclockwise rotation of the Yucatan Peninsula; and 5) formation of passive margins. In this study, I integrated 50,000 line kilometers of 2D seismic reflection, gravity, magnetic, refraction, and wells data to better constrain the timing, structure, and fault-controlled stratigraphy of these five, main tectonic events in the eastern Gulf of Mexico.

In **Chapter 2**, I identified the late Paleozoic, indentation-related, right-lateral, strike-slip faults that controlled 2-3-km-deep, right-stepping, pull-apart basins; these faults crosscut large areas of undeformed Paleozoic basins and are not reactivated until later Mesozoic rifting. I used regional, magnetic data to map Phase 1, Triassic, normal faults striking to the northeast that are consistent with parallel and alternating, basement highs and lows along the west Florida continental margin. I used seismic reflection data to map northwest-trending, marginal rift structures along the edges of the area of Jurassic oceanic crust that record the Phase 2 rifting between continental crust in Florida and the Yucatan basin.

In **Chapter 3**, I used deeply-penetrating, seismic data to better define the location and geometry of Jurassic slow-spreading ridge and fracture zones. 3-D gravity modeling was used to construct a depth to Moho map that integrates the depth to the top of oceanic basement and its Moho as observed on deeply-penetrating, seismic reflection lines. Crustal thickness variations in the oceanic crust are attributed to thicker crust forming more distant from the pole of rotation. The age of stratigraphic units overlying oceanic crust was used to date the initiation (early Kimmeridgian, 156 Ma) and cessation (late Berriasian, 138 Ma) of oceanic crust formation.

CONTENTS

CHAPTER I: INTRODUCTION TO THIS DISSERTATION

1.1 History and development of this dissertation

I was born and raised in Dongying, a city located in the Bohai oil-producing basin of eastern China. The main industries in Dongying are related to either oil exploration or oilfield services. My interest in geology began in high school when my father, Jingliang Lin, who spent his entire career as a petroleum engineer working for the China Sinopec company, explained to me that understanding geology is the first step to finding oil. Following my graduation from high school in May 2009, I spent four years studying geology at the China University of Petroleum in Beijing.

After my four years of university study, I applied and was accepted into the master's program in geology at the Missouri University of Science and Technology (MST) in Rolla, Missouri. My master's thesis supervisor at MST was Dr. Kelly Liu whose geophysical research area is seismology and seismic interpretation. After starting the master's program in September, 2013, I was selected by Dr. Liu to be one member of the five-person, American Association of Petroleum Geologists (AAPG) Imperial Barrel Award (IBA) team that competed in May, 2014, in the AAPG Mid-Continent section and received an honorable mention. In June, 2014, I began my master's thesis research on the topic of: *Seismic interpretation and facies identification of the Guantao Formation, Huagou Gas Field, Bohai Basin, China*. The 3D seismic data and wells used for the study were provided by China Sinopec.

In the fall of 2014, I visited, applied and was accepted into the Ph.D. program of geology at the University of Houston under the supervision of Dr. Paul Mann and the Conjugate Basins, Tectonics, and Hydrocarbons (CBTH) project. Upon arrival at UH in January, 2015, Dr. Mann proposed that I work in the eastern Gulf of Mexico (EGOM) using a combination of industry data sets from Spectrum and Dynamic which were both members of the CBTH consortium. We arranged permissions to use the 2009, Bigwave 2D seismic data set from Spectrum that provided a dense grid of seismic data over much of the eastern GOM and the 2011, Supercache survey of Dynamic that provided much wider-spaced, but deeply-penetrating seismic transects. During this same time, I obtained vintage, 1977-1983, 2D seismic data from the EGOM through the Marine Seismic Data Center at the University of Texas at Austin. I also ordered and obtained well data from the Bureau of Ocean Energy Management (BOEM) in New Orleans.

In 2016, I applied and was awarded a $2,750 grant from the AAPG grant-in-aid to carry out analysis of cores of the South Florida basin that were stored at the Florida Core repository at the Florida Geological Survey in Tallahassee, Florida. The objective was to carry out geochemical analyses to quantify the Cretaceous source rock potential of the South Florida basin using bitumen reflectance that could be measured in the petroleum geochemistry lab of Dr. Adry Bissada of the University of Houston. I made two trips to Tallahassee and returned 30 core samples to Dr. Bissada's Petroleum Geochemistry Lab at UH for geochemical analysis. Unfortunately, the predominately, carbonate samples from the South Florida margin did not contain enough organic matter for the proposed, geochemical analyses of the maturity of potential, carbonate, source rocks to be successful.

Below is a summary of meetings where I presented aspects of this dissertation research:

Meeting	Title	Award	Year
Sheriff Lecture, HGS-UH	Fault kinematics of Jurassic faults in the southeastern Gulf of Mexico compared to Basin-opening Models.		2015 Nov
Student Research Day, UH	Seismic stratigraphy and structure of a Late Jurassic, southeastward propagating zone of rifting and oceanic spreading separating continental crust of Florida and Yucatan, southeastern Gulf of Mexico.	2nd Place Poster Presentation, MS/ Ph.D. First Year Category	2016 May
GCAGS meeting, Corpus Christi, Texas	Kinematics of Jurassic rifting and oceanic spreading between the continental blocks of western Florida and the Yucatan Peninsula.		2016 Sep
Sheriff Lecture, HGS-UH	Along-strike, structural-volcanic variations of fossil, late Jurassic, southeastern Gulf of Mexico spreading ridge explained by plate reconstruction of Florida and Yucatan continental blocks		2016 Nov
AGU Fall meeting, San Francisco, California	Jurassic, slow-spreading ridge in the southeast Gulf of Mexico and its along-strike morpho-volcanic expression		2016 Dec
Student Research Day, UH	Basement and crustal structure of Jurassic oceanic crust in the eastern Gulf of Mexico		2017 May
GCAGS, San Antonio, Texas	Total tectonic subsidence analysis for evaluating location and magnitude of Late Triassic-Early Jurassic rifting in the eastern Gulf of Mexico	2nd Place, Gordon I. Atwater Poster award	2017 Sep
AAPG, Salt Lake City, Utah	Crustal structure of the Jurassic oceanic crust and thinned continental crust separating the conjugate, rifted margins of eastern Florida and the Yucatan Peninsula	Selected for AAPG student poster competition	2018 May

Below is a summary of academic awards from the University of Houston Department of Earth and Atmospheric Sciences and AAPG Foundation:

Award organization	Award	Amount	Year
AAPG Foundation	2016 Grant-in-Aid, M. Ray Thomasson Named Grant	Cash award of $2,750	2015 Jan
University of Houston Department of Earth and Atmospheric Sciences	Marathon Scholarship for outstanding work in Geology (EAS Graduate Student Award)	Cash award of $2,000	2016 May

During the winter of 2017, I returned to China for job interviews with Chinese oil companies and was offered a full-time position as a petroleum exploration geologist by China National Offshore Oil Corporation (CNOOC). I will begin working as an exploration geologist at CNOOC in Beijing in August, 2018.

1.2 Organization of this dissertation

This dissertation includes two, integrated chapters on the geological and geophysical study of the EGOM using 50,000 km of merged, industry, 2D seismic reflection data, well sets, and ship-track gravity and magnetic data. Based on this regional dataset, I compared the regional tectonic setting, plate reconstructions and regional gravity and magnetic maps of areas of full-thickness and extended continental crust deformed during both late Paleozoic continental collision and late Triassic-early Jurassic rifting. I used 2D seismic lines from the Spectrum and Dynamic data sets to illustrate specific structural and basinal features within this zone that include: 1) late

Paleozoic strike- slip faults; 2) Phase 1; 3)Triassic rifts; and 4) Phase 2, late Jurassic rifts and oceanic crust.

1.3 Summary of chapter 2

The long-term problem in understanding the structure of the EGOM and Florida is distinguishing late Paleozoic collision-related deformation during the assembly of Pangea from Triassic and Jurassic deformation related to the breakup of Pangea because many of these deeply-buried, features are poorly imaged on seismic reflection data and have not been drilled. I address this problem by mapping 50,000 km of 2D, seismic reflection data tied to 23 wells to produce a regional, basement structure map of the Florida margin of the EGOM.

From west to east, three, distinct, structural provinces are recognized: 1) **conjugate rift margins of the Yucatan peninsula and western Florida** that were rifted apart during Phase 2 GOM opening in the late Jurassic and separated by late Jurassic oceanic crust; basement and magnetic highs and lows on those two margins formed during late Triassic-middle Jurassic Phase 1 rifting are re-aligned by reconstructing the Yucatan-Florida conjugate margin prior to late Jurassic, seafloor spreading; regional maps of salt thickness show a southeastward thinning of salt towards thicker, continental crust in the southeastern GOM; 2) **a 45-km-wide zone of northwest-southeast-striking strike-slip faults and associated narrow basins of Paleozoic age**; I interpret these faults as late Paleozoic, indentation, right-lateral, strike-slip faults related to the northeastern edge of the South American continental promontory that collided with the North America plate to form the Alleghenian and Ouachita orogeny in the southern USA; one of these pull-apart basins is overlain by Jurassic diabase which is associated with rift-related volcanism in the central Gulf of Mexico and in southern Florida; and 3**) a zone of NE-SW, Triassic, rifting in the South Georgia area terminates on NW- SE Paleozoic strike-slip faults.** Wells and seismic data from NE Florida are used to illustrate the localized presence of Triassic, Phase 1 rifts bounding the northern edge of the early Paleozoic Suwannee Basin.

1.4 Summary of chapter 3

In this chapter, I describe an extinct, Jurassic, ridge-and-transform geometry in the eastern Gulf of Mexico (EGOM) using a combination of gravity, magnetic, and 2D seismic data collected by the oil industry. The marine gravity and magnetic data from the spreading ridge segments are characterized by circular gravity lows interpreted as large, volcanic centers formed along a slowly-spreading ridge (2.2-2.4 cm/yr). Basement mapping reveals that the EGOM oceanic ridge system is characterized by 30-60-km-long, ridge segments. The central areas of these ridge segments as terminated at the ridge-fracture zone intersections marked by associated, nodal basins.15-km-wide, 2-km-high axial volcanoes fill the central parts of the axial valleys of the spreading ridge. 2D seismic data tied to a deepwater well indicate that this axial volcanism ended during the earliest Cretaceous (Berriasian to Valanginian, 145-136 Ma), the cessation of seafloor spreading in the EGOM. The prevalence of lower crustal, dipping reflectors (LCDRs) observed from 2D seismic lines of the oceanic crust may be related to magma trapped within the ductile part of the lower crust as the basin opened. Basement faulting is revealed by two fault trends with associated gravity anomalies that are related to counterclockwise rotation of the Yucatan block. Spreading flowlines - generated from plate reconstruction parameters defined by the geometry of fracture zones for the entire GOM - indicate an excellent fit of the conjugate gravity and magnetic anomalies in the EGOM. My 3D gravity structural inversion results suggest that oceanic crust in the northwestern EGOM is thicker (6.4 km) than in southeastern EGOM (5.5 km) and is interpreted to represent faster spreading with thicker crust in locations more distant from the pole of rotation located in western Cuba.

CHAPTER II: CRUSTAL, STRUCTURAL, AND STRATIGRAPHIC EFFECTS OF PALEOZOIC COLLISIONAL AND STRIKE-SLIP FAULTING AND MESOZOIC RIFTING ON THE EASTERN GULF OF MEXICO AND SOUTHEASTERN USA

2.1. Introduction and objectives of this chapter

The Gulf of Mexico (GOM) is a hydrocarbon-rich, and geologically-complex basin formed from the late Triassic to earliest Cretaceous. The offshore maritime areas of the GOM are subdivided into the sectors of the United States, Mexico, and Cuba, with a shared central sector in the center of the basin (Salvador, 1987, 1991; Galloway, 2008) (Fig. 2.1). Research on the evolution of the GOM over the past, several decades has mainly been driven by offshore, petroleum exploration which has focused for decades on the western and central US GOM.

The study area for this chapter is the eastern GOM and western Florida margin which is shown as the boxed area on Figs 2.1a and b. Petroleum exploration is less advanced in the eastern GOM than the western and central GOM, due to a 1980 environmental moratorium declared by the state of Florida that prevents all offshore drilling in Florida waters. For this reason, there have been no exploration wells drilled after 1980 along the western margin of Florida and much of what we know about the Florida continental margin of the eastern GOM is linked to studies dating back to the 1970’s and 1980’s of land-based, exploration wells. Extensive seismic reflection data sets have been collected along the Florida margin during the moratorium period including the 2009, industry, seismic reflection data provided by Spectrum that I use in this chapter.

Oil exploration on the shelfal and deepwater sector of the Mexican GOM has lagged the exploration of the US GOM for a variety of political and technological reasons. In 2013, Mexico accelerated the pace of exploration in its shelfal and deepwater by opening these areas for international exploration. This event has allowed new seismic data sets to be collected along the northern Yucatan margin, which is the conjugate margin of the hydrocarbon-rich, northeastern GOM that includes the western Florida margin (Sandwell et al., 2014; Nguyen and Mann, 2016) (Figs. 2.1a, 2.1b).

For this dissertation, I have been kindly granted access to seismic data from Spectrum for both the Florida continental margin and its Yucatan conjugate margin (Fig. 2.1a). I have also had access to the results of the CBTH master's thesis work by Andrew Steier that also used an extensive grid of Spectrum, 2D seismic data from the northern Yucatan margin (Steier, 2018).

The overall objective of this chapter is to integrate these new, industry, offshore datasets with the many vintage (2009-2011), land-based studies of Florida. These previous Florida studies reveal a complex Paleozoic subsurface, basement structure mapped from deep wells, regional gravity, and regional magnetic data (Fig. 2.1b). Below are three main objectives of this chapter that are addressed using this regional compilation of offshore seismic data, on- and regional offshore gravity and magnetic data, and exploration wells.

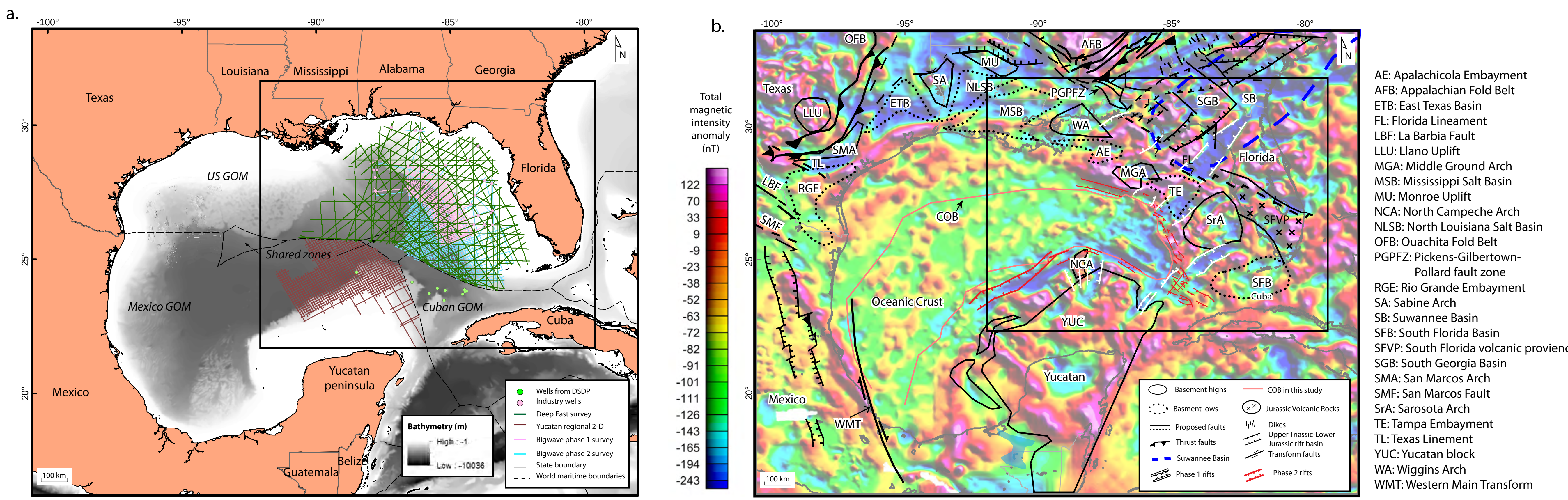

Figure 2.1 (a) Geographic setting of the boxed study area of the eastern Gulf of Mexico (EGOM) with a bathymetric basemap from GEBCO (Jakobsson et al., 2012). The dashed black lines separate the GOM into four, maritime sectors (US, Mexico, Cuba, and shared sector in the center). Colored lines show the 2D, seismic reflection datasets that I used in this chapter: Spectrum Deep East (green lines), Spectrum Bigwave Phase 1 (blue lines) and Spectrum Bigwave Phase 2 (pink lines), and Yucatan regional 2-D (red lines). Dots show the locations of industry wells (green) and wells from DSDP (pink) used in this study. (b) Total magnetic map of the GOM from (chapter 3, this dissertation) with an overlay of Paleozoic and Mesozoic tectonic features that include: **early Paleozoic Suwannee Basin** (Boote and Knapp, 2016); **late Paleozoic thrust and strike-slip faults and foreland basins** (Thomas, 1991); **GOM basement highs and lows** (Sawyer et al., 1991; Dobson and Buffler, 1997); **Triassic-Jurassic normal faults bounding basement highs and rifts** (McBride, 1991); **areas of Jurassic volcanic rocks in south Florida** (Byerly, 1991); the **continent-ocean boundary** (red line) based on Chapter 3 of this dissertation (2018); and **Phase 1 rifts** (white lines) and **Phase 2 rifts** (red lines) mapped in this study. Late Triassic-Lower Jurassic rift basins formed during the breakup of Pangea closely follow the same trends of Late Paleozoic thrust faults.

2.1.1 Role of strike-slip faulting in the late Paleozoic, Alleghenian orogeny

Previous studies have shown that the Lower Paleozoic basins in the subsurface of Florida, southern Georgia (Smith and Lord, 1997), and its offshore area (Boote and Knapp, 2016) are remarkably undeformed given their proximity to the deformed zone of resulting Alleghenian orogeny in the southeastern USA. Boote and Knapp (2016) proposed that the extensive and largely undeformed Suwannee basin located in the Georgia and Florida areas post-dates and overlies the Suwannee suture zone formed during the Alleghenian Orogeny.

Smith and Lord (1997) used wells, gravity, and magnetic data to infer three northwest-striking, right-lateral, strike-slip faults of late Paleozoic age beneath the onland area of northern Florida. I have used offshore, industry data to identify a fourth parallel, right-lateral, strike-slip fault of late Paleozoic age extending 800 km along the continental margin of northwestern Florida and coincident with the Florida Lineament of Christenson (1990). The width of the four parallel strike-slip faults spans a distance of 550 km and indicates the presence of major zone of northwest-striking, late Paleozoic right-lateral shearing during the Alleghenian orogeny (Fig. 2.1b). Following Thomas (1991), I attribute all four of these right-lateral, strike-slip faults to a zone of indentation in the Alleghenian orogeny by a continental indenter composed of the combined area of the Yucatan block and the South American plate.

2.1.2 Finding evidence for rifts and the two-phase opening model for the GOM

The Gulf of Mexico basin is formed by the breakup of Pangea and counterclockwise rotation of Yucatan block from the late Triassic to earliest Cretaceous (Salvador, 1987; Marton and Buffler, 1994, 1999) (Fig. 2.1b). Salvador (1987), and Eddy et al. (2016, 2018) have observed that few rifts have been recognized from drilling or 2D seismic reflection mapping from the subsurface of the GOM, which is puzzling given that previous, seismic refraction, magnetic, and gravity surveys have shown that the GOM is surrounded by an extensive area of thinned, continental crust (Dunbar and Sawyer, 1987; Sawyer et al., 1991; Galloway, 2008).

According to recent studies by Eddy et al. (2014, 2018), and Nguyen and Mann (2016), one explanation for the lack of visible rifts is that the GOM rifts occurred in two phases with the older phase of rifts of Triassic and early Jurassic age now obscured by thick, salt and passive margin deposits of the northern GOM. Around 5 km of salt was deposited during a short period (163-161 Ma) in a sag basin setting overlying rifts formed during the earlier, Phase 1 phase (Hudec et al., 2013). The eastern GOM has the advantage of having a thin or absent salt which allows better geophysical imaging of both the pre-salt (Phase 1) and post-salt (Phase 2) rifts. An important goal of this chapter is to use the Spectrum seismic reflection data to better illustrate both the pre-salt Phase 1 rifts of late Triassic-early Jurassic age, and the post-salt Phase 2 rifts of late Jurassic age. Moreover, the two phases of rifts have orthogonal trends in EGOM which is easier to identify than the central GOM: the older Phase 1 rifts trend northeast whereas the younger Phase 2 rifts trend more northwest.

Seismic imaging has improved to show sedimentary or volcanic reflectors beneath the base of the salt which earlier studies like Dobson and Buffler (1991), and Sawyer et al. (1991) referred to as “top basement”. For seismic imaging with limited penetration and in areas of few wells that penetrate basement, a challenge for this study is to infer the ages of reflector packages beneath the salt that could represent Paleozoic sedimentary rocks (Boote and Knapp, 2016; Boote et al., 2018), and Mesozoic sedimentary rocks occupying late Triassic to earliest Jurassic rift basins (Dobson and Buffler, 1991).

2.2 Tectonic setting

Six plate reconstructions showing representative stages in the Late Paleozoic and Mesozoic tectonic evolution of the GOM modified from previous, plate reconstructions by Seton et al. (2012), Domeier and Torsvik (2014), and Eddy et al. (2014) are shown on Fig. 2.2a:

1) **Late Paleozoic collisional phase** of the GOM that involves indentation and the formation of right-lateral, strike-slip faults in the northeastern GOM (Fig. 2.2a). The Alleghenian collisional event during the late Paleozoic (~320 Ma) in the southeastern USA forms the Appalachian-Ouachita fold-thrust belt and associated foreland basin by a northwestward motion of a continental indenter that includes the combined area of the Yucatan block and northern South America (Hatcher, 2002, 2010; Nance et al., 2012).

2) **Late Triassic beginning of Phase 1 rifting** (Fig. 2.2b). Initiation of Phase 1 GOM rifting began during the breakup of Pangea in the late Triassic-early Jurassic (~190 Ma) (Salvador, 1987; Eddy et al. 2014, 2018). Northeast-trending, rift basins with volcanism and dikes formed in response to the northwest-southeast extension in areas located south of the Ouachita segment of the Appalachian fold-thrust belt (Barnett, 1975; Van Houten, 1977; Salvador, 1987; Byerly, 1991) (Fig. 2.1b). These volcanic and non-marine sediments are correlative with northeast-trending, Upper Triassic-Lower Jurassic Newark Group along the eastern margin of the United States (Withjack et al., 1998). To the south of Upper Triassic-Lower Jurassic red beds, a broad zone of basement highs and lows formed from NW-SE extension in the first phase of rifting (Sawyer et al., 1991; Dobson and Buffler, 1991; Pindell and Kennan, 2009) (Fig. 2.2b).

An unusual, bimodal range of alkaline and silicic igneous activity within the Triassic-Jurassic South Florida volcanic province (SFVP) has been attributed to a hotspot influence in the South Florida area during the early Mesozoic (Barnett, 1975; Van Houten, 1977; Mueller and Porch, 1983; Smith, 1982) (Fig. 2.2b). Klitgord et al. (1984) proposed that the volcanism in the South Florida block (SF) was related to the breakup of Pangea by reconstructing South Florida block adjacent to the South Georgia Basin before Triassic-Jurassic rifting. However, the mechanism for the more than 300 km southeastward movement of South Florida block along proposed Bahamas Fracture zone requires a contemporary opening of the Central Atlantic and GOM (Klitgord et al., 1984). As the GOM formed ~20 Ma later than the Central Atlantic (Bird and Burke, 2006), the Bahamas Fracture Zone model is not favored in this study. An alternate nonfracture model with long-lived volcanism (~180 Ma) in the EGOM and South Florida was proposed by Beaman et al. (2017) and shown in the Fig. 2.1b.

3) Cessation or pause in **late early Jurassic (~170 Ma) Phase 1 rifting** (Fig. 2.2c). It is unclear if rifting completely ceases or is continuous with the Phase 2 rotation of the Yucatan block (Eddy et al., 2014).

4) **Late Jurassic (Callovian) salt deposition** in a largely unfaulted and continuous sag basin setting above late Triassic-late early Jurassic Phase 1 rifts (Fig. 2.2d). During Callovian time, Phase 1 rifting subsided and marine water entered a large sag basin that overlay the area of rifting probably through an Oxfordian marine strait crossing the area of west-central Mexico from the Pacific Ocean (Salvador, 1987). The arid climate in the large sag basin resulted in a thick salt basin, formed during a very short time interval (163-161 Ma) according to Hudec et al. (2013) (Fig. 2.2d).

5) **Late Jurassic, initiation of counterclockwise rotation of the Yucatan block with accompanying Phase 2 rifting at the margins of the Yucatan block**. Counterclockwise rotation of the Yucatan block along West Main Transform (WMT) along the eastern margin of Mexico separated the salt basin into two parts: the Louann salt basin in the US GOM and the Campeche salt basin in the Mexico GOM (Salvador, 1987; Hudec et al., 2013; Nguyen and Mann, 2016) (Fig. 2.2e). Salt deposition pre-dates formation of the oceanic crust of the deep GOM basin as only allochthonous salt is found overlying oceanic crust on both the US and Mexican margins (Hudec et al., 2013; Steier, 2018). The thickest area of salt occupies the broader, more extended crust in the US GOM, while a much thinner salt deposit occupies the narrow conjugate

margin of the Yucatan block (Salvador, 1991; Steier, 2018) (Fig. 2.2f). This unequal salt distribution in the GOM indicates an asymmetrical rift process during Phase 1 rifting - perhaps related to the reactivation of pre-existing, W-E striking, crustal weaknesses formed during the Late Paleozoic Alleghanian orogeny (Marton and Buffler, 1993). Phase 2 extension in the EGOM which changed from northwest-southeast to northeast-southwest show disparity in trends between Phase 1 and 2 rifts. Phase 2 rifts are orthogonal in many locations to the rifts formed during the earlier, Phase 1 event (Fig. 2.2e). Continued opening of GOM led to a series of NW-trending half-grabens formed in the Berriasian within the V-shaped area between Florida, Yucatan, and Cuba during Berriasian (Marton and Buffler, 1994, 1999; Escalona and Yang, 2013) (Fig. 2.2f).

6) **Earliest Cretaceous (Berriasian), cessation of Yucatan block rotation and the end of Phase 2 rifting and the beginning of the passive margin phase of GOM evolution** (Galloway, 2008) (Fig. 2.2f). The Yucatan block ceased its motion after rotation between 37° (Nguyen and Mann, 2016) to 42° (Marton and Buffler, 1994, 1999) away from its conjugate margin in western Florida during the earliest Cretaceous (Fig. 2.2f). The pink lines represent the mid-ocean-ridge and fracture zones identified by Nguyen and Mann (2016).

2.2.1. Summary of main tectonic events and their controls on stratigraphic megasequences

In the chart shown in Fig. 2.3, the stratigraphy of the northeastern and southwestern EGOM are correlated with six tectonic phases for GOM basin history including 1) pre-late Triassic pre-rift; 2) Late Triassic-middle Jurassic Phase 1 rifting; 3) Callovian sag basin (Louann-Campeche salt); 4) Oxfordian-Kimmeridgian Phase 2 rifting; 5) Late Jurassic-early Cretaceous Phase 2 oceanic spreading; and 6) early-late Cretaceous passive margin. The chronostratigraphic correlation for the northern part of the West Florida Basin is modified from Dobson and Buffler (1997), Goldhammer and Johnson (2001), and Snedden et al. (2014). The chronostratigraphic chart for the Campeche area of Mexico in the southwestern GOM is modified from Angeles-Aquino, and Cantú-Chapa (2001). The southeastern GOM stratigraphy is modified from Marton and Buffler (1999).

For the eastern GOM, Snedden et al. (2014) used an industry deepwater well in the northeastern GOM (well LL-399) to correlate the deepwater sequences that onlap the area of late Jurassic oceanic crust in the northeastern GOM. Snedden et al. (2013, 2014) identified three supersequences that progressively downlap onto oceanic crust: 1) Tithonian-Berriasian Cotton Valley-Bossier (CVB) (142-152 Ma); 2) Valanginian Cotton Valley-Knowles (CVK) (138-142 Ma); and Haynesville-Buckner (HVB) (152-155 Ma) (Eddy et al., 2014).

Figure 2.2 Six, plate reconstructions showing representative stages in the Late Paleozoic and Mesozoic, tectonic evolution of the GOM modified from previous, plate reconstructions by Seton et al. (2012), Domeier and Torsvik (2014), and Eddy et al. (2014). Green areas represent areas of unstretched, continental crust while orange areas represent areas of stretched, continental crust. Blue arrows represent the direction of motion of the South American plate relative to North America and the rotation of the Yucatan block. The structures are the same as those identified in Fig. 2.1b. (a) **Formation of Ouachita-Appalachian fold-thrust belt and associated foreland basin** by NW-SE collision between the South America plate, Yucatan block and North America plate at the end of Late Paleozoic Alleghanian orogeny (~320 Ma). Three, NW-striking, right-lateral strike-slip faults form during the indentation of North America and subdivide the continental crust of the Florida peninsula (Smith and Lord, 1997). (b) **Initiation of Phase 1 GOM rifting during the breakup of Pangea** in the late Triassic-early Jurassic (~190 Ma) (Eddy et al., 2014). (c) **Cessation of Phase 1 GOM rifting in early Jurassic** (~170 Ma). Red beds and dikes are formed along the Late Paleozoic fold belt. Phase 1 rifts mapped in this study are in white lines. It is unclear if rifting completely ceases or is continuous with the Phase 2 rotation of the Yucatan block. (d) **Deposition of the Louann-Campeche salt in a large, continuous sag basin formed above continental crust extended during Phase 1 rifting.** The pink polygon outlines the single salt basin restored by reuniting the Louann and Campeche salt basins. The cyan polygon shows the proposed source of Pacific seawater for the Louann- Campeche salt deposits from Salvador (1987). **(e) Onset of Phase 2, Late Jurassic rifting as Yucatan rotates counterclockwise relative to Florida and northern GOM areas.** Phase 2 extension in the EGOM changed from northwest-southeast to northeast-southwest, and formed rift (red lines) parallel to the COB. The rotation of Yucatan block initiated the formation of the Western Main Transform (WMF) and divided the single, pre-Phase 2, Callovian salt basin into two, separate basins (Louann salt basin in the US sector and Campeche salt basin in the Mexican sector) by formation of oceanic crust (area of central GOM shown by blue polygon). (f) **Phase 2 Yucatan block rotation and seafloor spreading had ceased by the earliest Cretaceous (Berriasian).** The pink lines represent the mid-ocean-ridge and fracture zones identified by Nguyen and Mann (2016).

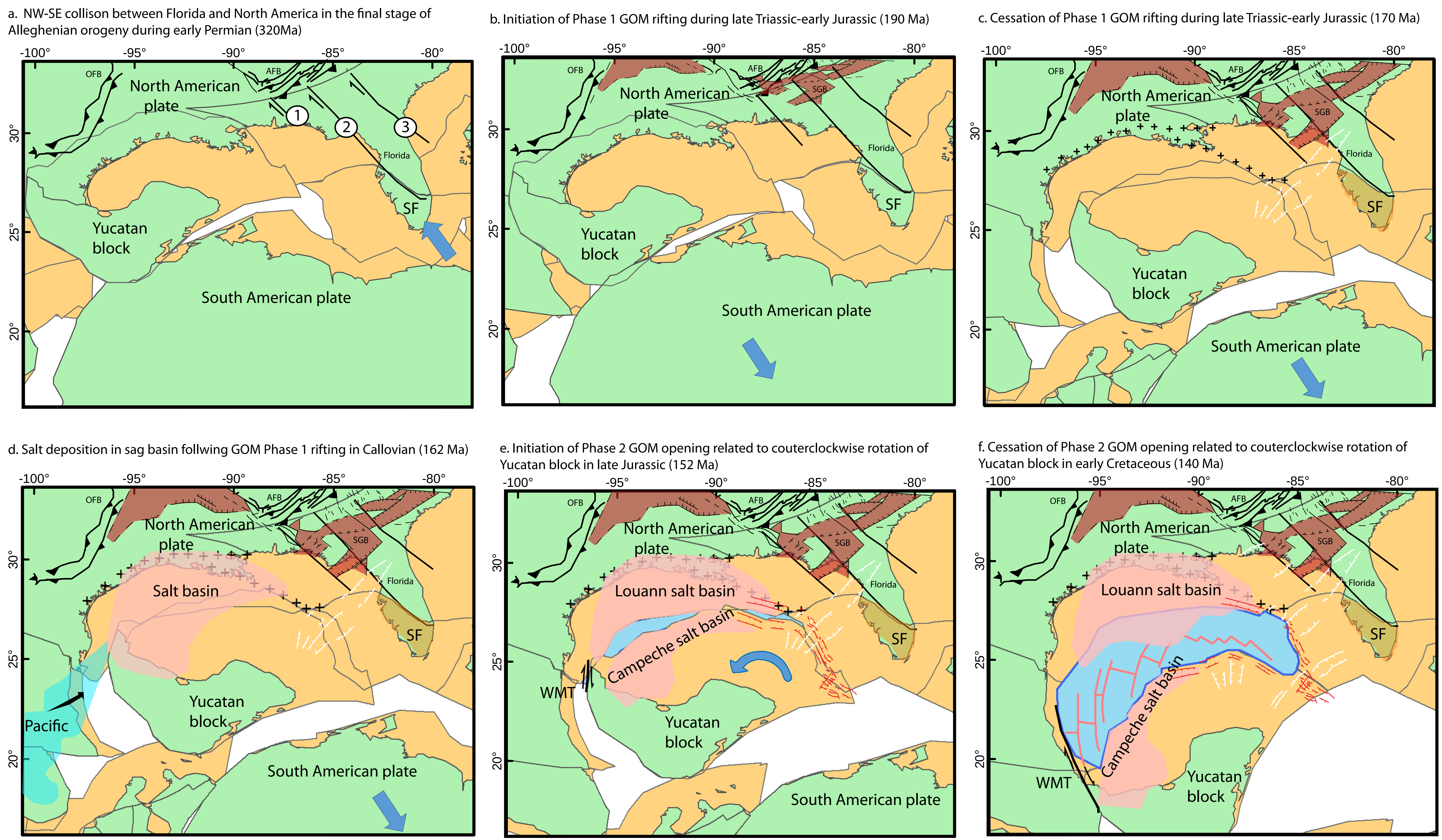
a. NW-SE collison between Florida and North America in the final stage of Alleghenian orogeny during early Permian (320Ma)
b. Initiation of Phase 1 GOM rifting during late Triassic-early Jurassic (190 Ma)
c. Cessation of Phase 1 GOM rifting during late Triassic-early Jurassic (170 Ma)
d. Salt deposition in sag basin follwing GOM Phase 1 rifting in Callovian (162 Ma)
e. Initiation of Phase 2 GOM opening related to couterclockwise rotation of Yucatan block in late Jurassic (152 Ma)
f. Cessation of Phase 2 GOM opening related to couterclockwise rotation of Yucatan block in early Cretaceous (140 Ma)
-100°
-95°
-90°
-85°
-80°
30°
25°
20°
OFB
AFB
SGB
North American plate
South American plate
Yucatan block
Florida
SF
Pacific
Salt basin
Louann salt basin
Campeche salt basin
WMT

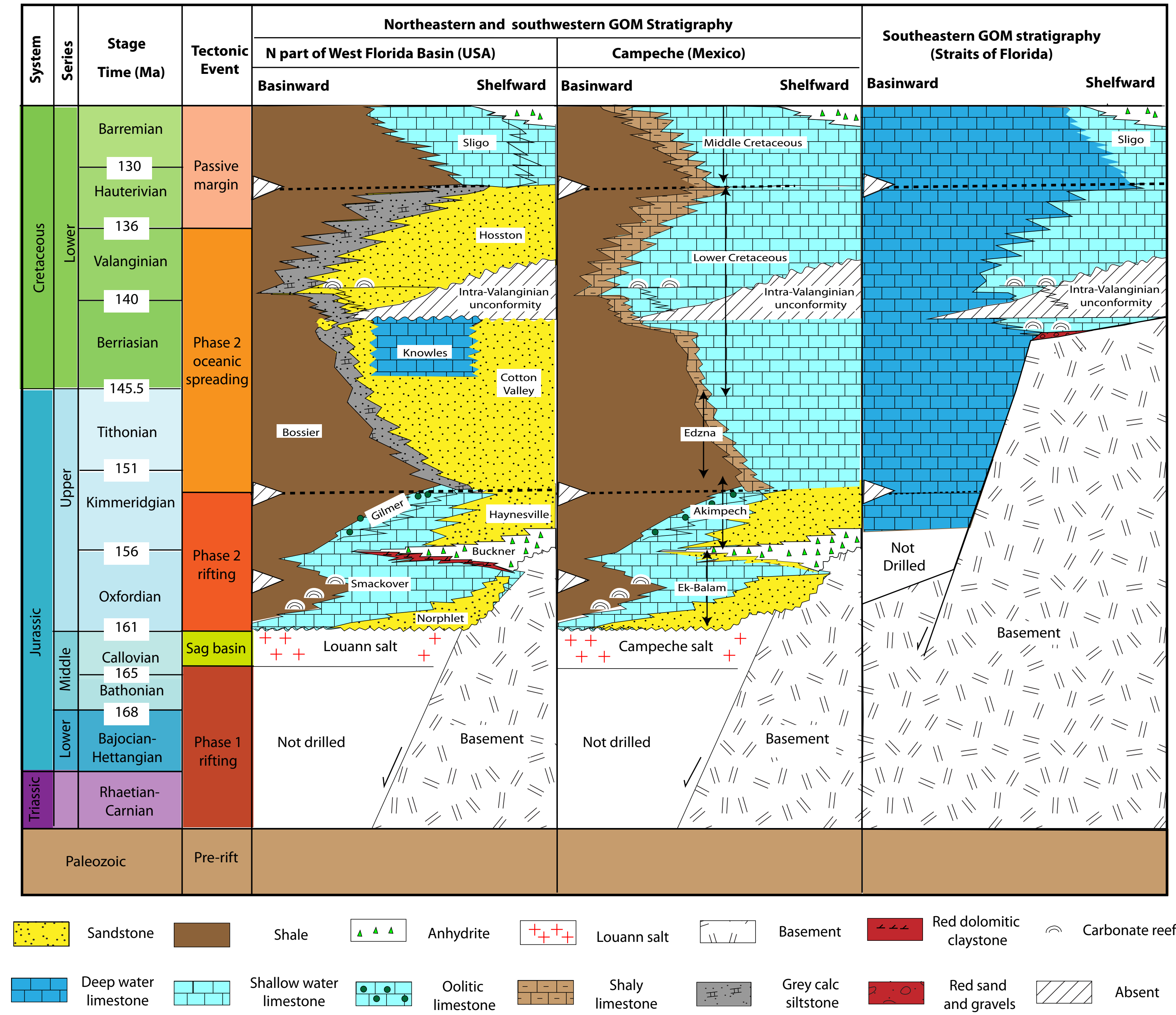

Figure 2.3 Stratigraphy of the northeastern and southwestern EGOM correlated with six, tectonic phases for GOM basin history including 1) **pre-Triassic, pre-rift**; 2) **Triassic-middle Jurassic Phase 1 rifting**; 3) **Callovian sag basin (Louann-Campeche salt)**; 4) **Oxfordian-Kimmeridgian Phase 2 rifting**; 5) **Late Jurassic-early Cretaceous Phase 2 oceanic spreading**; and 6) **early-late Cretaceous passive margin**. The chronostratigraphic chart for northern part of the West Florida Basin is modified from Dobson and Buffler (1997), Goldhammer and Johnson (2001), and Snedden et al. (2014). The chronostratigraphic chart for the Campeche area of Mexico in the southwestern GOM is modified from Angeles-Aquino, and Cantú-Chapa (2001). The southeastern GOM stratigraphy is modified from Marton and Buffler (1999).

No wells have penetrated synrift sedimentary rocks underlying the salt in the deepwater GOM where Upper Triassic-Lower Jurassic, Phase 1, rift-related, “red beds” are inferred from the regional, stratigraphic compilation of Salvador (1991). The absence of salt and pre-Berriasian sedimentary rocks in the southeastern GOM around Florida Strait indicate this tip of the southeastern, V-shaped, less rifted, continental region remained emergent during the Callovian when massive salt was being deposited in the central GOM (Marton and Buffler, 1999).

2.2.2 Types of crystalline basement beneath the eastern GOM and Florida

The base of late Jurassic Louann salt was commonly used to define “top basement” in several studies during the 1980’s and 1990’s of the eastern GOM (Addy and Buffler, 1984; Lord, 1986, 1987; Corso, 1987; Ball et al., 1988; Dobson and Buffler, 1991). This inferred “top basement” was a likely consequence of limited resolution of seismic imaging during the 1980’s and 1990’s rather than representing the “true top basement”. On the West Florida carbonate platform in the northeastern GOM, Ball et al. (1988) first interpreted a Triassic graben, a syncline, and a possible igneous intrusion using USGS 2D seismic reflection data as shown on Fig. 2.4a. Using a deeper-penetration, industry, seismic dataset from the northeastern GOM, Dobson and Buffler (1991) imaged Phase 1, Triassic rifts southeast of the South Georgia rift that were truncated by the Florida Lineament of Christenson (1990) (Fig. 2.4b). Dobson and Buffler (1991) also interpreted other rift features including normal block faulting (of probable Phase 1 Triassic age), and fault-resistant sedimentary layers or “hogbacks” (composed of either Paleozoic or Triassic sedimentary or igneous rocks).

In the onland area of Florida, the deepest, subsurface reflector - that could be mapped with confidence from 2D seismic images and tied to wells from the early 1980's - is the pre-Cretaceous, post-rift unconformity surface which truncates the lower Paleozoic and Triassic sedimentary rock sequences of the Suwannee Basin and the South Georgia rift (Applin, 1951; Applin and Applin, 1965; Klitgord et al., 1984) (Fig. 2.4b). In the subsurface of northern Florida, crystalline, basement rock types could be divided into two provinces: a northern area of pre-early Paleozoic calc-alkaline andesite in the north and a southern area of early Mesozoic volcanic rocks (Mueller and Porch, 1983; Bartok, 1993) (Fig. 2.4b). The boundary of these two regions partially coincides with the Florida lineament as mapped using gravity and magnetic data by Christenson (1990) (Fig. 2.4b).

Smith and Lord (1997) subdivided the northern region of the present-day land area of the Florida peninsula into four parts by three northwest-striking, right-lateral, strike-slip faults that strike subparallel to the Florida lineament proposed by Christenson (1990) lying 120 km to the west. These three strike-slip faults are labeled as 1, 2, and 3 on the map in Fig. 2.4b. Faults 2 and 3 form one fault-bounded edge of the Triassic age South Georgia rift (Fig. 2.4b). Smith and Lord (1997) proposed that these parallel, right-lateral faults formed the eastern edge of the Yucatan-South America indenter that pushed northwestward into the North American continent during the latest Paleozoic (Fig. 2.4b).

2.2.3 Tectonic setting and the extent of the early Mesozoic Suwannee Basin of northern Florida

The Suwannee Basin is a relatively undeformed early Mesozoic sedimentary basin overlying a complex, Precambrian basement in northern Florida and southeastern Georgia (Applin, 1951; Applin and Applin, 1965; Barnett, 1975; Boote and Knapp, 2016; Boote et al., 2018) (Figs. 2.2a, 2.4b, and Table 2.1). Extensive onshore wells in northern Florida and southern Georgia penetrate Lower Mesozoic, rift-related, sedimentary rocks at a depth of 600 m and are used to define the northeasterly trend of the South Georgia rift system extending as far north as the coastal area of Georgia (Smith and Lord, 1997; Boote et al., 2018) (Fig. 2.4b). The northeast trend of the Suwannee basin is well expressed in the regional magnetic map but the relative contribution of the late Paleozoic orogeny and Mesozoic rifting on this northeast trend is poorly understood (Fig. 2.1b).

Lower Ordovician quartzite and Middle Ordovician to Middle Devonian shale and sandstones were deposited in this Late Mesozoic continental platform or passive margin (Applin, 1951; Applin and Applin, 1965; Arden, 1974; Duncan, 1998; Boote et al., 2018) (Fig. 2.4b). Detrital zircons from Lower Mesozoic, clastic sedimentary rocks of the Suwannee basin reveal a Gondwanan (West African) origin for the Suwannee Basin (Mueller et al., 1994; Mueller et al., 2014) (Fig. 2.4b). From seismic reflection, refraction, and gravity data, the thickness of this Lower Mesozoic, rift-related sedimentary rocks onshore has been estimated to be in the range of 2.5-3 km (Boote and Knapp, 2016).

Two wells in offshore Georgia have penetrated Ordovician to Devonian quartzite, and Silurian to Devonian sedimentary and meta-sedimentary rocks that appear correlative with the onshore Suwannee Basin of northern Florida (Dillon and Popenoe, 1988; Poppe and Dillon, 1989; Poppe et al., 1995).

With velocity control taken from seismic refraction studies, the offshore Suwannee Basin adjacent to the southeastern coast of the USA has been extensively mapped using vintage, seismic reflection lines acquired in the 1970's and 1980's (Dillon and Popenoe, 1988; Boote and Knapp, 2016; Boote et al., 2018). The average thickness of Suwannee basin offshore of Georgia is estimated to be 4-6 km (Boote and Knapp, 2016).

In the offshore area of western Florida, only one, exploration well (Florida Middle Ground 252 #1) penetrates the 55 m of Lower Paleozoic sedimentary rocks (Applegate and Lloyd, 1985) (Fig. 2.2a). As this well is located on the northern edge of a northwest-trending, magnetic low that crosses northern Florida, the western end of the Suwannee basin in the eastern GOM may be defined by this magnetic low that is in turn truncated to the south by the northwest-trending, Florida lineament (Christenson, 1990) (Fig. 2.4b).

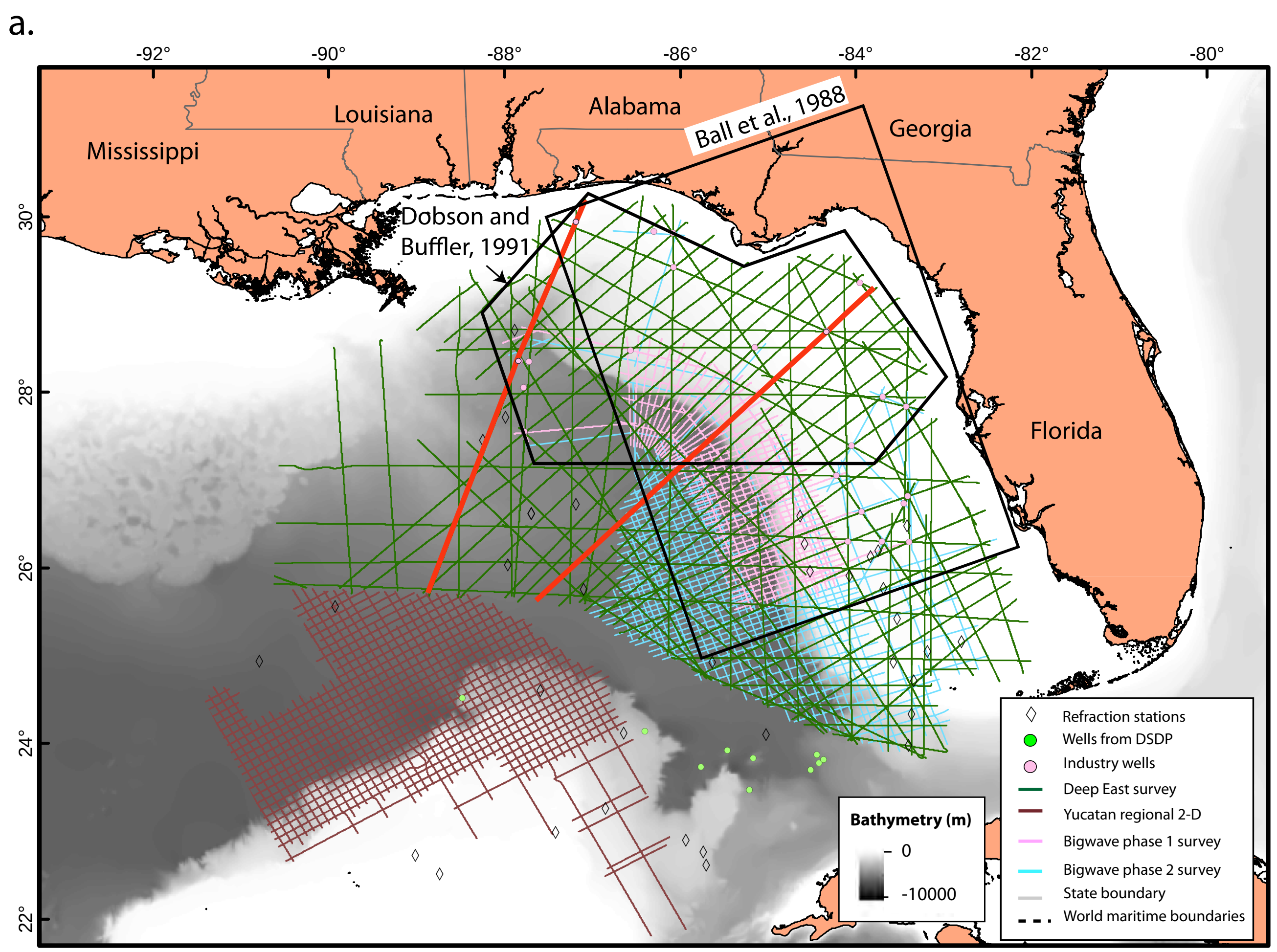

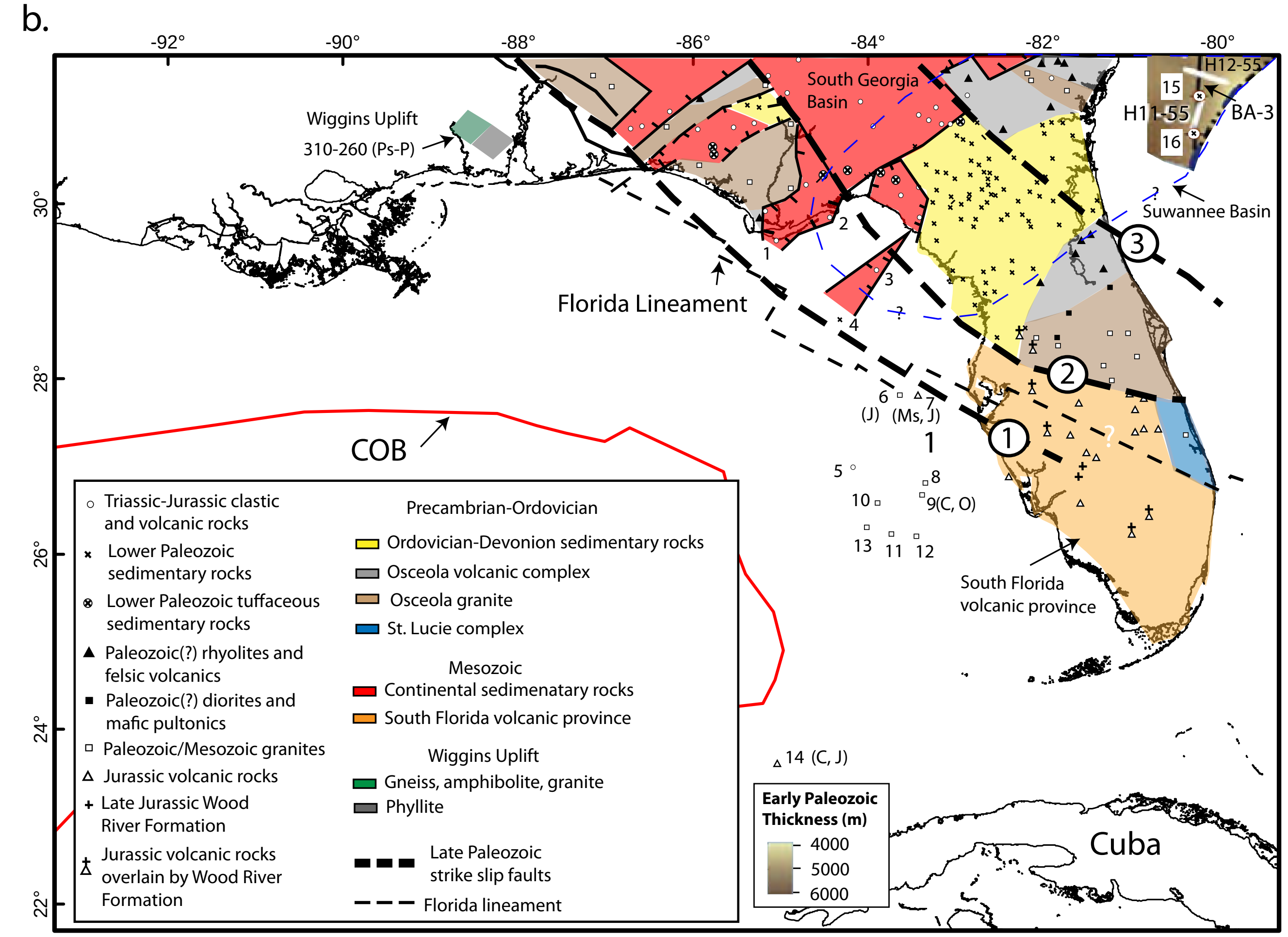

Figure 2.4 (a) Seismic reflection, refraction, and well data used in this study. Key to map symbols and color key for all lines is shown in Fig. 2.1a. Red lines show the locations of four, refraction profiles from the Gulf of Mexico Opening (GUMBO) project (Christeson et al., 2014; Eddy et al., 2014). The diamond symbol shows refraction stations from Ibrahim et al. (1981), and Ebeniro et al. (1986). Black polygons show areas of previous basement studies by Ball et al. (1988), and Dobson and Buffler (1991). (b) Basement well types and divisions compiled in this study. Onshore wells and location of Florida Lineament (FL) were compiled from Christenson (1990). Locations of right-lateral strike-slip faults shown as bold, dashed lines are from Smith and Lord (1997). Boundaries between differing basement types beneath Florida are modified from Dallmeyer (1987), and Smith and Lord (1997). Wells and thicknesses of the Lower Paleozoic from the east coast of the USA in Georgia and Florida are from Boote and Knapp (2016).

Table 2.1. Basement types of wells drilled in the Florida region used in this study.

Number	Wells	Pre-Cretaceous Sedimentary rocks		Crystalline rocks		Source
		Rock types	Drilled thickness (m)	Rock types	Drilled thickness (m)	
1	Mobil 224A	Triassic Eagle Mills	132.3			Barnett, 1975
2	Calco 224-A2	Triassic Eagle Mills	0			Applegate and Lloyd, 1985
3	Gainesville 707 -1	Triassic Eagle Mills	422.1	Paleozoic? sedimentary rocks	42.7	Applegate and Lloyd, 1985
4	Florida Middle Ground 252 -1	Lower Paleozoic clastic sedimentary rocks	54.9	Paleozoic? metamorphic rocks	436.8	Applegate and Lloyd, 1985
5	Elbow 915 -1	Paleozoic clastic sedimentary rocks?	273.7			Applegate and Lloyd, 1985
				Mesozoic?, altered, mafic, volcanic rocks	273.7	TOC inhouse memo from Christenson, 1990
6	Sr. Petersburg 7 -1			Early Cretaceous (~135 Ma) granite	102.7	Applegate and Lloyd, 1985; Smith, 1982
7	Sr. Petersburg 100 -1			Jurassic diabase and Mississippian rhyolite	322.5	Applegate and Lloyd, 1985; Smith, 1982; Ball et al., 1988
8	Charlotte Harbor 144 -1			Ordovician? rhyolite	16.5	Applegate and Lloyd, 1985
9	Charlotte Harbor 188 -1			Cambrian? granodiorite overlain by rhyolite	43.0	Applegate and Lloyd, 1986
10	Charlotte Harbor 265 -1			Lower Cambrian age granite overlain by rhyolite	311.8	TOC inhouse memo from Pindell, 1985
11	Charlotte Harbor 622 -1			Rhyolite?	39.6	Paleontology report from BOEM
12	Charlotte Harbor 672 -1			Ordovician rhyolite	37.2	K-Ar age date TOC in house memo
13	Vernon 654 -1			Cambrian? granite	196.9	Applegate and Lloyd, 1985; Pindell, 1985
14	DSDP 77-538A			Early Jurassic (190Ma) diabase dikes and Cambrian (500 Ma) metamorphic rocks	64.0	Buffler and Schlager, 1981
15	Transco 1005-1			Ordovician-Silurian sedimentary rocks	833.6	Poppe et al., 1995
16	COST GE-1			Devonian? sedimentary rocks	626.0	Poppe et al., 1995

Well information including basement ages is compiled from Applegate and Lloyd (1985), Pindell (1985), and Christenson (1990).

2.3 Data and methods used in this study

2.3.1 Regional grids of offshore, industry 2D seismic reflection data

For this study I used three regional grids of 2-D seismic reflection data to map the basement and salt distribution in the eastern Gulf of Mexico (EGOM), which are shown on the regional map in Fig. 2.4a. In the US sector of the eastern GOM, I used the 2-D Deep East survey that was acquired and processed most recently by Spectrum in 2007. The Deep East survey covers much of the eastern GOM with an average line spacing of ~50 km, a shot point interval of 37.5 m, and a two-way-time record length of 13-14 seconds. The seismic data were post-stack, and depth- migrated to a total depth of 40 km.

In the southeastern GOM, the Spectrum Big Wave survey has a closer line spacing that varies from 10 km in the Tampa Basin to 30 km in the South Florida Basin (Fig. 2.4a). The Big Wave survey had two phases of acquisition with Phase 1 in 2005 and Phase 2 in 2009. These surveys were only available for use in this dissertation in two-way travel time and were also used for detailed salt mapping in the southeastern GOM.

For the Yucatan margin of Mexico, a regional 2-D survey was acquired by Spectrum in 2016 (Fig. 2.4a). For this survey, the shot point interval is 25 m, the two-way-time record length is 15 seconds, and the average shot point spacing is 10 -m. This survey was also used in the CBTH master's thesis study by Steier (2018) on the northern Yucatan margin.

2.3.2 On- and offshore well data

Well data includes 23, publicly-available industry wells obtained from the US Bureau of Ocean Energy Management (BOEM) on the US GOM shelf margins and 10 academic wells obtained from the archives of the Deep Sea Drilling Project (DSDP) on the Yucatan and Florida margins (Fig. 2.4a). Locations of 12 wells penetrated the Paleozoic, and Mesozoic basement (Table 2.1) for all the areas shown in Fig. 2.4b. I also compiled the onshore basement types from onshore wells in Florida to better understand basement crustal provinces US GOM (Boote et al., 2018) (Fig. 2.4b).

2.3.3 On- and offshore gravity and magnetic grids

I incorporated the ship-track gravity and magnetic data obtained during the Deep East and Big Wave survey for this study (Figs. 2.5, 2.6). For the area outside the seismic survey, I used the global, satellite-derived, free air, gravity grid (Sandwell et al., 2014), and the Geological Society of America, Decade of North American Geology (DNAG) magnetic anomaly data (Finn et al., 2011) (Figs. 2.5a, 2.6a). The advantage of using the DNAG magnetic data set is that areas that lack data have not been infilled by interpolating surrounding areas of actual data that can produce spurious trends in the map.

2.3.4 Offshore, refraction data

Two regional refraction profiles from GUMBO projects (Christeson et al., 2014; Eddy et al., 2014), and 24 refraction stations (Ibrahim et al., 1981; Ebeniro et al., 1986) were compiled to produce a regional crustal province map of the study area (Fig. 2.4a). With these well and velocity control, I mapped the top of crystalline basement and base of salt - or its equivalent horizon - in depth along the Florida conjugate margin and in two-way travel time along the Yucatan conjugate margin. A basin-wide, Cretaceous-Tertiary boundary (KTB) has also been mapped using seismic, well and refraction control and compared to the mapping results of the KTB by previous studies (Sanford et al., 2016).

2.4 Regional maps of Paleozoic and Mesozoic basins and base of salt

2.4.1 Regional magnetic anomaly map and reconstructing the Florida-Yucatan conjugate margins

The pattern of regional magnetic anomalies along the Florida continental margin is dominated by alternating, northeast-southwest-trending magnetic highs and lows that reflect systematic variations in the depth to the top basement surface (Fig. 2.5a). A continuous, west-northwest-trending magnetic high (labeled as A1) (>120 nT) truncated this series of alternating highs and lows with an apparent, 35 km, left-lateral, strike-slip offset (Fig. 2.5a). The A1 lineament is roughly collinear and sub-parallel to the Florida Lineament of Christenson (1990), although Christenson depicted the Florida Lineament as having small 30-50-km-long, rectilinear, offsets along its 300-km length (Fig. 2.4b).

Two parallel, west-northwest-trending magnetic highs (labeled as A2, A3) (>120 nT) are shown in central Florida (Fig. 2.5a). In the South Florida Basin, a prominent, roughly, north-south magnetic anomaly (C) is observed to merge with anomaly A3 towards the north. Mesozoic volcanic rocks were penetrated in all wells adjacent to the linear magnetic high features (A1, A2, and A3) (Ball et al., 1988) (Fig.2.4b).

In Fig. 2.5a, I have used the magnetic map to identify the boundaries of all possible, northeast-trending, Phase 1, Triassic-early Jurassic rifts and the disruption of the trends of these rifts by the northwest-trending, A1 lineament. My 2D seismic reflection data does not penetrate deeply enough to verify the extent or age of proposed rifts from the magnetic data set (for example, imaging the basement structure and sedimentary fill of the South Tampa rift) (Fig. 2.5a). The South Tampa Embayment is defined by 6-km sag of overlying, passive margin sediments which appears to overlie the southwestward continuation and rifted, modification of the late Paleozoic, South Suwannee Basin.

Magnetic anomalies observed along the Yucatan margins of the Gulf of Mexico show a good match with the trends of magnetic anomalies along the Florida margin in the Southern Tampa Embayment (STE) and Sarasota Arch (SrA) when the Yucatan block is restored by a 42^{o} clockwise rotation into its early Jurassic, pre-rift position (Nguyen and Mann, 2016). Following the same restoration in the southeast GOM, the Chiquila Basin (CB) of the Yucatan margin and the South Florida Basin (SFB) of the Florida conjugate margin do not restore into an exact re-alignment (Fig. 2.5b). Steier (2018) also describes similar, prerift matches between basement arches inferred from magnetic highs along the northeastern Yucatan margin with similar basement arches defined along the GOM margin in the southeastern USA.

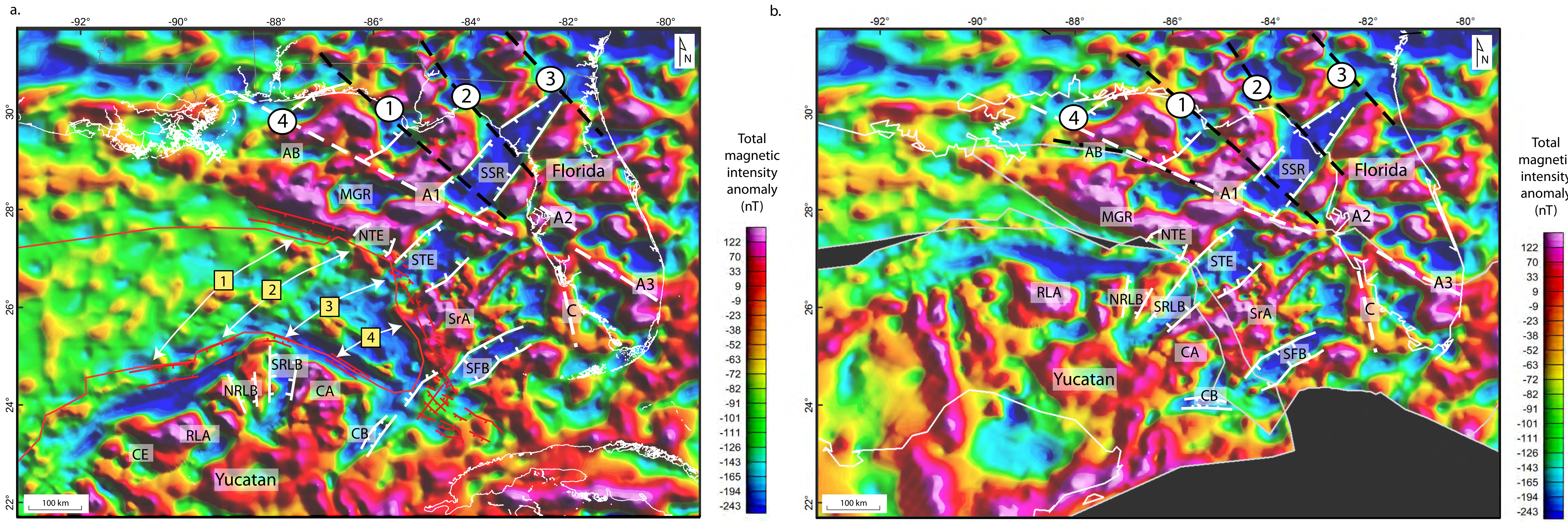

Figure 2.5 (a) Regional map of total magnetic anomalies in the eastern Gulf of Mexico. White double-headed arrows are small circle, flowlines calculated for single, GOM opening pole located near northwestern Cuba (22.41°, -84.33°) (Nguyen and Mann, 2016). Red lines show the location of COB described in Chapter 3 of this dissertation. Fault symbols are same as Fig. 2.1b. (b) Reconstruction of the Yucatan-Florida conjugate margins in the late Jurassic (~158 Ma) using the single pole of rotation by Nguyen and Mann (2016) as shown in Fig. 2.5a. White dash lines are inferred left-lateral strike-slip faults identified from magnetic and basement mapping. Black dash lines are inferred right-lateral strike-slip faults also inferred from magnetic data. On the Yucatan conjugate margin from west to east, the basement highs and lows include the Celestun Embayment (CE), Rio Lagartos Arch (RLA), Northern Rio Lagartos Basin (NRLB), Southern Rio Lagartos Basin (SRLB), Chiquila Arch (CA), and Chiquila Basin (CB) from west to east. On the Florida conjugate margin from northwest to southeast, the basement highs and lows include the Apalachicola Embayment (AB), Middle Ground Arch (MGR), Northern Tampa Embayment (NTE), Southern Tampa Embayment (STE), Sarasota Arch (SrA), and South Florida Basin (SFB). The NE-trending magnetic low inferred as Suwannee Basin (SB) in the North Florida shows a 35-km left-lateral offset with South Tampa Embayment (STE).

To the north of the inferred, Southern Tampa rift, the northeast-southwest alternating highs and lows are truncated by a high intensity, A1, magnetic anomaly high that trends to the northwest and parallel to the COB (Fig. 2.5a). The conjugate Yucatan margin exhibits a linear strong magnetic low along this part of the restored margin (Fig. 2.5a).

2.4.2 Free-air, gravity field and crustal boundaries of the eastern GOM

The regional, free-air gravity map shows the combined effects of water depth, variations in sediments thickness, and compositional variations of the crust and upper mantle (Fig. 2.6a). An abrupt change in the free-air, gravity anomaly from 0 to -30 mgal marks the continent-ocean boundary in the eastern GOM (Chapter 3, this dissertation) with this abrupt gravity change becoming more obvious in the southeastern GOM (Fig. 2.6a).

In the northeastern GOM, the gravity structure of the Florida continental margin is obscured by a thick, salt layer - while the salt-free or lesser-salt, Yucatan margin shows a clear, free-air, gravity expression of the intersection of the oceanic fracture zones and the COB that formed during the transition from rifting to oceanic spreading (Fig. 2.6a) (Steier, 2018; Chapter 3, this dissertation). The landward edge of the continental margin on both the Florida and Yucatan conjugate margin correlates well with the outer edge of the steep, Early Cretaceous carbonate escarpment (Galloway, 2008) (Fig. 2.6a).

The free-air gravity data reveals a similar pattern seen on the magnetic map of northeast-trending alternating highs around 50 mgal, and lows around -20 mgal that are truncated by linear, northwest-trending highs as defined by anomalies A1, A2, and A3 that are labeled on the map in Fig. 2.6a. The magnetic features (1, 2, 3) related to the South Georgia Basin are less recognizable as linear features on the regional, gravity map (Fig. 2.6a). In addition, the northeast- trending gravity lows (D1 and D2) in the range of 10-23 mGal reflect a thicker and elongate depocenter of lower Paleozoic sediments in the area of the proposed South Suwannee rift, and depocenter of thicker Paleozoic sedimentary rocks of the Suwannee basins suggested from both seismic reflection and well correlation (Christenson, 1990) (Fig. 2.6a).

2.4.3 Crustal thickness map from total, tectonic subsidence method

Dunbar and Sawyer (1987) calculated the present day-crustal thickness of the Gulf of Mexico region using total tectonic subsidence derived from the depth to basement taken from deep wells and seismic reflection data (Fig. 2.6b). With the assumption that the late Paleozoic, pre-rift crustal thickness was about 40 km (Fig. 2.2a), then $\beta=2$ is necessary to create the contact between thick, transitional crust and thinner, transitional crust. The thicker area of transitional crust along the western margin of Florida is composed of a moderately-thinned crust with the top of basement lying 2-12 km below sea level (Sawyer, 1991).

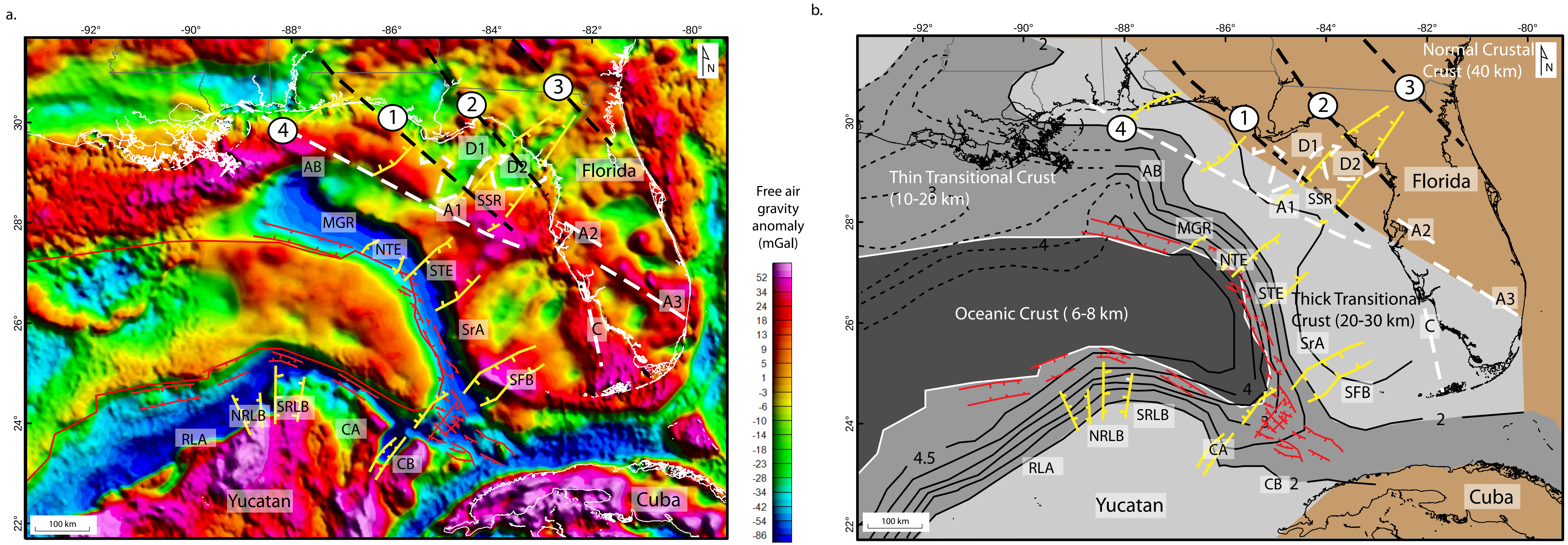

Figure 2.6 (a) Regional map of free-air gravity anomalies in the eastern Gulf of Mexico. NW-trending magnetic highs are correlated with linear, strike-slip faults mapped by Smith and Lord (1997). The northeast-southwest gravity lows (D1, D2) north of A1 correspond to the eastward, offshore extent of the Suwannee Basin. The South Suwannee rift (SSR) inferred from magnetic low anomalies is characterized as gravity highs similar to the rifts in the Northern Tampa Embayment (NTE) and Southern Tampa Embayment (STE). (b) Crustal provinces from Dunbar and Sawyer (1987), and Sawyer et al. (1991) based on areas of total tectonic subsidence. The thickness of normal continental crust shown in the brown color is assumed to be 40 km thick. The boundary between the thick transitional crust and unextended crust is roughly along the magnetic feature 1 shown in Fig. 2.6a. Yellow faults are late Triassic-early Jurassic formed during Phase 1 rifting, and red faults are late Jurassic faults formed in Phase 2 rifting.

The broad zone of arches and proposed, intervening lows formed by northeast-trending, Phase 1 rifts coincides with this zone of thinned, continental crust along the northern periphery of the GOM (Galloway, 2008). As the lows are all northeast-trending, I propose that they formed as late Triassic-early Jurassic, Phase 1, rift basins superimposed on the late Paleozoic folded belt. The thin, transitional crust was extended in an orthogonal direction during Phase 2 rifting when the Yucatan block counterclockwise rotated from Florida margin in the late Jurassic. The gravity and magnetic highs (A1, A3, C) that are shown on Figs. 2.5, 2.6 all coincide with the northern boundary of the thicker, transitional crust.

2.4.4 Regional map of the base of salt and pattern of salt distribution

The base of salt, mapped in the eastern GOM study area along the western margin of Florida reveals this same pattern of northeast-trending arches and intervening embayments that include these following features from northwest to southeast: 1) Apalachicola Embayment (AE); 2) Middle Ground Arch (MRA); 3) Tampa Embayment (TE); 4) Sarasota Arch (SrA); and 5) South Florida Basin (SFB) (Fig. 2.7a). All these northeast-trending, embayments filled by thicker, sag accumulations of Cretaceous, passive margin rocks are inferred to be fundamentally controlled by underlying, northeast-trending rifts whose fault-bounded edges are inferred from the regional, magnetic map in Fig. 2.5a.

The proposed Tampa rift is separated into two parts - the Northern Tampa rift (NTR) and the Southern Tampa rift (STE). Both of these inferred rifts are overlain by the Tampa Embayment (TE) that is expressed as a large sag in the passive margin section. The northern and southern parts of the Tampa rift are offset by a NW-trending basement low which is collinear and parallel to the Florida lineament of Christenson (1990) (Fig. 2.4b).

From northwest to southeast along the Florida margin, a shallowing trend in the embayments to the depth of top salt can be observed from -11000 m to the top of salt in the Apalachicola Embayment, to -6000 m to the top of salt in the South Florida Basin (Fig. 2.7). The average depth of arches also shows a north-to-south, shallowing trend from -5500 m to the top of salt in the Middle Ground Arch to -3500 m to the top of salt on the Sarasota Arch (Fig. 2.7a). Along the northern Yucatan margin, the basement contrasts with the Florida margin by showing broader highs with smaller and narrower, intervening basins (Fig. 2.7a).

The major basement arches of the Yucatan margin were identified on the basis of magnetic data and named by Steier (2018) according to nearby Mexican towns from west to east: Celestun Embayment (SE), Rio Lagartos Arch (RLA), Rio Lagartos Basin (RLB), Chiquila Arch (CA), and Chiquila Basin (CB) (Fig. 2.7a). The Rio Lagarto Arch is separated into two parts by an intervening basement high which was previously named the North Campeche Arch (NCA) by Buffler and Sawyer (1985) (Fig. 2.7a). The Chiquila Basin (CB) of the Yucatan margin is equivalent to the Jurassic rift previously described at the Catoche Tongue (Shaub, 1983; Schlager et al., 1984; Marton and Buffler, 1999).

The salt distribution in the southeastern GOM shows an asymmetric distribution with thicker salt deposited in the Florida margin attributed to asymmetric rifting with more crustal thinning in the central GOM and less crustal thinning along the Yucatan, conjugate margin (Marton and Buffler, 1993). The thickest area of salt (~1000-1500 m) mapped in detail by Steier (2018) was deposited north of Middle Ground Arch and west of Rio Lagartos Arch (Fig. 2.7a). Thin salt (~300-600 m) was remobilized and deformed as salt diapirs within the Tampa Embayment and Rio Lagartos Basin. Salt is absent above all the arches south of Tampa Embayment (Fig. 2.7a).

2.4.5 Pre-Paleozoic, crystalline basement

My depth to basement map shows that Phase 2, late Jurassic rift basins developed prior to initiation of seafloor spreading along the continent-ocean boundary (Fig. 2.7b). Wider, Phase 1, Triassic-early Jurassic rifts developed beneath embayments of the Florida and Yucatan margins and are inferred to have formed parallel to older, northeast-trending Paleozoic, basement fabric. Boote and Knapp (2016), and Boote et al. (2018) observe that early Paleozoic sedimentary basins of southern Georgia and northern Florida are remarkably flat and undeformed. For this reason, I propose that the prominent northeast-trending arches and basins along the western coast of Florida and expressed on the regional, gravity and magnetic maps is a result of Phase 1 rifting.

In addition to the regional northeast-trending, topographic, highs and lows on the Florida and Yucatan margins, two northwest-trending basement lows are found on the southeast flank of Apalachicola Embayment and the eastern flank of Tampa Embayment (Fig. 2.7b). A circular, basement low is found on the northeast flank of South Florida Basin (Fig. 2.7b).

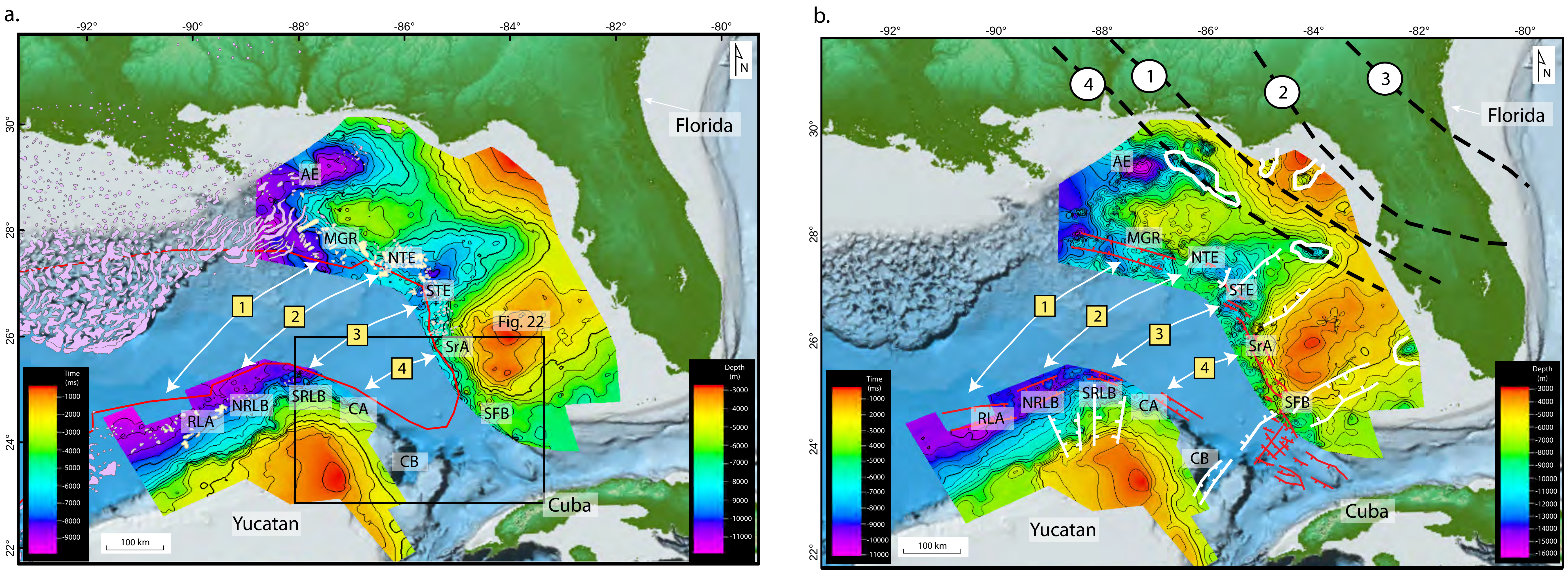

Figure 2.7 (a) Regional map of the depth to base of salt in the eastern GOM as I mapped from the Spectrum Deep East survey (the grid is shown in Fig. 2.1a). Yellow polygons are salt domes identified from seismic surveys in the study area. Purple polygons are salt areas compiled from the Huffman et al. (2004) for areas outside of my study area. Salt is thickest in basement lows in the stretched, continental areas of eastern GOM and completely absent from the southeastern GOM. (b) Regional map showing the depth to the top of crystalline (Paleozoic) basement mapped from the Spectrum Deep East survey. The top of the crystalline basement is shown in time from the Yucatan 2-D regional survey as these data were only available in time. The northeast-southwest trending basement highs and intervening lows in Florida and northwest-southeast trending basement highs and intervening lows match with the lineated, magnetic, anomaly patterns seen in Fig. 2.5. The linear northwest-southeast trending basement lows coincide with the A1 and C magnetic lineations seen on the magnetic maps of Figs. 2.4 and 2.5. These northwest-oriented linear trends are parallel to the three, late Paleozoic faults identified by Smith and Lord (1997). The northeast-southwest trending lows between Fault 1 and 2 are known to be Triassic rifts. Triassic Jurassic fault symbols are same as Fig. 2.1b.

2.5 Interpretations of Paleozoic and Mesozoic basins from seismic reflection and well data

2.5.1 Basement provinces defined by lithologies present in onshore wells and presence of strike-slip faults

Lithologic and age dating studies of cores taken from deep wells penetrating Paleozoic basement in Florida, south Alabama, and Georgia have defined three lithotectonic units: (1) the northeast-trending, Late Paleozoic, Suwannee Basin which was reactivated during Phase 1, Late Triassic-Early Jurassic rifting and was intruded by diabase dikes of Triassic age; (2) the "Osceola complex" of Chowns and Williams (1983) made up of a Paleozoic, granitic batholith and associated early Paleozoic volcanic rocks; and (3) the extensive Jurassic volcanic province of south Florida (Applin, 1951; Applin and Applin, 1965; Barnett, 1975; Dallmeyer, 1987) (Fig. 2.4b).

The distinctive Osceola basement complex is found in three, separate regions: 1) in northwest Florida around the city of Pensacola; 2) in northeast Florida and South Georgia; and 3) in central Florida. These three areas of early Paleozoic Osceola complex were interpreted by Smith (1982), and Smith and Lord (1997) to be the result of disruption by right-lateral offset on three, right-lateral, strike-slip faults labeled as faults 1, 2 and 3 on Fig. 2.4b. Fault 1 partially coincides with the Florida lineament as mapped by Christenson (1990). These three, Late Paleozoic strike-slip faults also appear to have been reactivated as left-lateral, strike-slip faults during Phase 1 rifting as all three faults form sharp, linear boundaries of the Triassic, South Georgia rift basin (Smith and Lord, 1997).

On the magnetic map in Fig. 2.5a, the three, strike-slip faults appear to extend for 350-550 km to the area north of the Suwannee Basin. These faults from Smith (1982) are parallel to a major, late Paleozoic, right-lateral, strike-slip faults I describe in the next section from the western shelf of Florida. The NE-trending linear trend of the Suwannee basin as observed on the basement map constrained by deep wells (Fig. 2.4b) aligns with a magnetic high on the regional total magnetic map on Fig. 2.5a, and a gravity low on regional free air gravity map on Fig. 2.6a which may reflect a late Triassic rift effect on the early Paleozoic Suwannee basin.

2.5.2 Mapping of the Paleozoic strike-slip basins in the western shelf of Florida adjacent to the Suwannee basin

In the offshore, West Florida Basin, I interpret three, elongate, northwest-trending, pull- apart basins as forming along a major right-lateral, Paleozoic, strike-slip fault that is at least 100 km long and parallels the continental margin area of thinned continental crust (Figs. 2.6a, 2.7b). This fault is collinear and parallel to fault A1 defined on the regional map in Fig. 2.5a and also parallel to the Florida lineament described by Christenson (1990). This fault zone is parallel to Paleozoic, strike-slip faults 1-3 as described by Smith (1982) and Smith and Lord (1997) and located 150 km to the east on the Florida peninsula (Fig. 2.6a, b).

From northwest to southeast, I have named the three basins the Destin Dome Basin (DDB), the Elbow Basin (ELB), and the Pully Ridge Basin (PRB) (Figs. 2.7, 2.8). From 2D seismic sections through the center of the basins, high-amplitude reflectors at a depth of 34 km below sea level are interpreted as the Moho (Figs. 2.9, 2.10). An elevated Moho at a depth of 2-3 km is observed beneath the main depocenters of Destin Dome and Elbow Basins (Figs. 2.9, 2.10). In cross-section, all three basins exhibit a downward-tapering, "negative flower structure" typical of pull-apart basins (Figs. 2.9, 2.10, 2.11). The symmetrical, 15-25-km-wide, 2-3 km-deep basins align in a right-stepping pattern along a single, linear fault trace that would indicate right-lateral shear. From a seismic reflection line across the linear fault trace, a possible 20-km-deep strike-slip fault was observed within the basement and supports the linearity of the fault that connects the two basins separated by a distance of 200 km (Fig. 2.11b).

In the northern Elbow basin, Jurassic granite was recovered from the St. Petersburg well 007-1 (PB 007 #1) (Fig. 2.9d). The only nearby well penetrating the basement is St. Petersburg 100-1 (SP 100 #1) that was drilled on the northeastern flank of the Elbow Basin, and penetrated Mississippian rhyolite and interbedded Jurassic diabase (age from Ball et al., 1988) (Fig. 2.10). This well confirmed the Late Paleozoic age of the deformed fill in the main depocenter of the strike-slip basins along with the presence of Jurassic volcanic rocks that may have accompanied crustal thinning and elevation of the Moho. The Jurassic volcanic rocks extend to the area with the prominent, linear magnetic high (A1) (Fig. 2.4a). In the Destin Dome Basin, the 50-100-m-thick, subhorizontal layer overlying the folded sediment layers is inferred to correlate with Late Jurassic diabase formed during the Phase 1 rifting event and corresponds to a prominent, magnetic high (Figs. 2.7, 2.8).

On the Florida peninsula, several, deep, exploration wells were drilled into Triassic-Jurassic volcanic rocks near the magnetic features labeled A2 and A3 (Fig. 2.4b). Although no well has been drilled into the Pully Ridge Basin, volcanic rocks are also likely to occur in this basin based on the presence of prominent, positive, magnetic anomalies. The linear shape of these three basins aligned along a major sub-vertical fault zone, their locations at right-steps in the fault trace, and their symmetrical and deep geometry in cross sections all support their tectonic origin as pull-apart basins formed along a late Paleozoic, right-lateral, strike-slip fault zone (Fig. 2.4b). Mississippian rhyolite drilled in the Elbow Basin supports these basement lows as forming during the Late Paleozoic, Alleghenian orogeny (Hatcher, 2002, 2010).

Two northeast-southwest trending lows in the east flank of Middle Ground Arch are truncated southwest by strike-slip fault 1 as proposed by Smith and Lord (1997) (Fig. 2.7b). The Gainesville 707 #1 well confirmed the presence of Triassic sedimentary rocks in the southern basin (Fig. 2.4b). The northern basin was also interpreted as a Triassic rift overlying the Early Paleozoic Suwannee Basin as correlated from onshore wells and with gravity anomaly D1 (Fig. 2.6a).

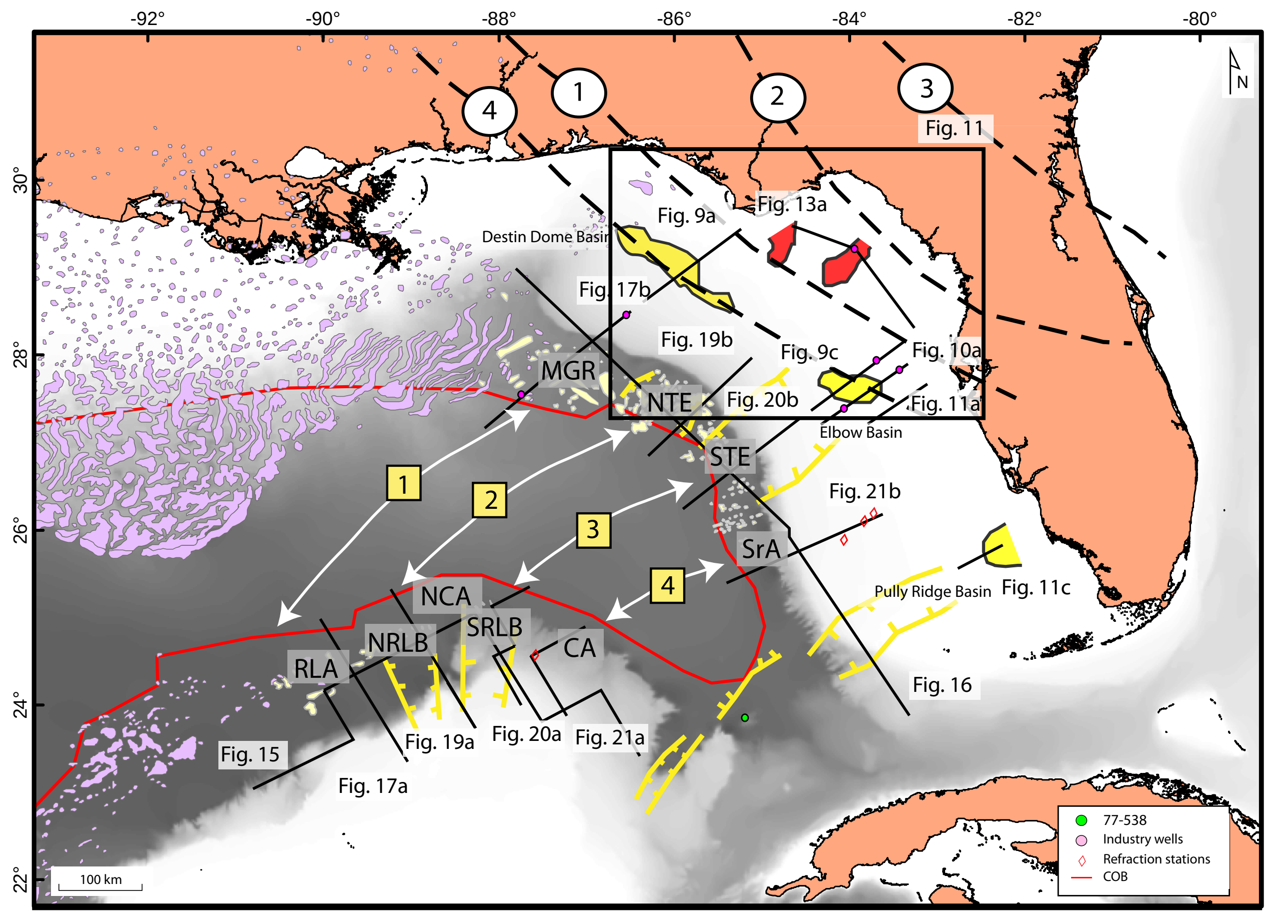

Figure 2.8 Regional map showing Paleozoic, strike-slip faults, and salt distribution on both conjugate margins. Locations of the 2D seismic lines are shown for the following figures in this chapter: Figs. 2.9, 2.10, 2.11, 2.13, 2.15, 2.16, 2.17, 2.19, 2.20, 2.21. Fault symbols are same as Fig. 2.6b.

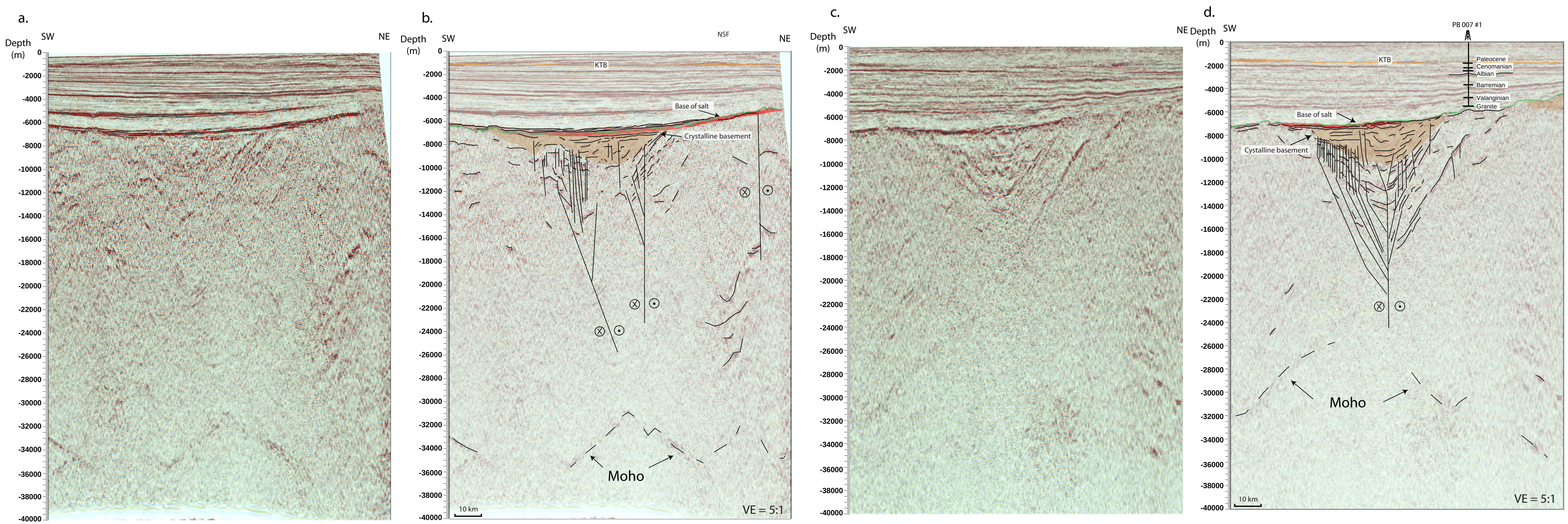

Figure 2.9 (a) Uninterpreted southwest-northeast, deep-penetrating, seismic line crossing the Destin Dome Basin (DDB) (location of line is shown on Fig. 2.8) at 5 to 1 vertical exaggeration. The Moho beneath is elevated under the heavily faulted basin which forms a strike-slip-related, flower structure. (b) Interpreted southwest-northeast, deep-penetration, seismic line crossing the Paleozoic, Destin Dome Basin (DDB) at 5 to 1 vertical exaggeration. Orange horizon is the Cretaceous-Tertiary boundary (KTB), and the green horizon is base of Louann salt. Black lines delineate prominent reflectors within the Paleozoic fill of the basin shown in brown color between inferred, crystalline basement and base of Louann salt. (c) Un-interpreted, southwest-northeast, deep-penetration seismic line crossing the Paleozoic, Elbow Basin (EB) at 5 to 1 vertical exaggeration and showing a similarly, uplifted Moho to the Destin Dome basin shown in Fig. 2.9a. (d) Interpreted, southwest-northeast, deep-penetration seismic line crossing the Elbow Basin (EB) at 5 to 1 vertical exaggeration. Well PB 007 #1 penetrated a Mesozoic granite within the basement.

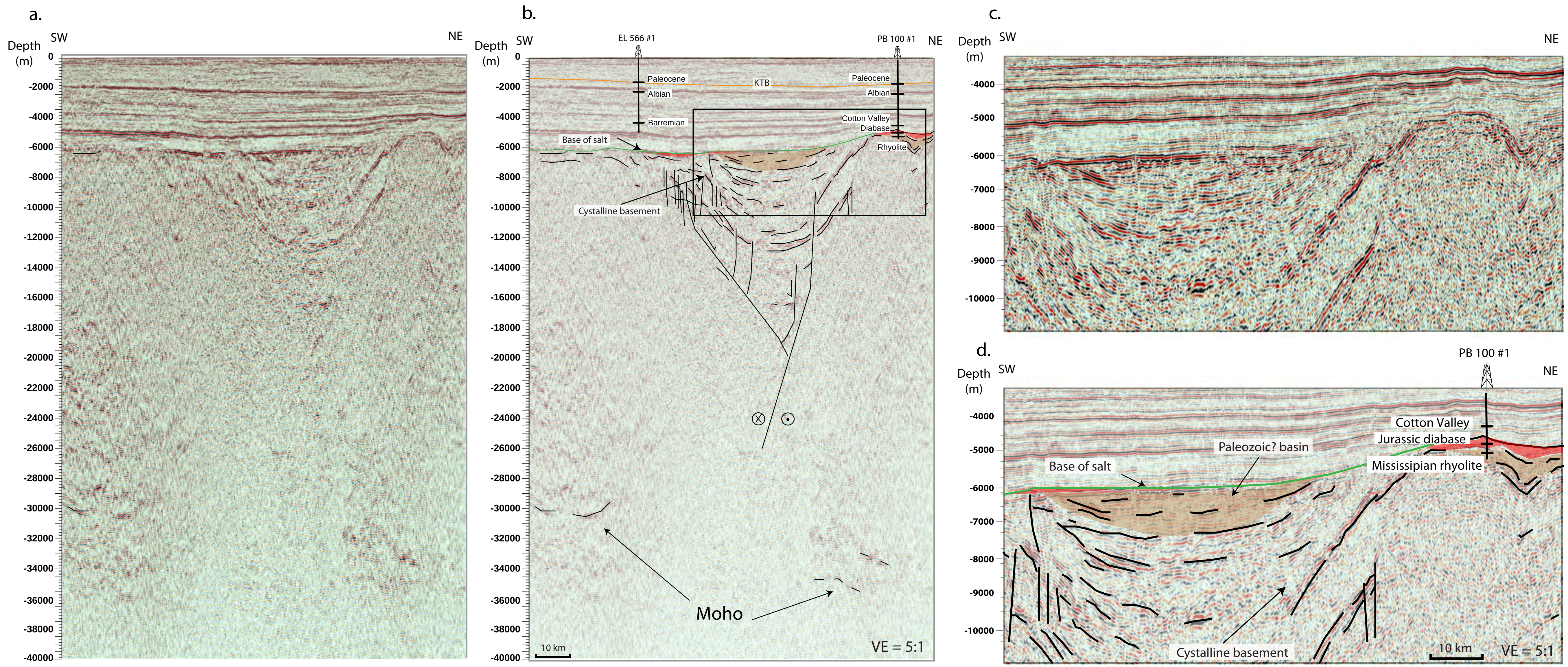

Figure 2.10 (a) Uninterpreted, southwest-northeast, deep-penetration seismic line crossing the Elbow Basin (EB) south of the line shown in Fig. 2.9c at 5 to 1 vertical exaggeration. (b) Interpreted, southwest-northeast, deep-penetration seismic line crossing the Elbow Basin (EB) south of the line shown in Fig. 2.9d at 5 to 1 vertical exaggeration. Well PB 100 #1 penetrated Jurassic diabase and Mississippian rhyolite on the northeast boundary of the Elbow pull-apart basin. (c) Zoom of the seismic line of the Florida margin shown in Fig. 2.10a to show seismic well correlation from well PB 100 #1 with the same vertical exaggeration. (d) Zoom of the seismic line of the Florida margin shown in Fig. 2. 10b to show seismic well correlation from well PB 100 #1 with the same vertical exaggeration .

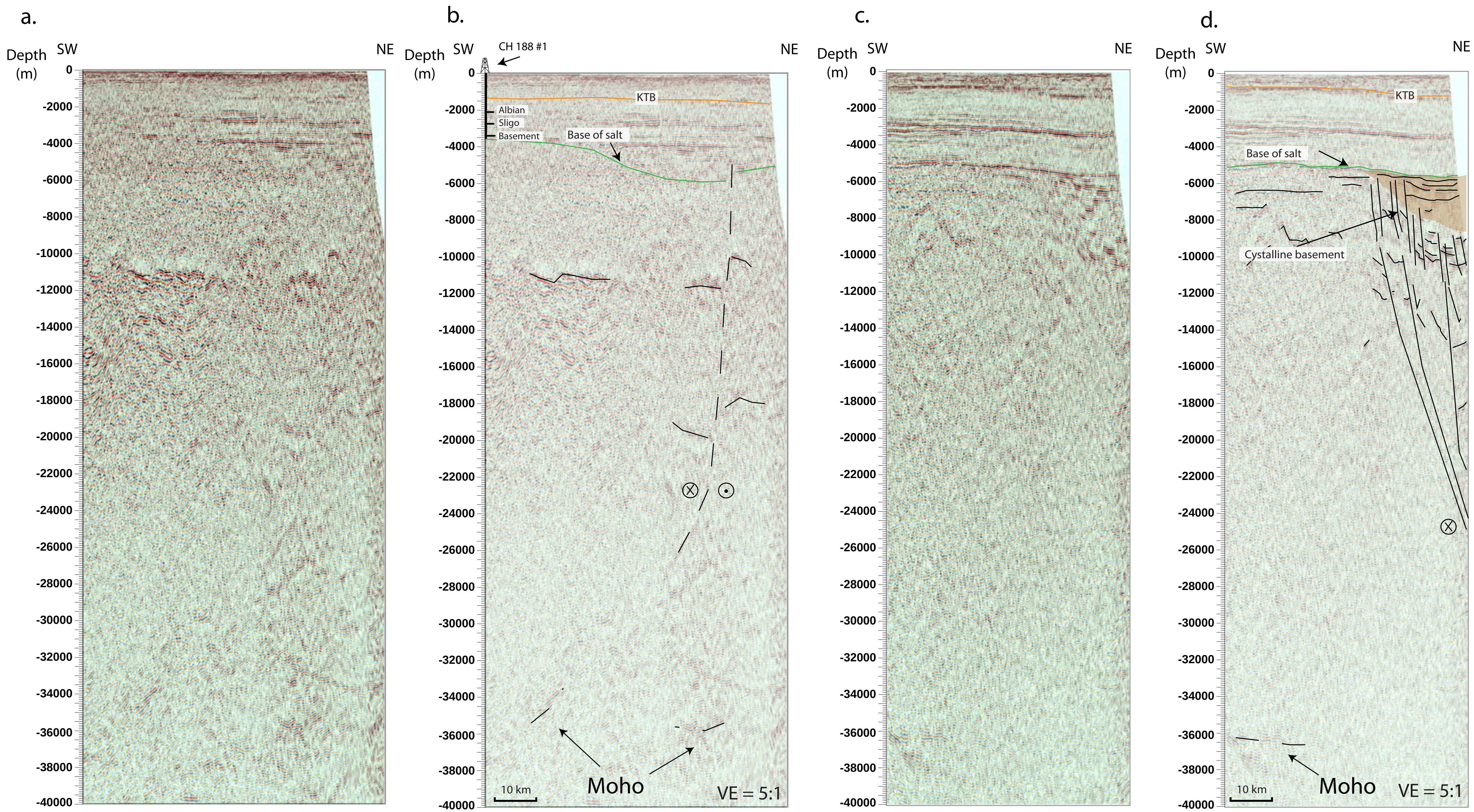

Figure 2.11 (a) Uninterpreted, southwest-northeast, deep-penetration seismic line crossing south of the Elbow Basin (EB) at 5 to 1 vertical exaggeration. (b) Interpreted, southwest-northeast, deep-penetration seismic line crossing south of the Elbow Basin (EB) at 5 to 1 vertical exaggeration. A possible 20-km-long strike-slip fault with 2-km offset is located at the projection of Paleozoic strike-slip fault identified in this study. (c) Uninterpreted southwest-northeast, deep-penetration seismic line crossing the Pully Ridge Basin (PRB) at 5 to 1 vertical exaggeration. Although only half of the Marco Basin is within this seismic section, the flower structure features of the Marco basin are similar to those of the Elbow basin as shown in Fig. 2.10a. (d) Interpreted, southwest-northeast, deep-penetration seismic line crossing the Pully Ridge Basin (PRB) at 5 to 1 vertical exaggeration. The magnetic feature indicates the presence of volcanic rocks within the Marco basin although this interpretation would require well data to verify.

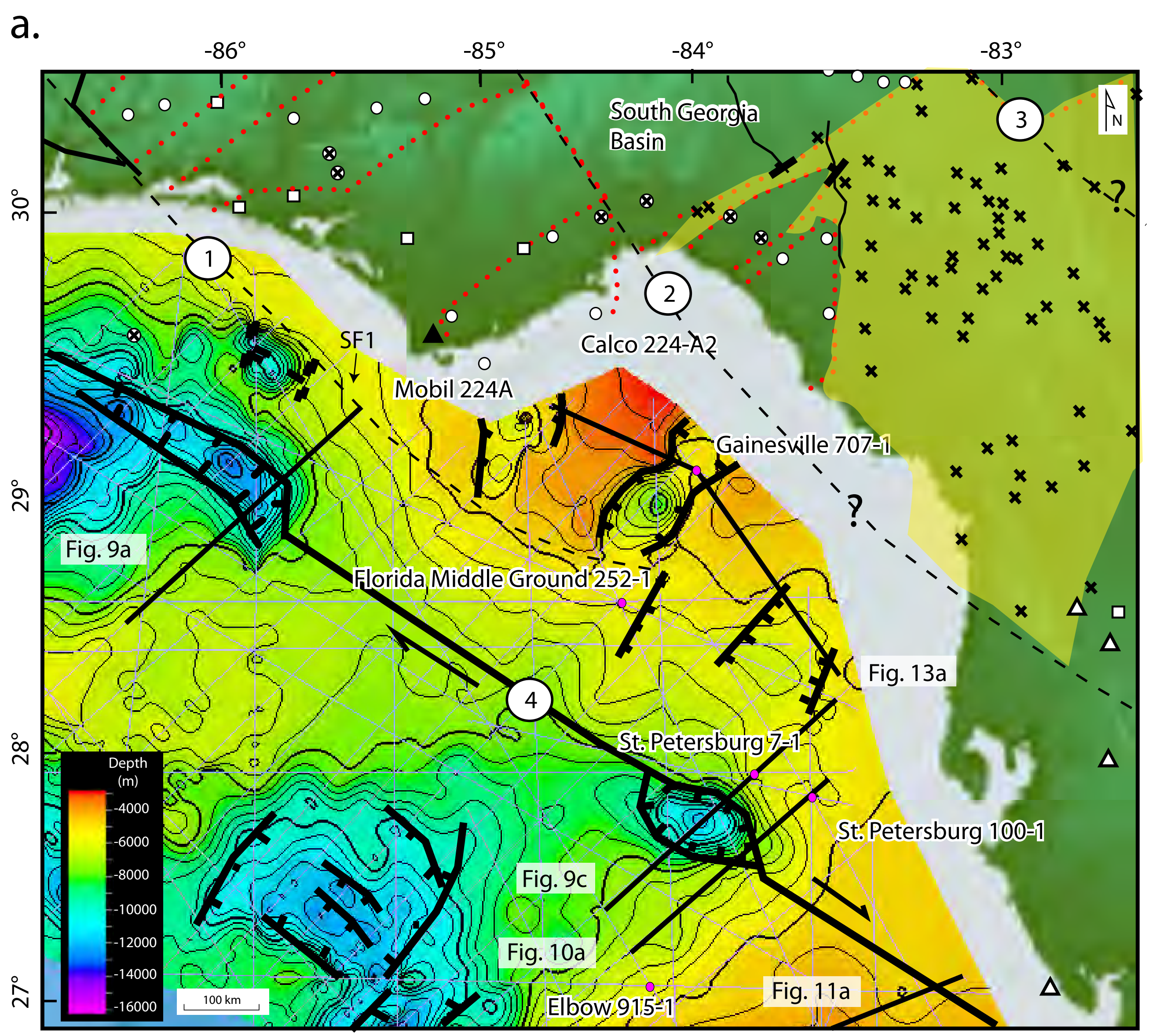

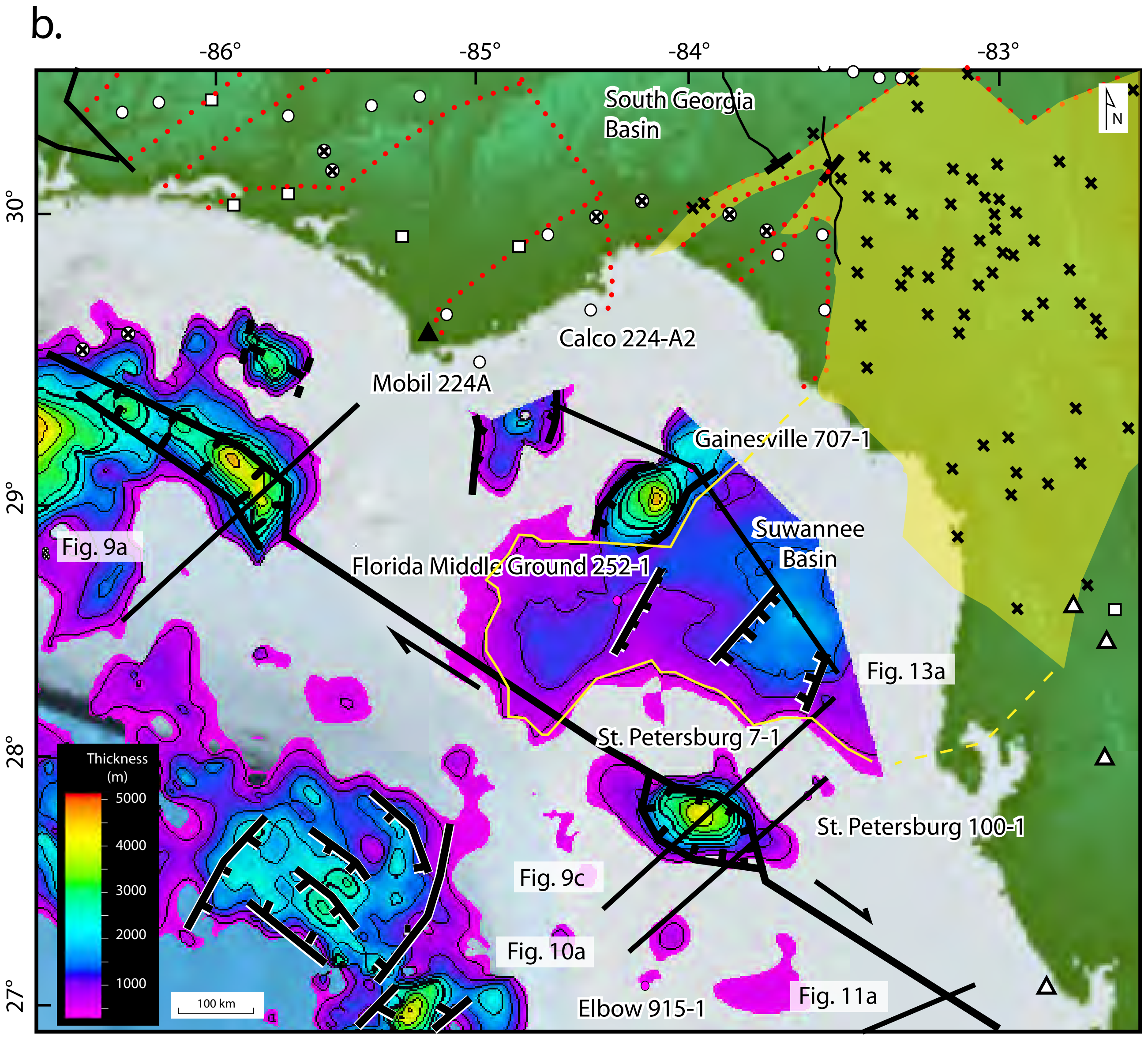

Figure 2.12 (a) Regional map of the depth to the top of the crystalline basement map in the area of the northern part of the West Florida Shelf. Thin purple lines show seismic grid used to make the map. Black lines onshore are published seismic lines from McBride (1991). The shapes and occurrence of the Destin Dome and Elbow, Paleozoic basins at right-steps in the fault supports the interpretation of right-lateral strike-slip along this fault that is consistent with similar, right-lateral faults mapped by Smith and Lord (1997) to the land area of Florida to the northeast. (b) Isopach map of Paleozoic and Mesozoic basins in the northern area of the West Florida Shelf. The early Paleozoic Suwannee and northeast-southwest trending Triassic faults produced by Phase 1 rifting are orthogonal to the trend of the early Paleozoic fault and associated pull-apart basins.

2.5.3 Subsurface geology of the onshore Triassic, South Georgia rift

South Georgia Triassic basin has been extensively drilled by onshore wells in north Florida and south Alabama and Georgia (Fig. 2.12) (McBride, 1991). Drilling results show South Georgia Triassic basin downfaulted the northern Suwannee basin that was then filled with Upper Triassic-Lower Jurassic red beds (Eagle Mills formation) and diabase (McBride, 1991). The offshore extent of the South Georgia rift to the southwest is not well defined (McBride, 1991).

Chowns and Williams (1983) summarized deep well information from the onland area of Florida and combined the well information with potential fields data to define the outline of the of South Georgia rift. Wells show that the South Georgia rift contains at least 3500 m of red beds (Fig. 2.4b).

McBride (1991) identified several, northwest-trending, half-grabens from north-south, and north-northwest-trending, 2D seismic reflection lines crossing the central part of the South Georgia rift in northern Florida. The largest rift depocenter in west Georgia is more than 100 km wide and 7 km in deep.

I used their southern, two seismic sections to compare to rift features I have mapped offshore using the Spectrum 2D seismic grid (Fig. 2.12). The northward-dipping, normal, boundary faults are inferred from abrupt truncations of southward-dipping reflectors interpreted as rift fill that is truncated by the post-rift unconformity (McBride, 1991). On this line, the half-graben is 7 km wide and 4 km deep and has an average, sediment velocity of 3.0 km/s (McBride, 1991).

2.5.4 Using offshore wells and seismic data to define South Georgia rifts beneath the West Florida shelf

On the West Florida shelf, three wells have penetrated Triassic-Jurassic clastic and volcanic rocks in rift basins (Fig. 2.12). The Mobile 224A well penetrated 132 m of coarse-grained, Eagle Mills formation at 4210 m below sea level along with a diabase sill around 4200 m below sea level (Barnett, 1975). The Calco 224-A2 well encountered diabase at 3177 m below sea level and bottomed in Triassic Eagle Mills Formation at 3208 m (Applegate and Lloyd, 1985). The Gainesville 707-1 (GV 707) well penetrated the 422 m of Triassic, Eagle Mills Formation at 2773.4 m and drilled 42 m into the Paleozoic sedimentary basement (Applegate and Lloyd, 1985).

This Paleozoic sedimentary rock in these wells correlates with grey, Paleozoic siltstone found in the well Florida Middle Ground 252-1 and in numerous, onland wells that bottomed in Paleozoic sediments (Fig. 2.12) (Applegate and Lloyd, 1985). The Triassic section is composed of more than 300 m of Triassic red beds and contains a series of volcanic and volcanoclastic rocks that grade upward into the red bed sequence (Bartok, 1993). The redbeds are dated with pollen as late-middle Triassic which is the same age as the Triassic volcanic complex within the Newark graben of New Jersey (Applegate and Lloyd, 1985; Byerly, 1991; Bartok, 1993).

Basement and isopach maps show northeast-trending and north-trending trending Triassic basins along the southwestern edge of the onshore South Georgia Basin, and another Triassic basin aligned with the northern boundary of the Suwannee basin (Fig. 2.12). Fig. 2.13 is a northwest-southeast, cross-section through these Triassic and Paleozoic depocenters.

Strong, wavy reflectors mark the base of offshore Suwannee Basin that is bounded by normal faults (Fig. 2.13). Towards the northwest, Paleozoic, reflector packages become more chaotic in the lower parts of the basin. Several, higher-amplitude reflectors present at 8000 m below sea level may correspond to igneous sills formed during Triassic rifting and act to obscure the lower part of the Paleozoic section of the Suwannee Basin on 2D seismic reflection lines (Fig. 2.13).

The Triassic rift basins contain both late Triassic red beds and middle Triassic volcanic rocks correlating with a section drilled in the GV 707 well (Fig. 2.13). The middle Triassic layer had a consistent thickness of about 500 m and is confined within a rift basin (Fig. 2.13). The late Triassic section varies from 1500 m in the depocenter and pinches out towards the Suwannee Basin (Fig. 2.13). Following the geometry of offshore Triassic basin and potential field data, the fault boundaries of the South Georgia Basin is reinterpreted on Fig. 2.12. These rifts coincide with negative gravity feature D1 which correlates with a strong, magnetic anomaly (Figs. 2.6a, 2.14).

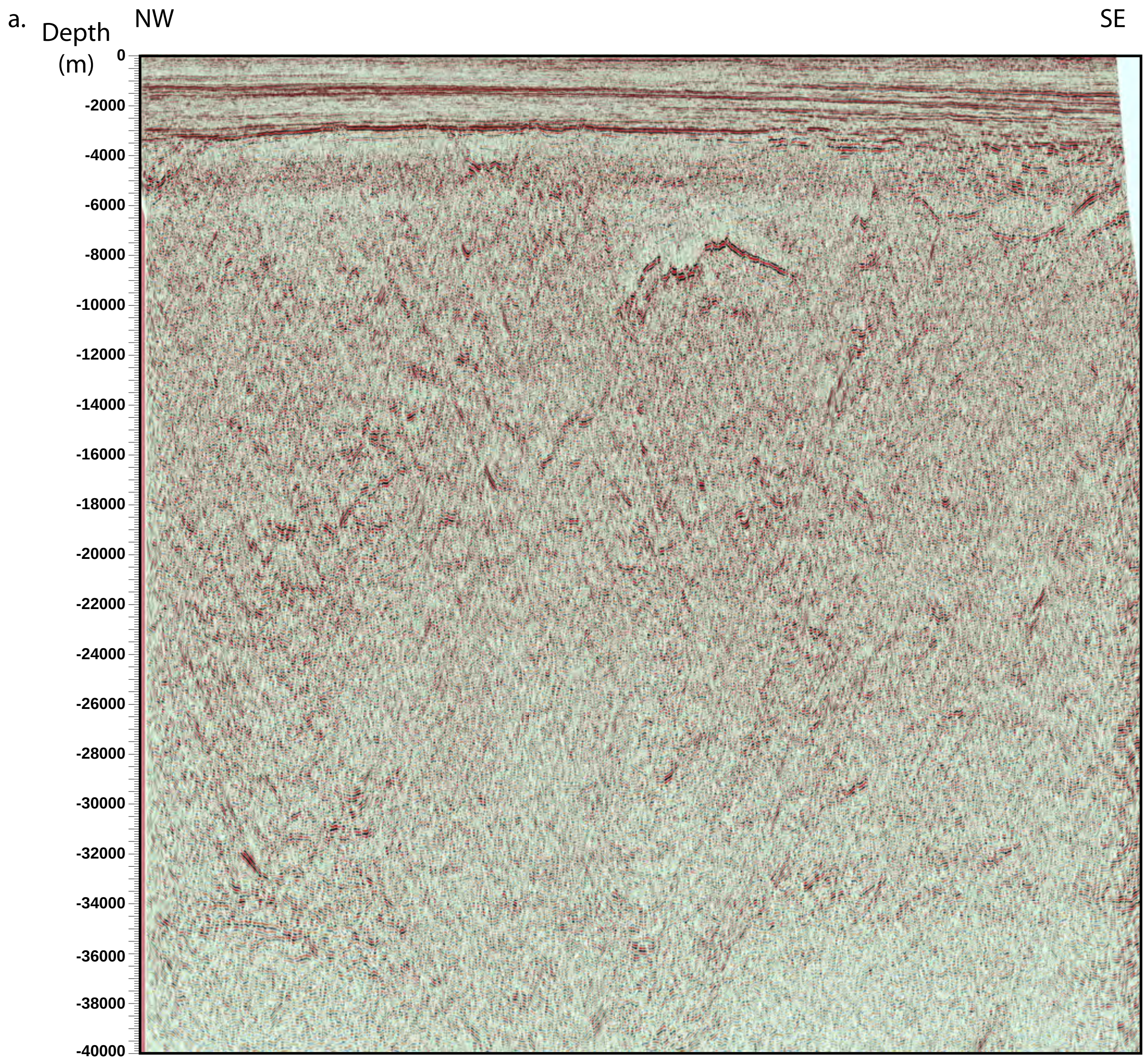

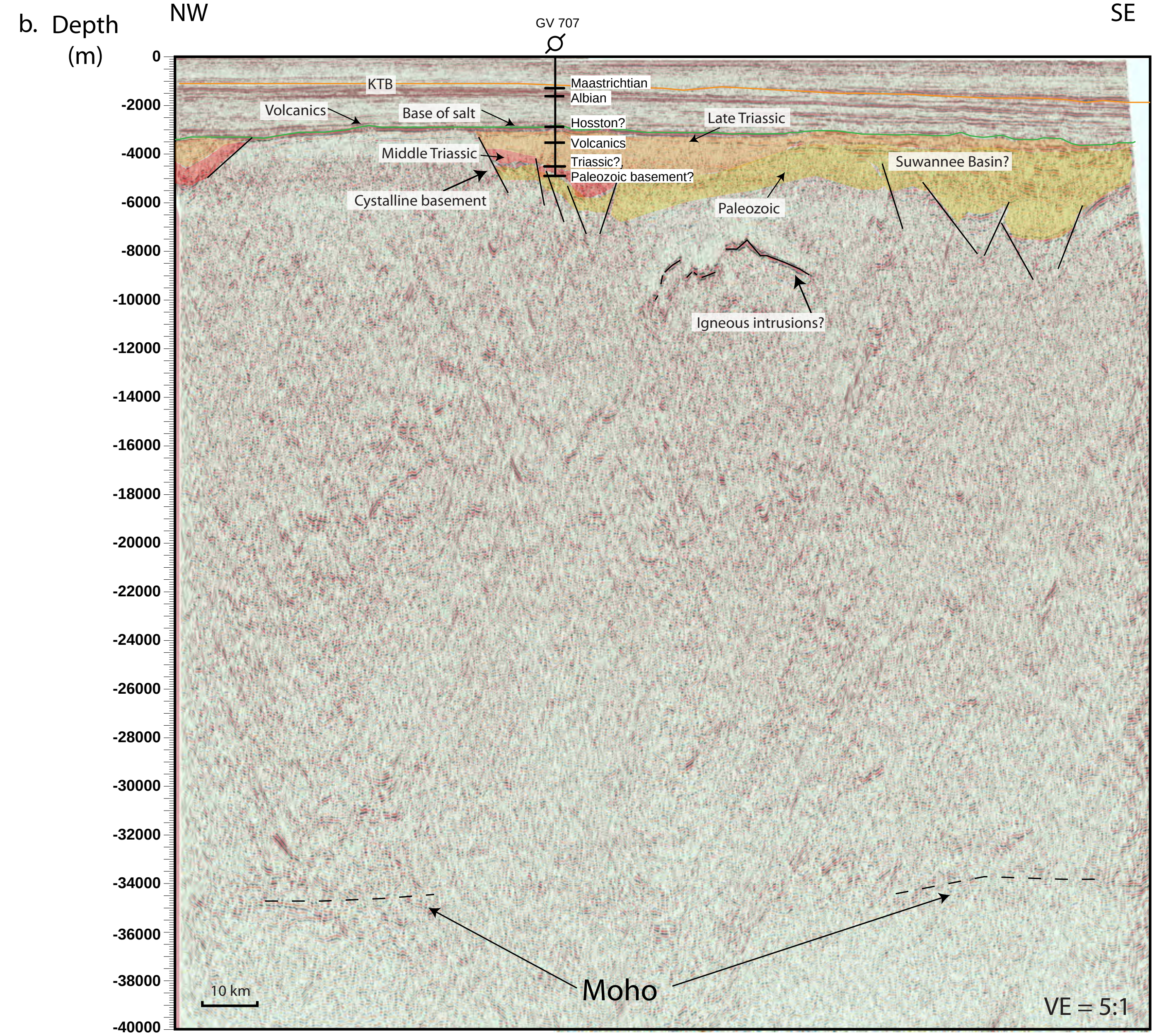

Figure 2.13 (a) Uninterpreted, northwest-southeast, deep-penetration seismic line crossing the southeastern, Triassic, South Georgia rift (SGS) and the Paleozoic Suwannee Basin (SB) at 5 to 1 vertical exaggeration. The high amplitude layer around 4 km below the post-rift unconformity is interpreted as igneous intrusions during Triassic rifting. (b) Interpreted, northwest-southeast, deep-penetration seismic line crossing southeast of the South Georgia rift (SGR) and the Paleozoic Suwannee Basin (SB) at 5 to 1 vertical exaggeration. Yellow, red, and orange background represent the possible extent of the basins are color-coded: Lower Paleozoic (yellow), Middle Triassic (red), and Late Triassic sediments (orange). Triassic rifting of Phase 1 reactivated the northern edge of the early Paleozoic Suwannee Basin.

2.6 Late Jurassic conjugate rift margins in western Florida and the Yucatan Peninsula

The Phase 2, Late Jurassic, rifted margin consists of broad, basement highs and intervening lows that can be re-aligned across the Florida and Yucatan, conjugate margins (Figs. 2.14, 2.15, 2.16). The northeast-trending, basement fabric can be related to Phase 1 rifting which formed the NE trending basement lows as rifts that are best expressed on the magnetic map in Fig. 2.5a.

To better compare the basement structures and salt distribution variation along Yucatan and Florida margin, I have interpreted the same, four conjugate basin pairs as proposed by Steier (2018): (1) the Rio Lagartos Arch (Yucatan) and Middle Ground Arch (Florida), (2) the Rio Lagartos Basin (Yucatan) and Tampa Embayment (Florida), (3) the Chiquila Arch (Yucatan) and Sarasota Arch (Florida), and (4) the Chiquila Basin (Yucatan) and South Florida Basin (Florida) (Fig. 2.14). The Rio Lagartos Basin on the Yucatan margin and Tampa Embayment on the Florida margin are divided into northern and southern basins by a basement high (Figs. 2.15, 2.16).

The South Florida basin forms a broad, regional depression that overlies a prominent, linear magnetic low shown on Fig. 2.5a that I interpret as a rift that has not been imaged using the currently-available, seismic reflection data. In contrast, the Yucatan conjugate margin exhibits the Chiquila basin which is a 1500-m-wide, 1.4 seconds (2100 m)-deep half graben (Fig. 2.15).

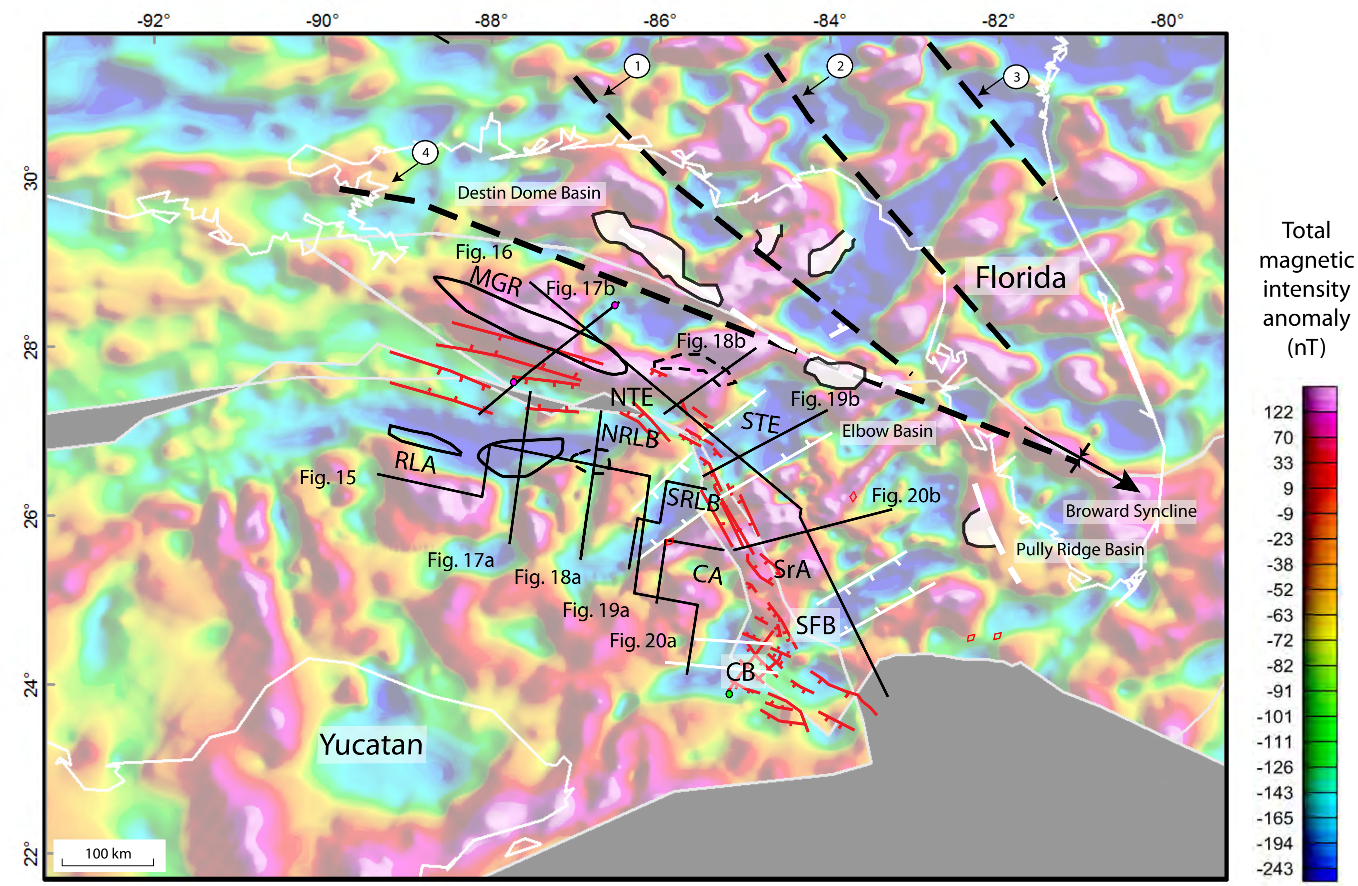

Figure 2.14 Late Jurassic, pre-phase 2, reconstruction using Gplates at 158 Ma of the regional map of total magnetic anomalies. Late Triassic-early Jurassic faults, and late Jurassic faults are shown in white and red lines, respectively. Interpreted, basinward dipping reflectors (BDRs) are shown by black polygons and correspond to magnetic highs in Florida margin, and magnetic lows in Yucatan margin.

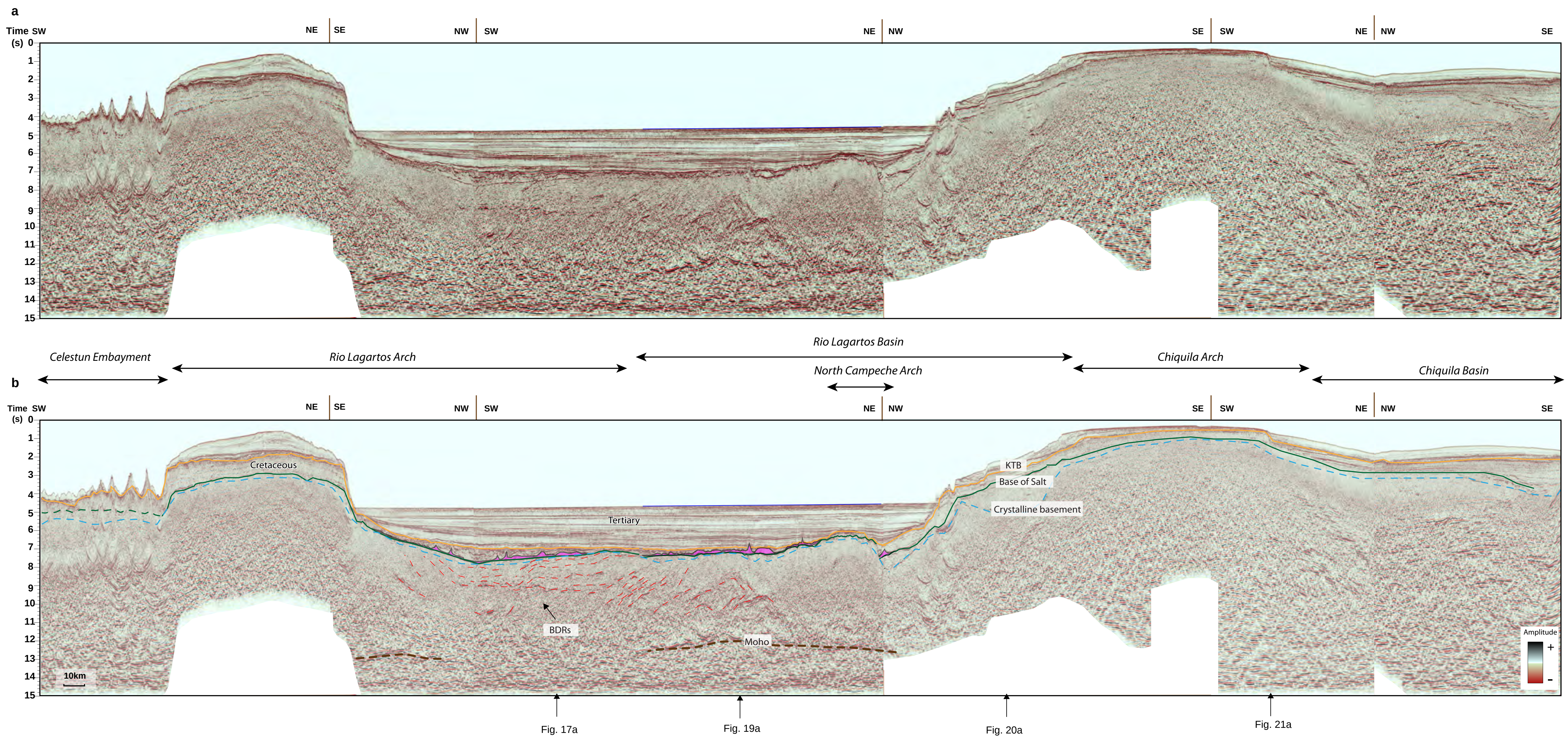

Figure 2.15 (a) Uninterpreted, southwest-northeast, deep-penetration seismic line crossing the continental shelf of the northern Yucatan peninsula (location of seismic lines is shown in Figs. 2.8 and 2.13). From west to east, broad basement highs and lows are named here and include: the Celestun Embayment (CE), the Rio Lagartos Arch (RLA), the Northern Rio Lagartos Basin (NRLB), the Southern Rio Lagartos Basin (SRLB), the Chiquila Arch (CA), and the Chiquila Basin (CB). (b) Interpreted, southwest-northeast, deep-penetration seismic line shown in Fig. 2.15a. Abbreviations for horizons are the same as used in Fig. 2.5a. Color-coded lines include: Orange, green, blue and brown lines are Cretaceous-Tertiary boundary (KTB) (orange), Base of salt (green), crystalline basement (blue), and Moho (brown). The dashed line indicates the lack of confidence for interpretation in areas of low seismic quality. The red dashed lines show the possible extent of basinward dipping reflectors (BDRs) in the area between the Rio Lagartos Arch and Rio Lagartos Basin.

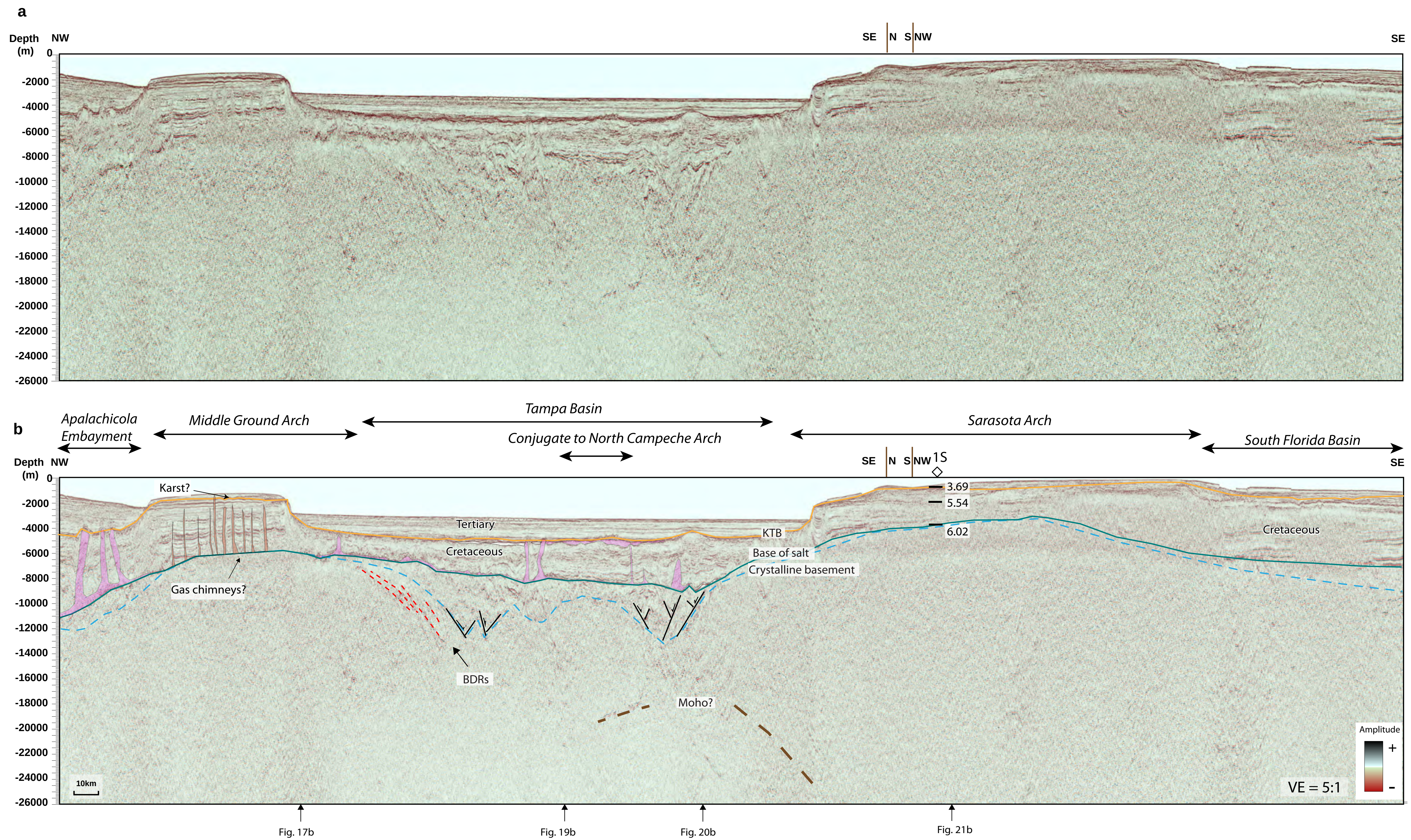

Figure 2.16 (a) Un-interpreted, northwest-southeast, deep-penetration seismic line from the continental shelf of Florida at 5 to 1 vertical exaggeration (location of seismic lines is shown in Figs. 2.8 and 2.13). Broad basement highs and lows represent the Apalachicola Embayment (AB), Middle Ground Arch (MGR), Northern Tampa Embayment (NTE), Southern Tampa Embayment (STE), Sarasota Arch (SrA), and South Florida Basin (SFB) from northwest to southeast. (b) Interpreted northwest-southeast, deep-penetration seismic line shown in Fig. 2.15a. Basin dipping reflectors (BDRs) are present between the Middle Ground Arch and North Tampa Embayment and conjugate to BDRs on the Yucatan margin.

On the Yucatan margin, high-amplitude basinward dipping reflectors (BDRs) underlie the base of salt on the Rio Lagartos Arch and the Northern Rio Lagartos Basin (Fig. 2.15). On the Florida margin, similar BDRs are observed on the conjugate Middle Ground Arch and the North Tampa Basin (Imbert, 2005; Christeson et al., 2014) (Fig. 2.16). Salt diapirs were observed emanating from the basement lows of the Rio Lagartos Basin and Tampa Embayment of the Florida and Yucatan conjugate margins, respectively, and pinch out onto the Chiquila Arch and Sarasota Arch.

2.6.1 Comparison of seismic reflection lines crossing the Rio Lagartos Arch (Yucatan conjugate margin) and the Middle Ground Arch (Florida conjugate margin)

I compared seismic profiles from the northern region of the study area across the conjugate pairs of the Rio Lagartos Arch (Fig. 2.17a) and the Middle Ground Arch (Fig. 2.17b). Both conjugate margins show high-amplitude, basinward-dipping reflectors (BDRs) outboard of the Cretaceous-Cenozoic, West Florida carbonate escarpment and beneath the base of salt.

The Yucatan seismic profile shows a 2-second-travel-time (3 km) thick, BDRs with a sediment velocity of 3 km/s that occupies a belt of BDRs that is 28-km-wide (Fig. 2.17a). With a salt velocity of 4 km/s, the 30-km-wide 0.1 second-high salt diapirs on the updip of BDRs has an average thickness of 200 m, and the 30-km wide 0.8s-high salt diapirs downdip from the BDRs has an average thickness of 1600 m (Fig. 2.17a). A basement high on the top of BDRs provides a sloping surface for deposition of post-rift sediments beneath the Cretaceous-Tertiary Boundary (KTB) that overlies the salt detachment (Steier, 2018) (Fig. 2.17a). The 1600-m-high, salt diapirs were concentrated within a symmetrical marginal rift on the seaward side of the extended continental crust and pinch out onto a 0.2 s (200 m) basement step-up between continent ocean boundary (COB) (Hudec et al., 2013). Steier (2018) mapped the westward continuation of the marginal rift in the Yucatan margin westward into the Campeche area. On the platform, a 4-km wide cave is present in a karsted zone of the KTB (Fig. 2.17a).

The Florida seismic profile shows a similar BDR wedge about 28-km wide and 5- km deep (Fig. 2.17b). Several high-amplitude low-continuous, wavy reflectors are observed beneath the Florida escarpment with ~3-4.5 km, thicknesses inferred to be part of a package of BDRs (Fig. 2.17). The salt layer is continuously distributed in a 70-km wide extended continental crust with salt rollers in the updip area and mild compression in the downdip area.

The extended continental crust is composed of a series of basinward-dipping, half-grabens underlying the 3-5 km high salt diapirs. A marginal, symmetrical rift is located on the seaward end of extended continental crust similar to the Yucatan margin (Steier, 2018). Salt diapirs with similar vertical heights are present above this symmetrical marginal rift and pinch out onto a 300 m basement step-up that marks the continent-ocean boundary (COB) (Hudec et al., 2013; Rowan, 2018).

Above the platform basement, a 3-km-high group of chaotic reflectors disturbs an area of strong, parallel reflectors (Fig. 2.18). I interpret these features as gas chimneys associated with the formation of natural gas. Dobson and Buffler (1991) recognized extensive basement-involved, normal faulting of the Middle Ground Arch, and suggested possible Triassic clastic rocks filled these rifts.

2.6.2 Comparison of seismic reflection lines crossing the Northern Rio Lagartos Basin (Yucatan conjugate margin) and Northern Tampa Embayment (Florida conjugate margin)

The 2D seismic line shown in Fig. 2.19 compares the conjugate margins of the Northern Rio Lagartos Basin and the Northern Tampa Embayment. In the Northern Rio Lagartos Basin, the salt distribution and rift geometry is similar to the previously observed features of the Florida margin observed on the seismic section in Fig. 2.17.

The Moho interpretation in this profile is characterized by high-amplitude, landward-dipping reflectors (LDRs) near the COB (Fig. 2.19). A set of high-amplitude, subparallel, folded reflectors within this 5 second, two-way time (15 km) thick crust are shown in the lower crust of the Yucatan margin (Fig. 2.18a).

The width of the salt distribution of Florida margin in the area of the Northern Tampa rift decreases from 70-km to 40-km. There is an absence of similar BDRs beneath the Florida escarpment, although a one-km-high, outer high is present near the COB (Fig. 2.17b).

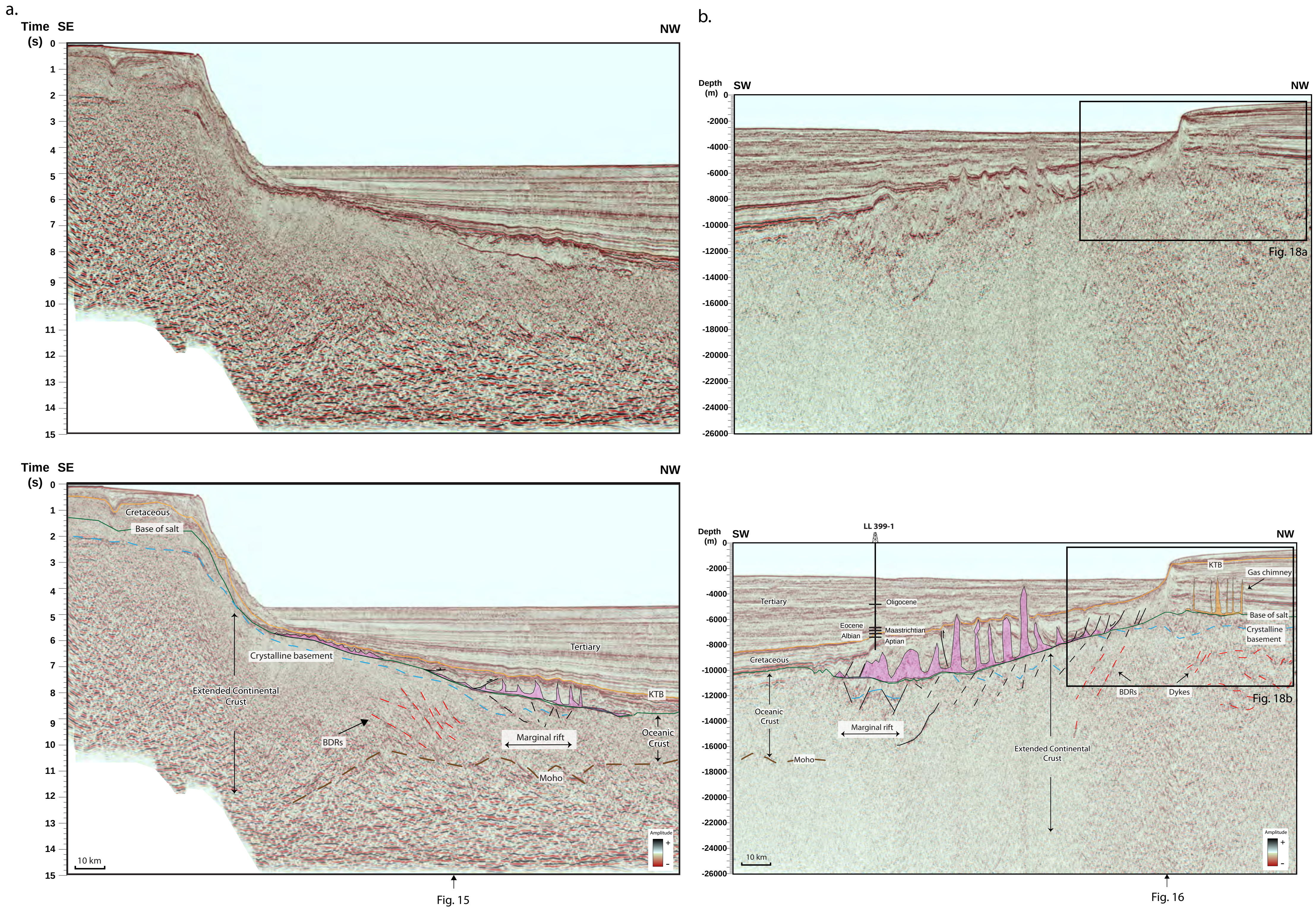

Figure 2.17 (a) Un-interpreted and interpreted, southeast-northwest, deep- penetration seismic line crossing the Rio Lagartos Arch (RLA), Yucatan. (b) The un-interpreted and interpreted, southwest-northeast, deep-penetration seismic line crossing the Middle Ground Arch (MGA) on its conjugate margin in Florida. Salt diapirs distributed over a wider, extended area of continental crust on the Florida margin than on its conjugate margin in Yucatan. Both conjugate margins show the presence of BDRs beneath the salt roller nearest the carbonate escarpment.

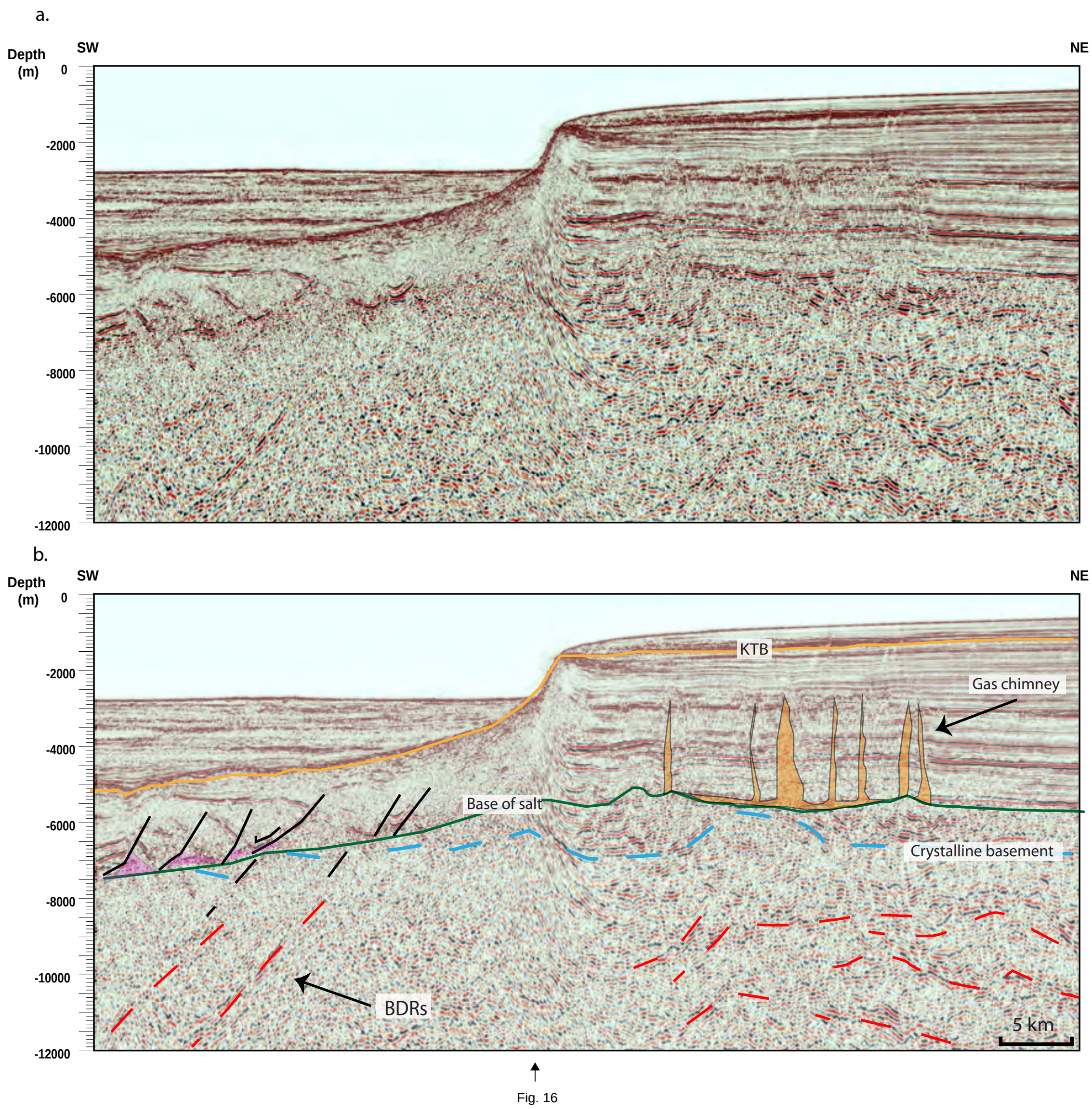

Figure 2.18 (a) Zoom of the seismic line of the Florida margin shown in Fig. 2.17a. (b) Zoom of the seismic line of the Florida margin shown in Fig. 2.17b to illustrate interpreted BDR's underlying salt rollers along with gas chimneys overlying the crystalline basement of Florida.

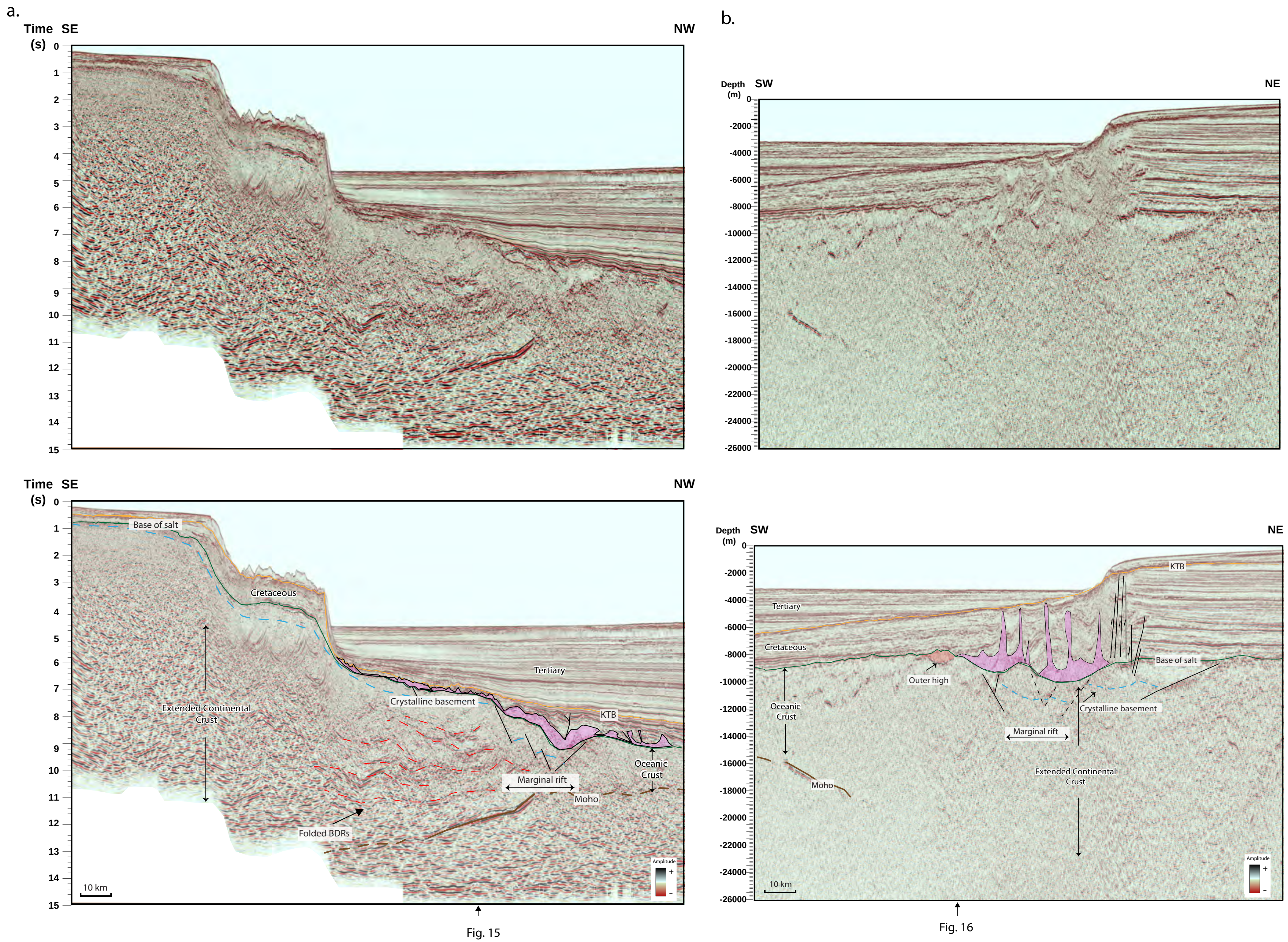

Figure 2.19 (a) Un-interpreted and interpreted, southeast-northwest, deep-penetration seismic line crossing the Northern Rio Lagartos Basin (NRLB) on the Yucatan margin. High-amplitude reflectors underneath the salt are folded and dip subparallel to the seismic Moho. (b) Un-interpreted and interpreted, southwest-northeast, deep-penetration seismic line from Northern Tampa Embayment (NTE) on the Florida margin. An outer high is shown on the seaward boundary of salt. Concentrated salt in a marginal rift similar to that present on the Yucatan margin (Steier, 2018).

2.6.3 Comparison of seismic reflection lines from Southern Rio Lagartos Basin (Yucatan conjugate margin) and Southern Tampa Embayment (Florida conjugate margin)

Fig. 2.20 compares seismic profiles through the conjugate margins of the South Rio Lagartos Basin and the South Tampa Embayment. In the South Rio Lagartos Basin, low-amplitude, salt rollers are concentrated in the basement low and confined by the outer basement high marking the COB. Similar, high- amplitude, subparallel reflector packages are present within the 5 seconds (~15 km) thick crust. The distribution of these subparallel reflectors is in a narrow belt that is adjacent to the COB (Fig. 2.19a). Beneath the basement of the Florida platform, a 2 second two-way time (~3 km thick) basin is located 15 km inboard of Cretaceous-Cenozoic, carbonate escarpment (Fig. 2.20a).

The seismic reflection line across the proposed Southern Tampa rift shows fewer, salt diapirs with 200-m to 500-m high diapirs emanating from the marginal rifts compared to 800-m to 1500-m high salt diapirs observed on the seismic reflection line across the area of the Northern Tampa rift (Fig. 2.20b). BDRs are not present under Florida escarpment, but are near the outer high marking the COB (Fig. 2.20b).

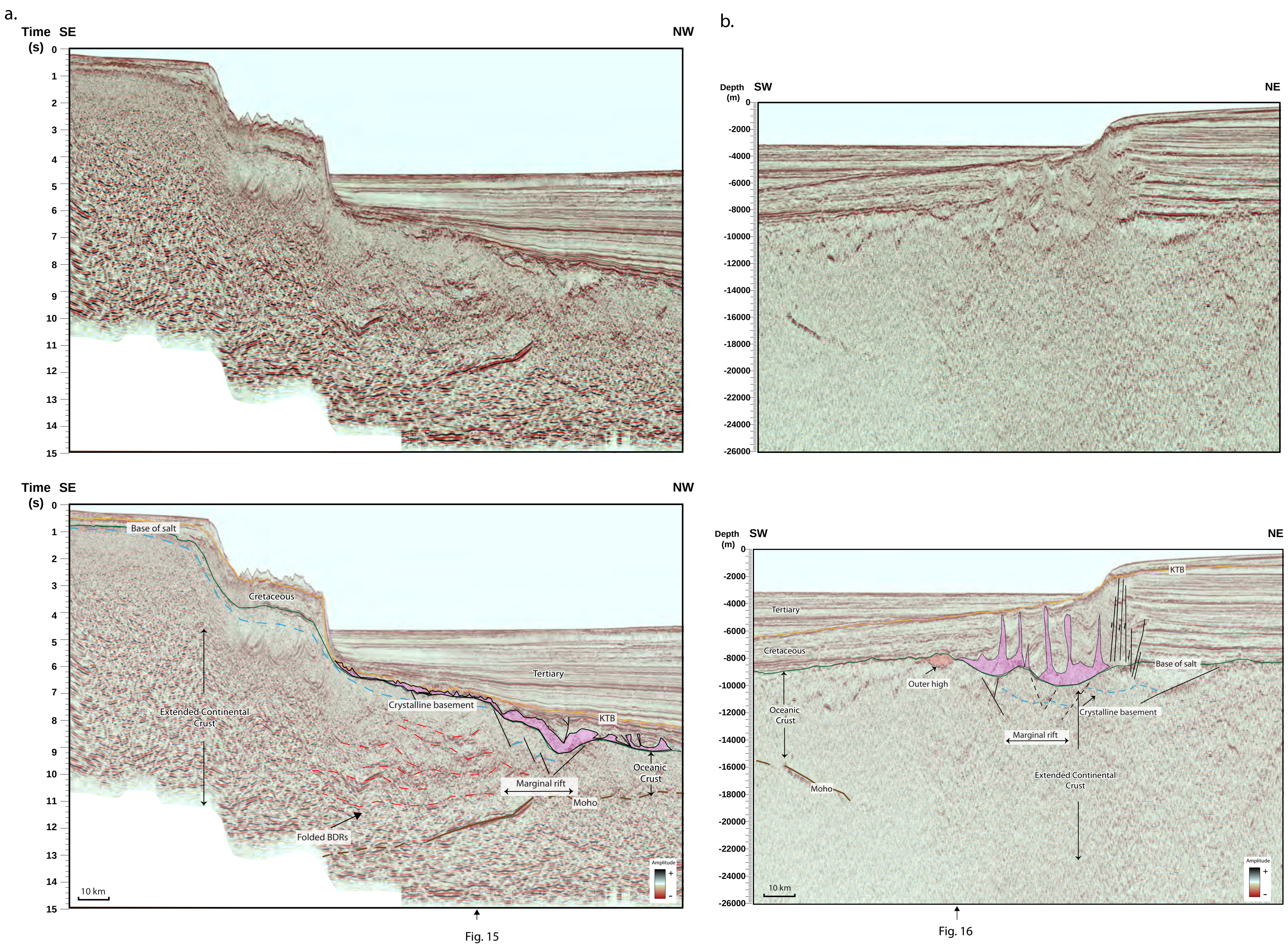

Figure 2.20 (a) Uninterpreted and interpreted, southeast-northwest, deep-penetration seismic line from Southern Rio Lagartos Basin (SRLB) on the Yucatan margin. Only salt rollers are present and stopped by the basement high in the extended continental crust. (b) Un-interpreted and interpreted, southwest-northeast, deep-penetration seismic line from Southern Tampa Embayment (STE). On both conjugate margins, a marginal rift on thinned, continental crust is present that forms a low what concentrates a larger, volume of salt. The seaward high of the marginal rift is the “step-up fault” bounding the higher-standing area of oceanic crust.

2.6.4 Comparison of seismic reflection lines from Chiquila Arch (Yucatan conjugate margin) and Sarasota Arch (Florida conjugate margin)

Seismic profiles from the Chiquila Arch (Fig. 2.21a) and Middle Ground Arch conjugate margins (Fig. 2.21b) are compared in the southern region of the study area. No related volcanic features or salt features are observed on these conjugate margins. Refraction data indicates that the top of basement on the Yucatan margin is correlated with the top of 5.9 km/s velocity layer at 2.3 s (-4.05 km in depth) at station 11W from Ibrahim et al. (1981). On the Florida conjugate margin, the acoustic basement is correlated with the top of 5.81-5.95 km/s velocity layer at 3 km below sea level from three, refraction stations of Ebeniro et al. (1986). The sediment thickness on the carbonate platform is around 2.5 km on both margins (Fig. 2.21).

Mounded features above the post-rift unconformity are inferred to represent Cretaceous carbonate reefs that formed in the early, passive margin stage of both conjugate margins (Fig. 2.22). From the seismic profile of the Yucatan margin, two, 0.6 s (1.5 km) high mounds with a velocity of 5 km/s) are interpreted as pinnacle reefs that grew on the upper part of the basement slope (Fig. 2.21a). On this conjugate pair, an 800-m-high pinnacle reef is 5-km-wide and is also present on the upper part of the basement slope (Fig. 2.21b). Relatively thicker Cretaceous passive margin sediments were deposited on the Florida margin than on the Yucatan margin.

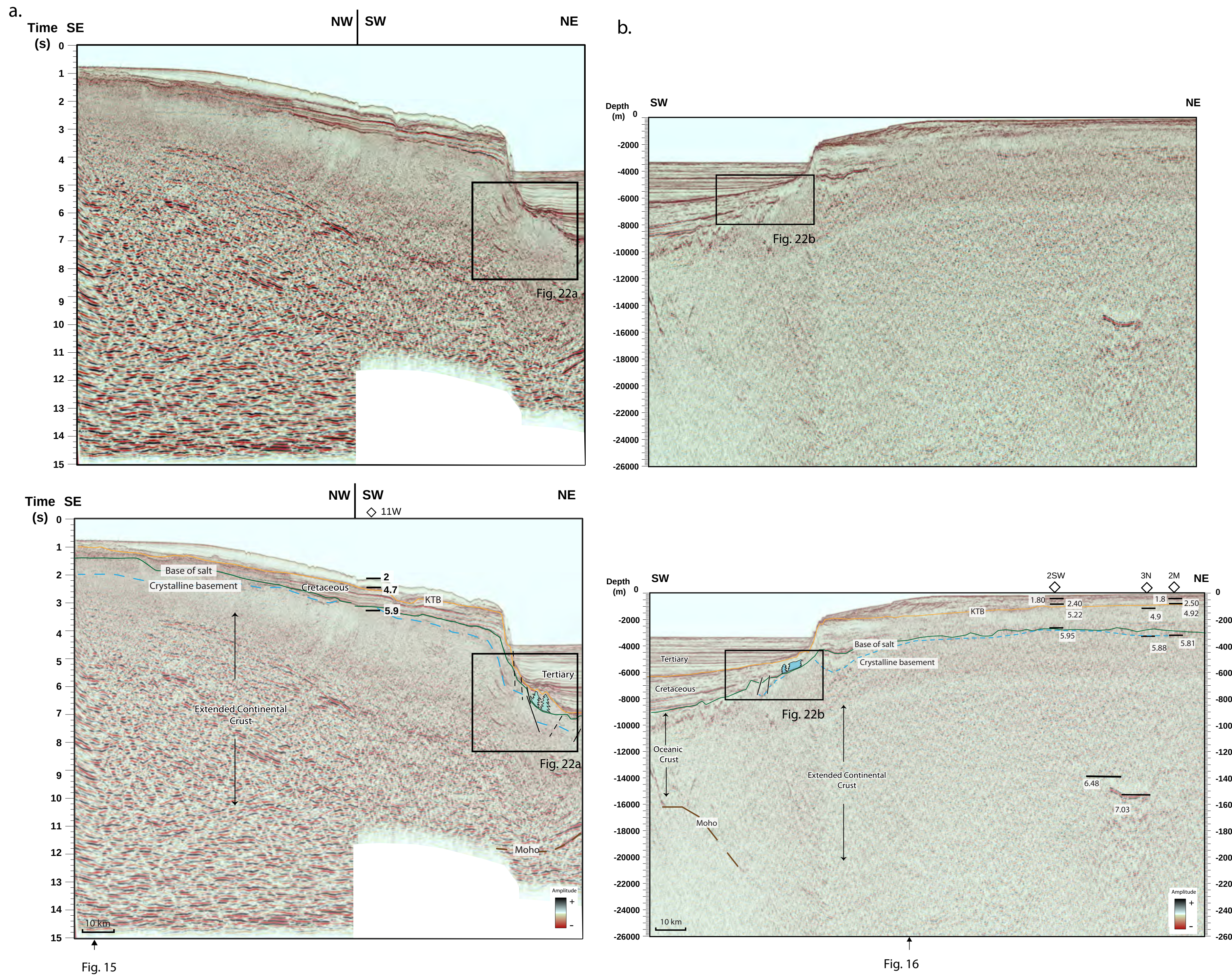

Figure 2.21 (a) Uninterpreted and interpreted, southeast-northwest, deep penetration seismic line from Chiquila Arch (CA), Yucatan. (b) Uninterpreted and interpreted, southwest-northeast, deep penetration seismic line from its conjugate margin on the Sarasota Arch (SrA) on the Florida margin. The top basement reflector correlates well with a sudden velocity change to around 5.8 km/s as seen on refraction data (Ibrahim et al. 1981; Ebeniro et al., 1986). Mounded, carbonate features on both conjugate margins are enlarged on Fig. 2.22.

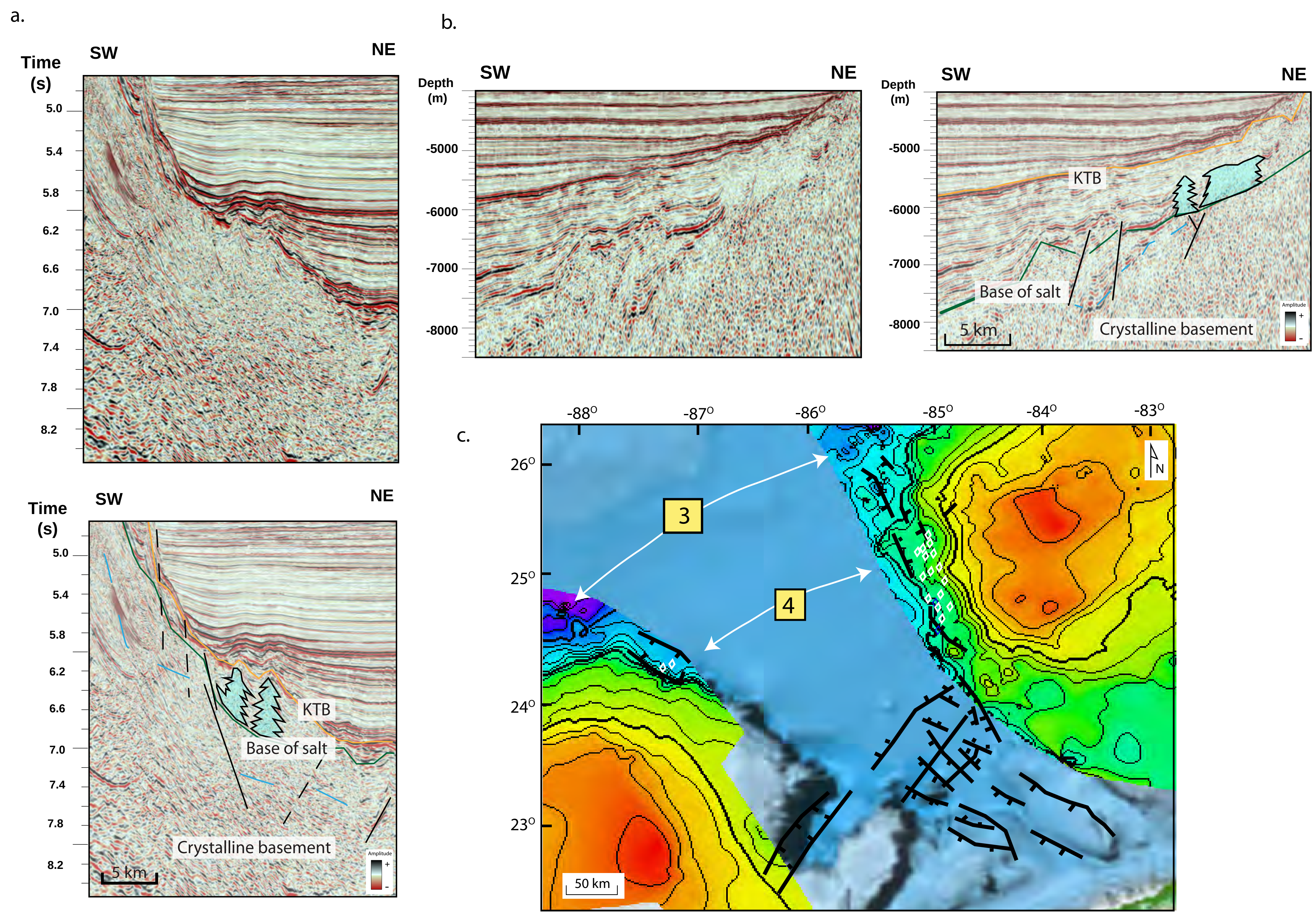

Figure 2.22 (a) Zoom of mounded, carbonate features of the Yucatan margin as shown on Fig. 2.21a. (b) Zoom of mounded, carbonate features of the Florida margin as shown on Fig. 2.21b. These carbonate mounds are inferred to be early Cretaceous in age as they are tilted on rift-related, fault blocks on the Yucatan margin. (c) Zoom of base of salt shown on Fig. 2.7. White rhombuses represent Cretaceous carbonate reefs mapped in the study area.

2.7 Discussion

2.7.1 Defining a broad zone of indentation-related, right-lateral, strike-slip faults in Florida and the eastern GOM

Beneath the west Florida shelf, linear zone of three, symmetrical, 15-25-km-wide, 2-3 km-deep basins align in a right-stepping pattern along a single, linear fault trace (Fig. 2.8). In cross section, all three basins exhibit a downward-tapering, "negative flower structure" typical of pull-apart basins (Figs. 2.9, 2.10). I interpret their origin as right-stepping, pull-apart basins along a northwest-striking, late Paleozoic strike-slip fault related to collision-related indentation of the combined Yucatan-South America continent into the southern margin of the North American continent (Thomas, 1991) (Fig. 2.11).

The 100-km-long, late Paleozoic strike-slip fault zone (labeled number 4 on Fig. 2.14) is mapped using northwest-southeast trending gravity and magnetic highs (A1) that are collinear with two elongate, Paleozoic, pull-apart basins: Destin Dome basin, and Elbow basin (Fig. 2.5). This fault zone is collinear and parallel to fault A1 defined on the regional map in Fig. 2.5b and to the Florida Lineament described by Christenson (1990) (Fig. 2.4a). This fault zone is parallel to Paleozoic strike-slip faults 1-3 as described by Smith (1982), and Smith and Lord (1997) 150 km to the east (Fig. 2.6a, b).

For the Pully Ridge Basin, its synclinal structure coincides with a gravity and magnetic low feature labeled A3 (Fig. 2.13). No basement rock older than Mesozoic has been drilled in South Florida onshore, but the Mesozoic volcanic rocks could correlate with Jurassic diabase penetrated in the Destine Dome Basin. Therefore, I propose that late Palezoic, right-lateral strike-slip fault zones best explain the locations and tectonic origins of the all observed, gravity and magnetic highs (A1, A2, A3, C) (Fig. 2.13).

The three, subparallel, late Paleozoic strike-slip faults (labeled 1, 2, 3 on Fig. 2.14) proposed by Smith and Lord (1997) correlate with northwest-trending, magnetic anomalies in North Florida. Like the three, strike-slip faults described by Smith and Lord (1997) 150 km to the east, I interpret this broad zone of right-lateral, strike-slip faulting as also forming along the eastern, continental edge of the Yucatan-South America, continental "indenter" (Fig. 2.2a) with later, minor, left-lateral, fault reactivation during Mesozoic, Phase 1 rifting (Figs. 2.2b, 2.2c) and 2 (Fig. 2.2e).

2.7.2 Origin of deep, Paleozoic basins on the western shelf of Florida

From the termination of the South Georgia rift zone in southern Alabama, the early Mesozoic basaltic province is offset over 400 km to the northwest into the state of Mississippi (Fig. 2.23c). This offset is roughly collinear with the northwestward, a continuation of the Pickens-Gilbertown-Pollard fault zone in Mississippi (Byerly, 1991) (Fig. 2.23c). Thomas (2004) proposed that the large-scale offset between Appalachian-Ouachita thrust belts and the associated Grenville basement terranes corresponded to the Alabama- Oklahoma transform formed during pre-orogenic rifting in the Laurentian margin (Fig. 2.23a).

Late Triassic-early Jurassic closely followed the northeast-trending, basement trends of late Paleozoic Appalachian-Ouachita orogeny belt (Fig. 2.23b). Late Paleozoic strike-slip faults identified in this study parallel the offset between Appalachian fold belt and Ouachita fold belt, and are equally spaced along the Suwannee-Wiggins suture

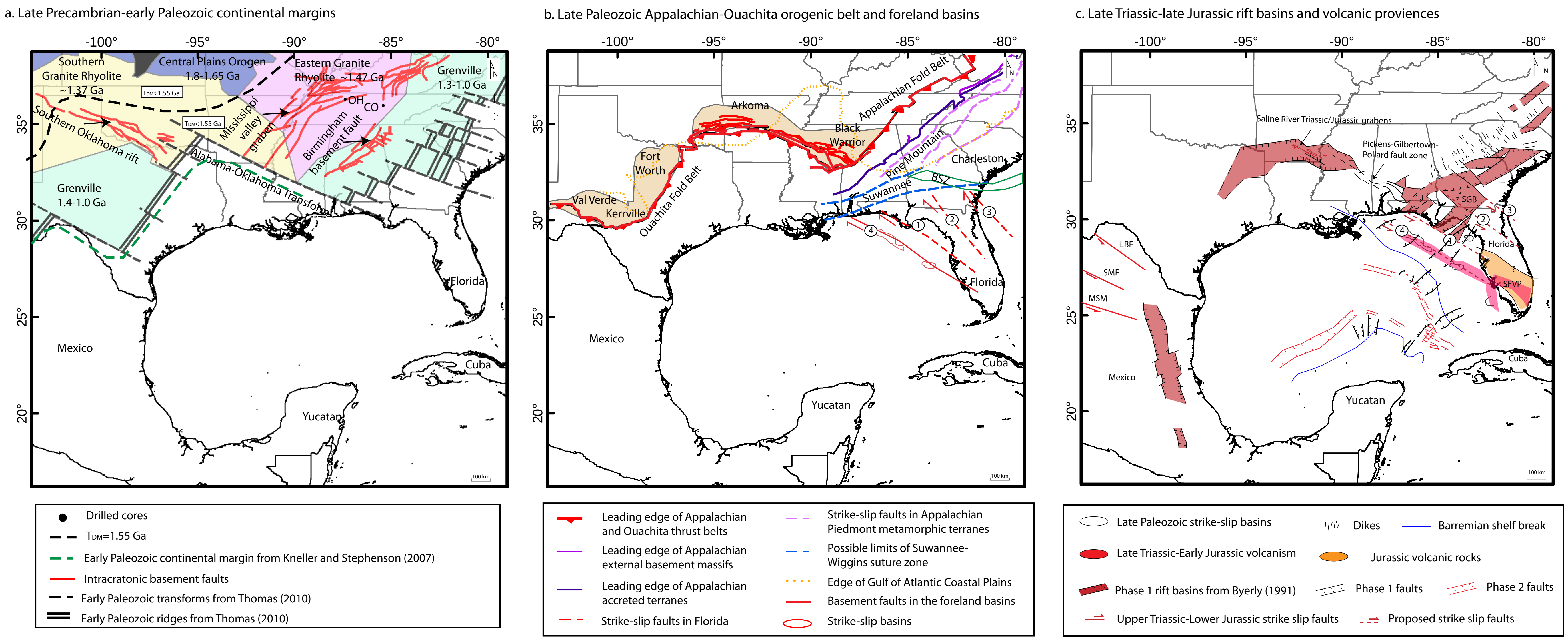

Figure 2.23 Summary of three major stages in the evolution of the eastern GOM. Faults known to be active during each of the three stages are highlighted in red. (a) The larger scale structures of the Gulf of Mexico and Florida margins were originally formed during the opening of the Paleozoic, Iapetus during the late Precambrian and early Cambrian as proposed by Thomas (1991). An 840-km, right-lateral offset of the Grenville Precambrian province and the southern margin of the North America plate formed during Iapetus opening. (b) Northeastward-directed, collision of the South America plate and Yucatan block acted as an indentor that reoccupied the area that these plates had vacated during the earlier, Paleozoic, rifting event. Fault trends in the southern Appalachians or the southeastern USA converge towards the area of the embayment in the area of the northern GOM suggesting that shortening was larger in the indentor area and that the northeast side of the indentor was formed by a broad zone of right-lateral, strike-slip faults (Thomas, 1991). (c) The breakup of Pangea occurred as Yucatan, and South America plates pulled away from the site of the late Paleozoic collision and reactivated the collision-related, right-lateral faults as rifting-related, Phase 1 rift faults (Byerly, 1991). A northwest-southeast right-lateral strike-slip fault with magmatism is interpreted on one of the late Paleozoic strike-slip faults (fault number 4 on Fig. 2.5). Phase 2 faults (red lines) are more concentrated at the edges of oceanic crust and orthogonal to the Phase 1 faults (black lines). Phase 2 marginal faults in the northwestern Yucatan are mapped by Steier (2018).

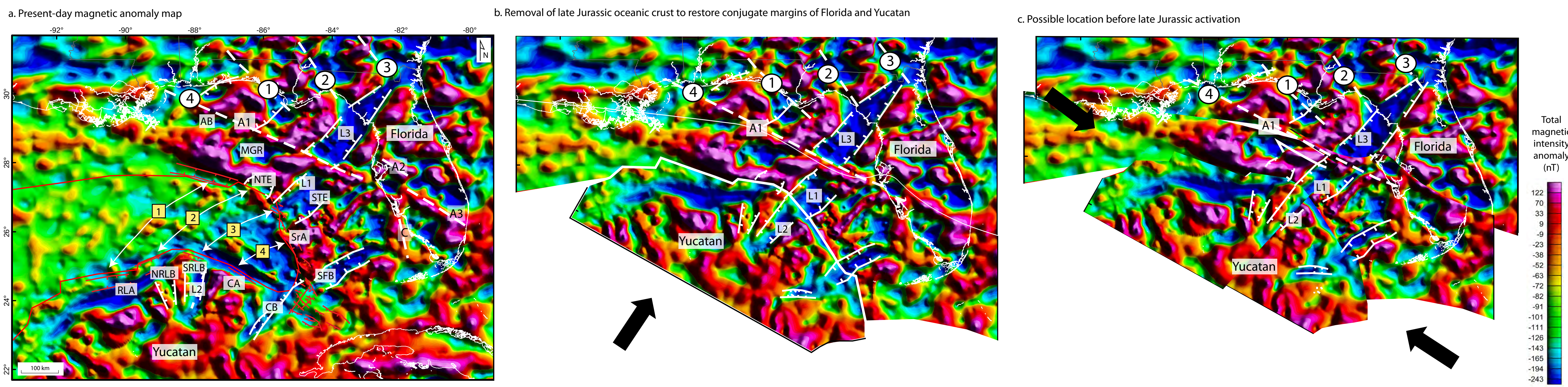

Figure 2.24 (a) Present-day, total magnetic anomaly map of the eastern GOM with an overly of Phase 1 rifts (white lines) and Phase 2 rifts (red lines). (b) Removal of late Jurassic oceanic crust in the eastern GOM using the single, pole of rotation of Nguyen and Mann (2016) to restore the Florida-Yucatan conjugate margins. The Southern Tampa rift (L1) and the South Suwannee rift (L3) on the Florida margin exhibit an apparent, 35-km-long, left-lateral offset which I interpret as forming during the period of Triassic-Jurassic rifting and left-lateral reactivation of older, right-lateral, Paleozoic faults (Fig. 2.23c). (c) The apparent, 35 km of apparent, left-lateral motion is restored prior to the Triassic-Jurassic rift phase.

zone (Fig. 2.23b). I interpret this 35-km-wide zone of Paleozoic, right-lateral, strike-slip faults as indentation, strike-slip faults related to the northwestward motion of the northeastern edge of the South American continental promontory that collided with the North America plate.

2.7.3 Realigning conjugate margins in Florida and Yucatan

Linear magnetic highs and intervening basement lows are orthogonal to the northwest-southeast, opening direction on both margins (Fig. 2.24a). This basement relief that is best expressed on magnetic data (Fig. 2.5a). I interpret the basement relief to have formed during late Triassic- middle Jurassic, Phase 1 rifting (Fig. 2.2c). The Tampa rift and the Rio Lagartos rift on the Florida-Yucatan, conjugate margins can be re-aligned in the northeast-southwest direction after Yucatan is rotated about 40 degrees clockwise (Fig 2.24b). The close, fit of the basement topography of the conjugate margins from magnetic data indicates that the proposed Tampa and Rio Lagartos formed as a single, linear rift during northwest-southeast- directed extension during Phase 1 rifting of Late Triassic-Early Jurassic age.

2.7.4 Reactivation and possible reversal of motion on Paleozoic, strike-slip faults during Phase 1 Triassic rifting

A 100-km-long, late Paleozoic strike-slip fault closely follows a linear, magnetic high and has been described previously as fault A1 defined on the regional map in Fig. 2.5a and as the Florida Lineament by Christenson (1990) (Fig. 2.4b). This fault zone is parallel to Paleozoic strike-slip faults 1-3 (1, 2, and 3) as described by Smith (1982), and Smith and Lord (1997)150 km to the east on the Florida peninsula (Fig. 2.6a, b).

The high intensity of these anomalies could result from the subsurface presence of rift-related, red bed, lithologies that are known to be downfaulted along the edges of the South Georgia rift (Fig. 2.5). The 35-km-long, left-lateral offset between a magnetic low, the Southern Tampa Rift (L1) and South Suwannee rift (L3) indicate a possible, early Jurassic, Phase 1, left-lateral reactivation of this previously, right-lateral, Paleozoic strike-slip fault. On Fig. 2.24c, a restoration of 35 km of left-lateral offset closely realigns the linear, magnetic trends of L1 and L3. I propose a minimum of 35 km of left- lateral motion on this fault during the Phase 1 Triassic rift phase that reactivated the previous, Paleozoic fault zone (Fig. 2.25).

2.7.5 Regional distribution of Middle Jurassic salt distribution in relation to its underlying, crustal types

Based on salt mapping on 50,000 line kilometers of merged, industry, 2D seismic reflection data sets, I divide the thinned, continental crust of Florida that flanks the deepwater area of oceanic crust into three structural provinces: 1) the 220 km-long, northwestern segment of thinned, transitional, continental crust; overlying this area of thinned crust is salt varying from 1 to 4 km high, 60-70 km wide; 2) the central segment of crust along the Florida margin is 260 km long and forms a V-shaped area from 70 km to 25 km wide; salt diapirs are associated with this crustal province; and 3) the southern segment of extended crust along South Florida is 110 km long and 20 km wide and shows no evidence for the presence of salt (Fig. 2.55); isolated Cretaceous carbonate reefs grow on the basement highs during the early Cretaceous, post-rift, passive margin phase (Fig. 2.22).

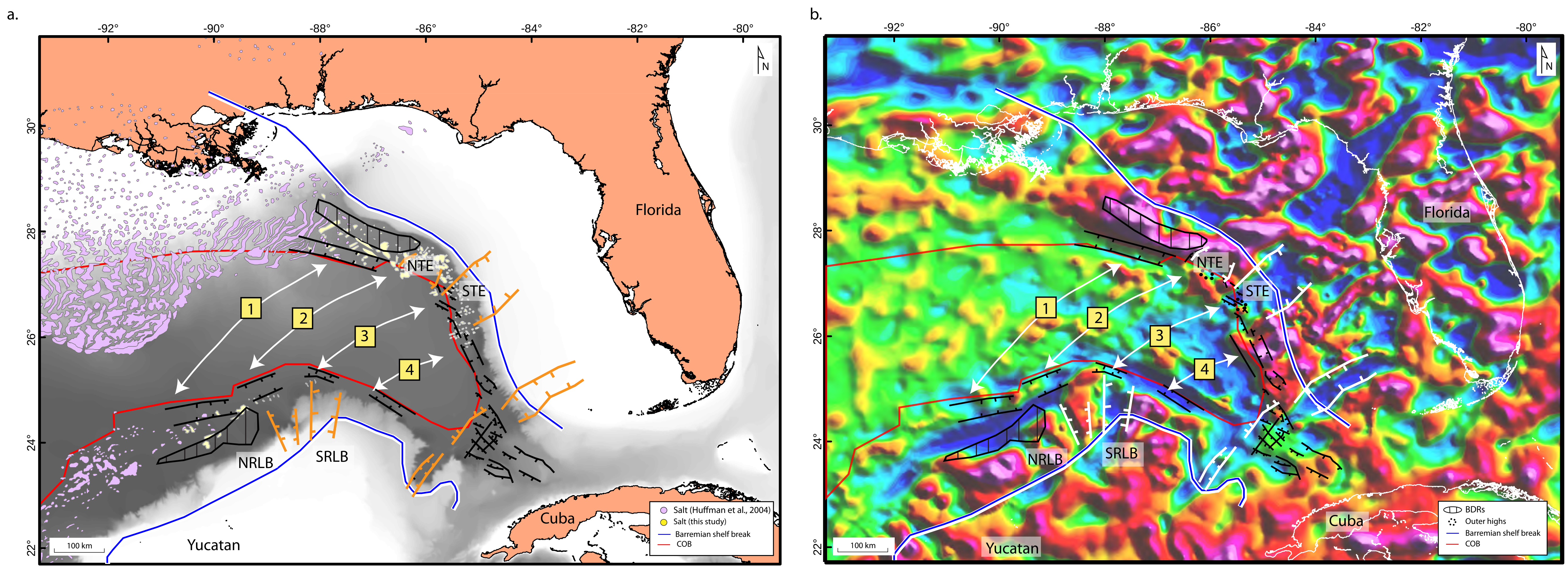

Figure 2.25 (a) Distribution of salt controlled by Phase 1 rifts in orange, and Phase 2 rifts in black. (b) Regional map of extended, continental crust overlying the regional map of the total magnetic anomaly. The outer marginal rifts and BDRs in Yucatan are conjugate to the Florida margin, encircle the area of oceanic crust, and formed during Phase 2 rifting). Phase 1 rift trends (white lines) trend northeast and are at right angles to these younger, Phase 2 rift trends (black lines).

On the conjugate Yucatan margin, the northwestern segment is overlain by 30 km salt rollers, and 30 km-wide, 1600-m high salt diapirs (Steier, 2018). The central segment is dominated by salt rollers and pinches out towards regional highs and southern segment (Steier, 2018) (Fig. 2.25). The asymmetrical salt distribution reflects asymmetric rifting during Phase 1 GOM opening with a wider, rifted margin in the northern GOM and a narrow, less extended margin along the Yucatan peninsula (Marton and Buffler, 1993). The lack of salt in the southern segment of the margin indicates that the southeastern GOM did not pass below sea level during the Phase 1 period of late Triassic-early Jurassic rifting (Marton and Buffler, 1993).

The regional distribution of the thickest, salt bodies in the eastern GOM is likely controlled by the presence of poorly-imaged, rifts that underlie the base of salt especially along the middle segment of the conjugate margin (Fig. 2.25). The thinnest area of salt is associated with elevated shoulders of the symmetrical, marginal rift near the COB. This marginal rift in the most distal zone of stretched, continental crust has identified by various names by previous workers on both the Florida and Yucatan conjugate margins: 1) **Inner ramp** of Hudec et al. (2013) in the northern GOM; 2) **Outer marginal trough** in Florida and the Yucatan margin by Pindell et al. (2014) and Rowan, (2018); 3) **Salt trough** in the northeastern GOM by Imbert (2005); and 4) **Outer marginal rift** on the northern Yucatan margin by Steier (2018). Pindell et al. (2014) proposed that the outer marginal trough is formed by rapid, marginal collapse following the end of late Jurassic, phase 2 rifting, and that this collapse provides the space for thick salt deposition. Rowan (2018), proposed that the symmetrical marginal trough changes from basinward-dipping rifts inboard to deeper depressions that result from slow sedimentation proximal to the shelf. Steier (2018) used subsidence plots to show that post-rift subsidence in the Cretaceous and Cenozoic was gradual and did not reflect any rapid pulses of margin subsidence.

2.7.6 Paleozoic basement faulted during Phase 2 rifting

Deep-penetration seismic reflection data allow identification of rifts and pre-rift basement beneath the base of salt (Fig. 2.25). In the northern segment, BSRs are observed beneath salt diapirs (Eddy et al., 2014). In the middle segment, outer highs located between the extended continental crust and oceanic crust are present on the Florida margin while wavy BDRs are observed on the Yucatan, conjugate margin (Fig. 2.25).

In the northeastern GOM, the extent of BDRs has been mapped and interpreted as magma-rich, seaward-dipping reflectors (SDRs) from their geometry and their associated, magnetic highs (Imbert, 2005; Imbert and Philippe, 2005; Pascoe et al., 2016). A high- velocity lower crust (HVLC) below the possible BDRs also supports the volcanic margin interpretation of the northeastern GOM (Eddy et al., 2014, 2018). In contrast, other workers have interpreted this margin as a magma-poor margin (Pindell et al., 2014; Rowan, 2014, 2018). Rowan (2018) interpreted the area of BDRs as asymmetrical, sedimentary, sag sequences deposited within rifts.

I interpret the BDRs as faulted and gently folded area of stratified, Paleozoic basement based on the good corrletion between BDRs present on both conjugate margins with no obvious faults underlying the BDRs (Figs. 2.14, 2.17, 2.19). The high-velocity lower crust (HVLC) identified from Eddy et al. (2014, 2018) underlies one of the three, late Paleozoic, pull- apart basins (Destine Dome Basin) that were mapped in this study. Therefore, the HVLC underlying the BDRs outboard of the Florida escarpment could also have formed during the late Paleozoic and prior to the Mesozoic opening of the GOM.

2.7.7 Implications of observations in this chapter for a revised plate model for the eastern GOM and the southeastern USA

The basement geometry study in the EGOM provides insights for reconstructions during the late Paleozoic collision and Triassic-Jurassic rifting (Figs. 2.26a-2.26f). Collision-related, indentation, right- lateral strike-slip faults formed around the Alabama promontory when Gondwana (South America and the Yucatan block) collided with the North American plate (Smith and Lord, 1997). A major right-lateral, Paleozoic strike-slip fault is indicated by the alignment of northwest- trending, pull-apart basins with sub-vertical, flower structures in profile (Fig. 2.26a).

The Late Triassic-Early Jurassic, Phase 1 rift phase formed NE-trending, rift basins parallel to the NE structural grain of the Ouachita-Appalachian fold-thrust belt (Fig. 2.26b). The South Georgia Basin is bounded by orthogonal, northwest-striking, late Paleozoic strike-slip faults that were likely reactivated during the later rift phase.

The eastern GOM extended in a northwest direction to form the Tampa rift along the Florida margin and the Rio Largartos Basin in the Yucatan margin (Fig. 2.26d). These Phase 1 rifts are best expressed on regional magnetic maps (Fig. 2.5a), but are too deep to be well imaged on the 2D seismic data that I had available for my study. During the middle Jurassic (163-165 Ma), a 6-km-thick salt unit deposited as a sag basin in the central GOM and thinner, ~0-1.5 km salt unit was deposited in the EGOM and pinched out onto thicker and less extended, continental crust of the Sarasota Arch in the southeast (Marton and Buffler, 1999; Hudec et al., 2013) (Fig. 2.25d).

As Yucatan block rotated counterclockwise away from Florida in the late Jurassic, the eastern GOM began to open during a northeast-southwest, Phase 2 rifting began that was orthogonal to the earlier, Phase 1, late Triassic-early Jurassic rifting (Fig. 2.26e). Rifts formed during Phase 1 rifting were separated as conjugate margins by the formation of oceanic crust in the deep GOM (Fig. 2.26e). The eastern GOM reached its present-day geometry in the Valanginian (Snedden et al., 2014; Marton, 1995; Marton and Buffler, 1999) (Fig. 2.26f).

Figure 2.26 Modified, Late Paleozoic and Mesozoic tectonic stages from the reconstructions shown in Fig. 2.2. (a) **Formation of Ouachita-Appalachian Fold Belt at the end of Late Paleozoic Alleghanian orogeny.** I have added a fourth, Paleozoic strike-slip fault to the previous, three, northwest-striking, right-lateral, strike-slip faults proposed by Smith and Lord (1997). I interpret these faults as forming as right-lateral, indentation faults during the northwestward collision of the South America plate and the Yucatan block during the late Paleozoic collision. (b) **Beginning of Phase 1 continental rifting of Late Triassic to Early Jurassic (190-170 Ma) occurred during the breakup of Pangea.** White lines are Rio Lagartos Basin (RLB), and Tampa Embayment (TE) formed during Late Triassic to Early Jurassic rifting. The previously, right-lateral, Paleozoic strike-slip faults are reactivated as left-lateral strike-slip faults. (c) **Cessation of Phase 1 GOM rifting in early Jurassic** (~170 Ma). (d) **Louann-Campeche salt was deposited in a sag basin overlying Phase 1 rifts.** Pink polygons outline the thick salt distribution restored from present-day geometry. Yellow polygons outline the salt domes formed by thin salt layer. (e) **Late Jurassic, Phase 2 rifting as Yucatan rotated counterclockwise from its conjugate margin in Florida.** Phase 2 rifts trend (red lines) in the EGOM changed from northwest-southeast to northeast-southwest. The rotation of Yucatan block separated the NE-SW trending rift basin (white lines) into two basins (Rio Lagartos Basin in the US, and Tampa Embayment in Mexico) by the formation of oceanic crust shown as the blue polygon. (f) **In the earliest Cretaceous, Oceanic spreading ceases, and the passive margins continue to develop into the late Cretaceous and Cenozoic.**

a. NW-SE collison between Florida and North America in the final stage of Alleghenian orogeny during early Permian (320Ma)

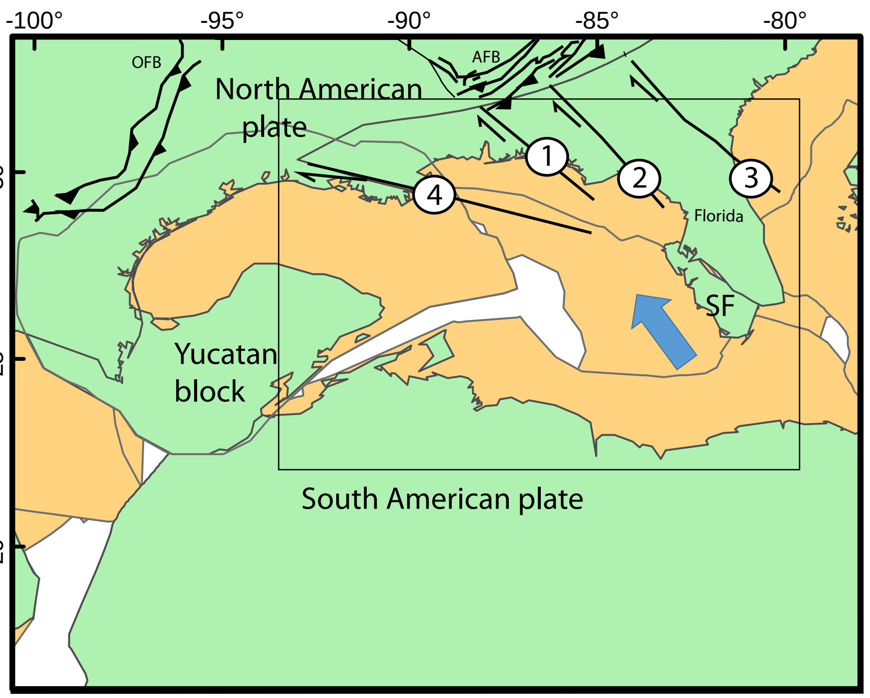

b. Initiation of Phase 1 GOM rifting during late Triassic-early Jurassic (190 Ma)

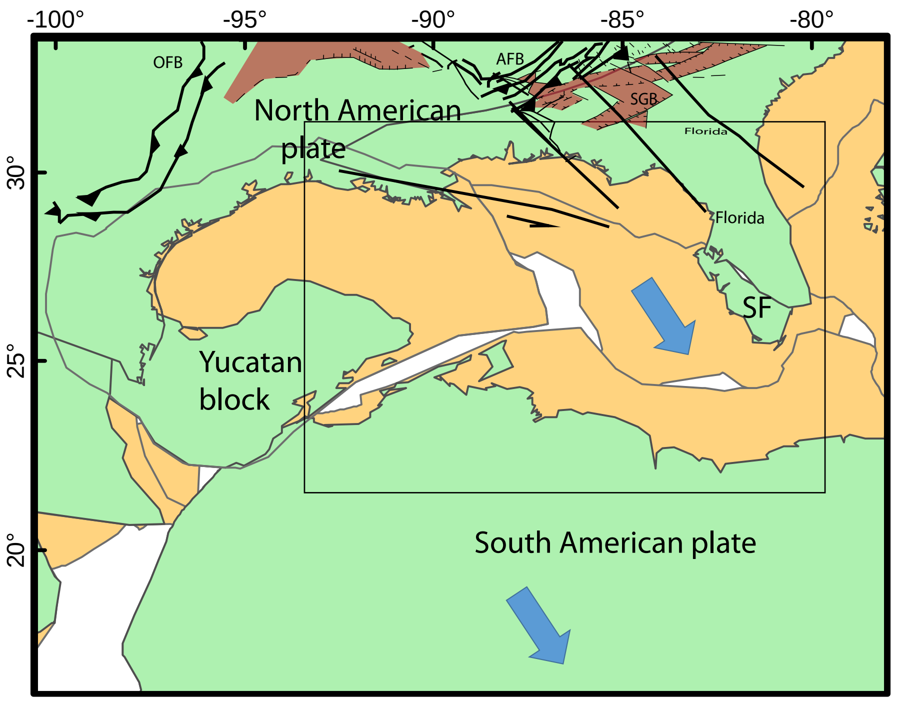

c. Cessation of Phase 1 GOM rifting during late Triassic-early Jurassic (170 Ma)

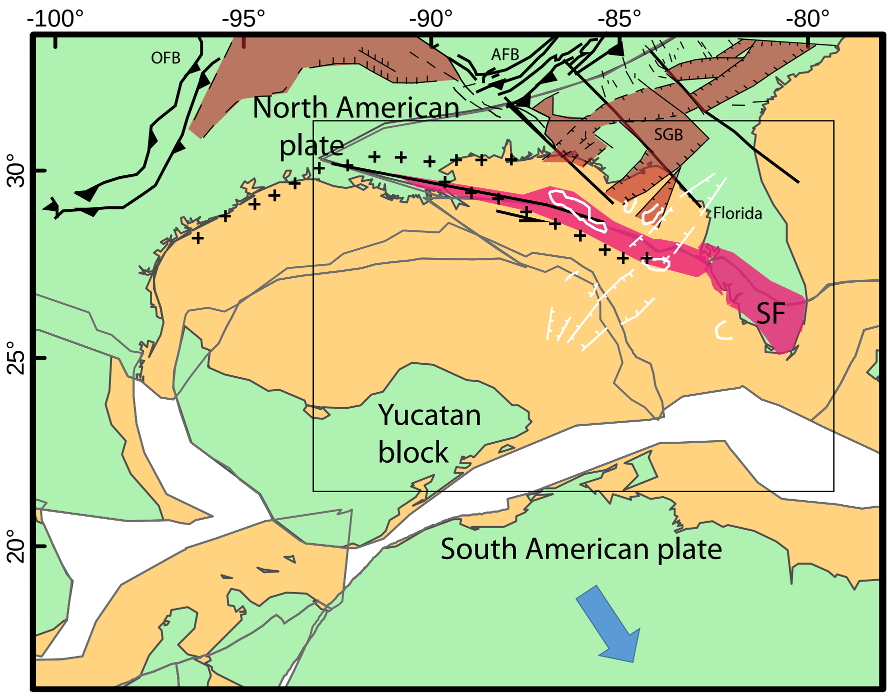

d. Salt deposition in sag basin follwing GOM Phase 1 rifting in Callovian (162 Ma)

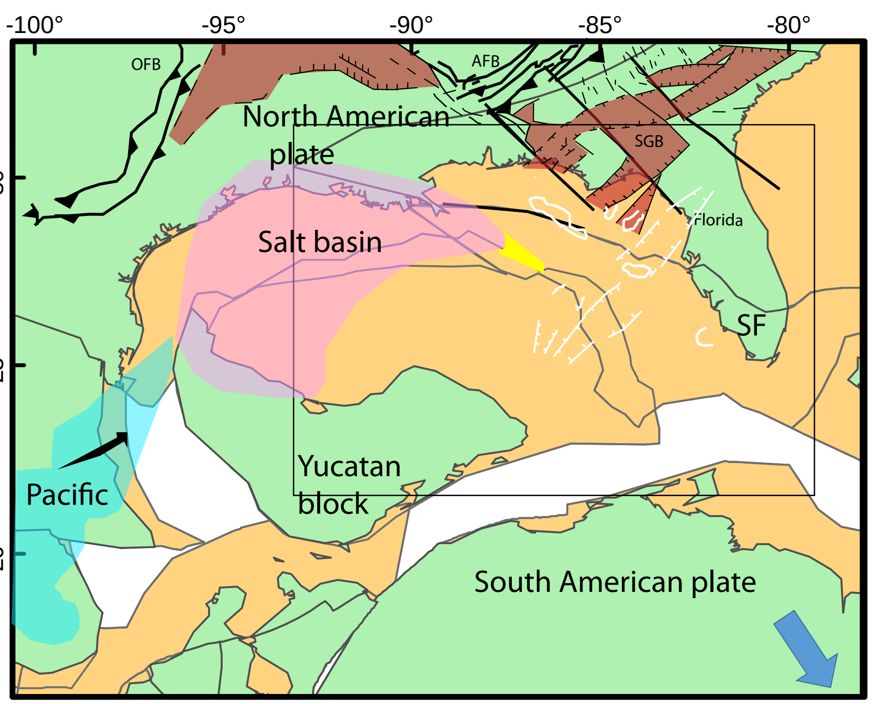

e. Initiation of Phase 2 GOM opening related to counterclockwise rotation of Yucatan block in late Jurassic (152 Ma)

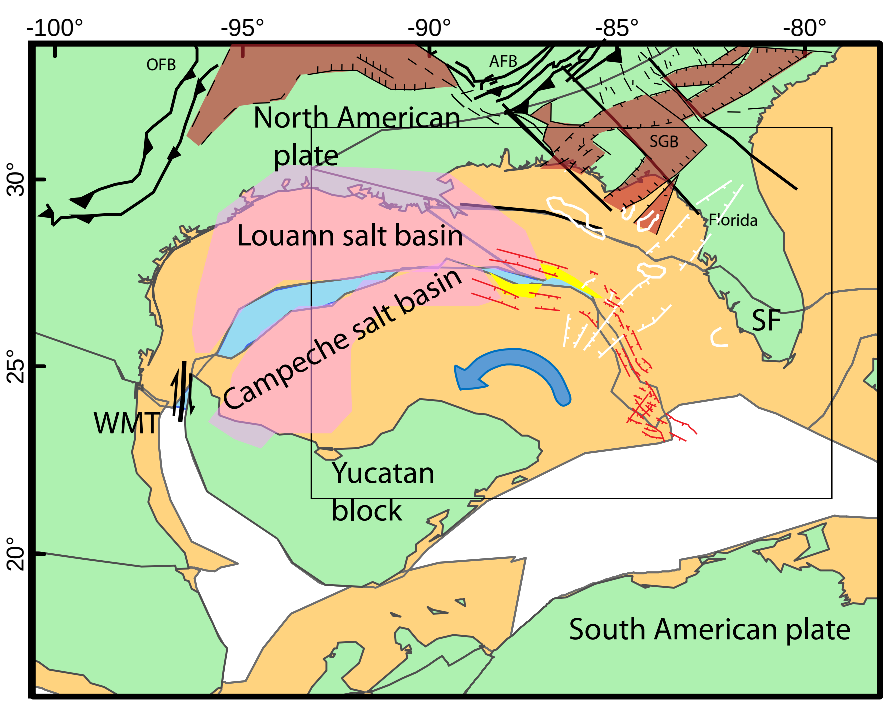

f. Cessation of Phase 2 GOM opening related to counterclockwise rotation of Yucatan block in late Jurassic (152 Ma)

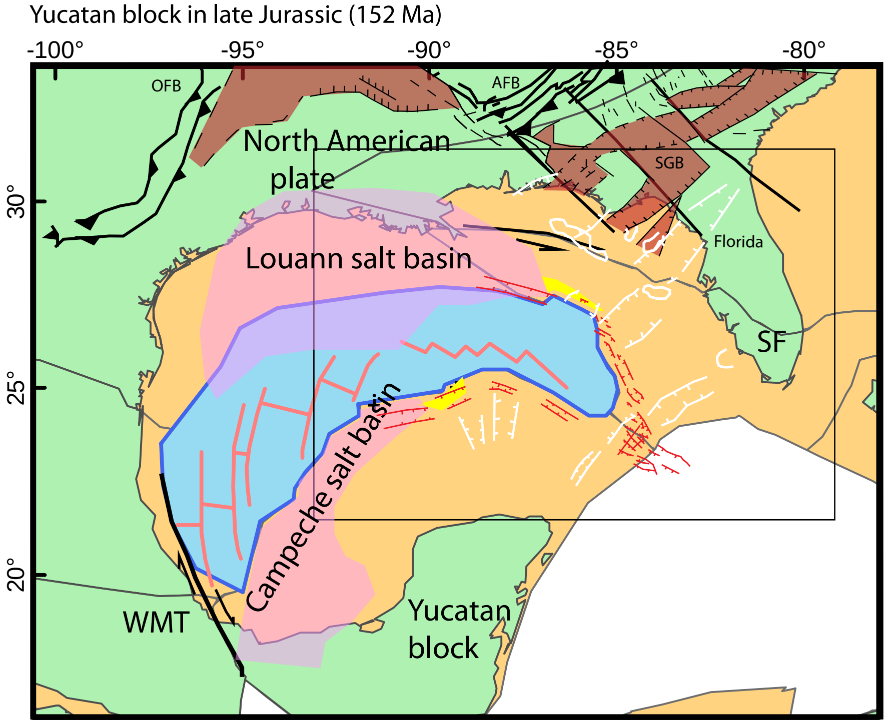

2.8 Conclusions

1. A series of six plate reconstructions (Fig. 2.26) are used to summarize the complex, Triassic to Recent tectonic setting for the GOM geologic evolution which consists of the following phases: 1) pre-Triassic, pre-rift; 2) Triassic-middle Jurassic Phase 1 rifting; 3) Callovian sag basin (Louann-Campeche salt); 4) Oxfordian-Kimmeridgian Phase 2 rifting; 5) Late Jurassic-early Cretaceous Phase 2 oceanic spreading; and 6) early-late Cretaceous passive margin.

2. A fourth 45-km-wide and linear zone of right-lateral, northwest-southeast-striking, strike-slip faulting, and associated pull-apart basins of late Paleozoic age formed during late Paleozoic Alleghanian orogeny. This fault zone is collinear and parallel to fault A1 defined on the regional map in Fig. 2.5a, to the west offset of Florida lineament described by Christenson (1990). This fault zone is parallel to Paleozoic, strike-slip faults 1-3 as described by Smith (1982), and Smith and Lord (1997) 150 km to the east (Figs. 2.6a, 2.6b). These older, Paleozoic faults were reactivated as left-lateral transtensional faults and pull-apart basins during Phase 1, Triassic-Jurassic NW-SE rifting as indicated by an uplifted Moho and thin sub-parallel sediments draping areas of magnetic and basement highs.

3. A zone of NE-SW, Triassic rifting in the offshore South Georgia area that terminates on inferred, late Paleozoic strike-slip faults (Fig. 2.12). Confinement of Triassic rift sediments along northwest faults indicates that earlier, right-lateral faults were reactivated during the rift phase.

4. Basement and magnetic highs and lows on the conjugate margins are inferred from magnetic data to represent Phase 1 rifts and can be precisely re-aligned by

reconstructing the Yucatan-Florida conjugate margin prior to the period of late Jurassic, seafloor spreading; salt distribution maps also show that these NE-SW-trending, basement highs, and lows were formed by the late Jurassic; salt thins towards the southeast onto thicker and less extended continental crust of the Sarasota Arch. The Yucatan margin has a narrower and thinner belt of salt distribution than the conjugate margin of Florida block which is consistent with asymmetrical continental rifting (more rifting to the north) and asymmetrical salt distribution (more salt to the north) (Fig. 2.25).

5. The BDRs near the Middle Ground Arch and Northern Tampa Embayment in the Florida margin, and Rio Lagartos Arch and North Rio Lagrartos Basin are likely not volcanic in origin. Instead, I proposed the BDRs are faulted and gently folded Paleozoic basement similar as the late Paleozoic basins identified from this study (Fig. 2.14).

REFERENCES

Addy, S.K., and R.T. Buffler (1984), Seismic stratigraphy of the shelf and slope, northeastern Gulf of Mexico, American Association of Petroleum Geologists Bulletin, 68(11), 782-1789, doi:10.1306/ad46199e-16f7-11d7-8645000102c1865d.

Ángeles-Aquino, F. J. (2006), Monografía petrolera de la Zona Marina: Asociación Mexicana de Geólogos Petroleros, 71, 77 p.

Ángeles-Aquino, F. J., and A. Cantú-Chapa (2001), Chapter 14: Subsurface Upper Jurassic stratigraphy in the Campeche Shelf, Gulf of Mexico, in The western Gulf of Mexico Basin: Tectonics, sedimentary basins, and petroleum systems, edited by C. Bartolini, R. T. Buffler, and A. Cantú-Chapa, American Association of Petroleum Geologists Memoir, 75, Tulsa, Oklahoma, 343-352.

Applegate, A. V., and J. M. Lloyd (1985), Summary of Florida petroleum production and exploration, onshore and offshore, through 1984, Florida Geological Survey, Information circular, 101, 1-69.

Applin, P.L. (1951), Preliminary report on buried pre-Mesozoic rocks in Florida and adjacent states, US Geological Survey Circular 91, 1–28.

Applin, P.L., and E.R. Applin (1965), The Comanche Series and associated rocks in the subsurface in central and south Florida, USGS Professional Paper 447, 84 p.

Arden Jr., D.D. (1974), A geophysical profile in the Suwannee Basin, northwestern Florida, Georgia Geological Survey Bulletin 87, 111–122.

Ball, M.M., R.G. Martin, R.Q. Foote, and A.V. Applegate (1988), Structure and stratigraphy of the western Florida shelf: part I multichannel reflection seismic data, Preliminary USGS Open-File Report 88-139.

Ball, M.M. (1991), Reassessment of the Bahamas Fracture Zone, American Association of Petroleum Geologists Bulletin 75, 3, 7-10.

Barnett, R.S. (1975), Basement structure of Florida and its tectonic implications, Gulf Coast Association of Geological Societies Transactions, 25, 122-142.

Bartok, P. (1993), Prebreakup geology of the Gulf of Mexico-Caribbean: Its relation to Triassic and Jurassic rift systems of the region, Tectonics, 12(2), 441-459, doi:10.1029/92tc01002.

Beaman, M., J., Koch, S. Paulson, and S Krueger (2017), The Florida-Bahamas Lineament and Gulf of Mexico Opening: To Move or Not to Move?, in AAPG Annual Convention and Exhibition Abstracts.

Bird, D., and K. Burke (2006), Pangea breakup: Mexico, Gulf of Mexico, and Central Atlantic Ocean, in Society of Exploration Geophysicists Technical Program Expanded Abstracts, 1013-1017a.

Boote, S. K., and J. H. Knapp (2016), Offshore extent of Gondwanan Paleozoic strata in the southeastern United States: The Suwannee suture zone revisited, Gondwana Research, 40, 199-210, doi:10.1016/j.gr.2016.08.011.

Boote, S. K., J. H. Knapp and P. A. Mueller (2018), Preserved Neoproterozoic Continental Collision in Southeastern North America: The Brunswick Suture Zone and Osceola Continental Margin Arc, Tectonics, 37(1), 305-321, doi:10.1002/2017tc004732.

Buffler, R. T., and D. S. Sawyer (1985), Distribution of crust and early history, Gulf of Mexico basin, Gulf Coast Association of Geological Societies Transactions, 35, 333-344, doi:10.1306/ad461d59-16f7-11d7-8645000102c1865d.

Byerly, G. R. (1991), Igneous activity, the Gulf of Mexico Basin, in The Geology of North America J, edited by A. Salvador, Geological Society of America, Boulder, Colorado, J, 91-108, doi:10.1130/dnag-gna-j.91.

Chowns, T. M., and C. T. Williams (1983), Pre-Cretaceous rocks beneath the Georgia coastal plain, US Geological Survey Professional Paper, 1313, 1-42, doi:10.1306/c1ea497d-16c9-11d7-8645000102c1865d.

Christenson, G. (1990), The Florida lineament, Gulf Coast Association of Geological Societies Transactions, SL, 99-115.

Christeson, G., H. Van Avendonk, I. Norton, J. Snedden, D. Eddy, G. Karner, and C. Johnson (2014), Deep crustal structure in the eastern Gulf of Mexico, Journal of Geophysics Research: Solid Earth, 119(9), 6782–6801, doi:10.1002/2014JB011045.

Corso, W. (1987), Development of the Early Cretaceous northwest Florida carbonate platform, Ph.D. Dissertation, University of Texas at Austin, Austin, Texas, 136 p.

Dallmeyer, R. D. (1987), 40Ar/39Ar age of detrital muscovite within Lower Ordovician sandstone in the coastal plain basement of Florida: Implications for West

African terrane linkages, Geology, 15(11), 998-1001, doi:10.1130/0091-7613(1987)15<998:aaodmw>2.0.co;2.

Dillon, W.P., and P. Popenoe (1988), The Blake plateau basin and Carolina trough, The Geology of North America, I-2, 291–328, doi:10.1130/dnag-gna-i2.291.

Dobson, L.M., and R. T. Buffler (1991), Basement rocks and structure, northeast Gulf of Mexico, Gulf Coast Association of Geological Societies Transactions, 41, 191-206, doi.org/10.1306/0c9b1ead-1710-11d7-8645000102c1865d.

Dobson, L.M., and R. T. Buffler (1997), Seismic stratigraphy and geological history of Jurassic rocks, northeastern Gulf of Mexico, American Association of Petroleum Geologists Bulletin, 81(1), 100-120, doi:10.1306/522b42a3-1727-11d7-8645000102c1865d.

Domeier, M., and T. H. Torsvik (2014), Plate tectonics in the late Paleozoic, Geoscience Frontiers, 5(3), 303-350, doi:10.1016/j.gsf.2014.01.002.

Dunbar, J. A., and D. S. Sawyer (1987), Implications of continental crust extension for plate reconstruction: An example from the Gulf of Mexico, Tectonics, 6(6), 739-755, doi:10.1029/TC006i006p00739.

Duncan, J.G. (1998), Geological history of an accreted Terrane: Paleozoic stratigraphy of the North Florida Basin, Suwannee Terrane, Ph.D. Dissertation, Florida State University, Tallahassee, Florida, 80 p.

Ebeniro, J. O., W. P. O'Brien, and F. J. Shaub (1986), Crustal structure of the south Florida platform, eastern Gulf of Mexico: An ocean-bottom seismograph refraction study, Marine Geophysical Researches, 8(4), 363-382, doi:10.1007/bf02084019.

Eddy, D., H. V. Avendonk, G. Christeson, I. Norton, G. Karner, C. Johnson, and J. Snedden (2014), Deep crustal structure of the northeastern Gulf of Mexico: Implications for rift evolution and seafloor spreading, Journal of Geophysical Research: Solid Earth, 119(9), 6802–6822, doi:10.1002/2014JB011311.

Eddy, D., H. V. Avendonk, G. Christeson, I. Norton (2018), Structure and origin of the rifted margin of the northern Gulf of Mexico, Geosphere, 14(4), 1-14, doi:10.1130/GES01662.1.

Escalona, A., and W. Yang (2013), Subsidence controls on foreland basin development of northwestern offshore Cuba, southeastern Gulf of Mexico subsidence controls, northwestern Offshore Cuba, American Association of Petroleum Geologists Bulletin, 97(1), 1-25, doi:10.1306/06111212002.

Finn, C., M. Pilkington, A. Cuevas, I. Hernandez, and J. Urrutia (2001), New digital magnetic anomaly database for North America, The Leading Edge, 20(8), 870-872, doi:10.1190/1.1487297.

Jakobsson, M., L. A. Mayer, B. Coakley, J. A. Dowdeswell, S. Forbes, B. Fridman, H. Hodnesdal, R. Noormets, R. Pedersen, M. Rebesco, H.-W. Schenke, Y. Zarayskaya A, D. Accettella, A. Armstrong, R. M. Anderson, P. Bienhoff, A. Camerlenghi, I. Church, M. Edwards, J. V. Gardner, J. K. Hall, B. Hell, O. B. Hestvik, Y. Kristoffersen, C. Marcussen, R. Mohammad, D. Mosher, S. V. Nghiem, M. T. Pedrosa, P. G. Travaglini, and P. Weatherall (2012), The International Bathymetric Chart of the Arctic Ocean (IBCAO) Version 3.0, Geophysical Research Letters, 39(12), 1-6, doi: 10.1029/2012GL052219.

Hatcher, R. D. (2002), Alleghanian (Appalachian) orogeny, a product of zipper tectonics: Rotational transpressive continent-continent collision and closing of ancient oceans along irregular margins, Special Paper-Geological Society of America, 364, 199-208, doi: 10.1130/0-8137-2364-7.199.

Hatcher, R. D. (2010), The Appalachian orogen: A brief summary, From Rodinia to Pangea: The Lithotectonic Record of the Appalachian Region: Geological Society of America Memoir, 206, 1-19, doi:10.1130/0-8137-2364-7.199.

Hudec, M., I. Norton, M. Jackson, and F. Peel (2013), Jurassic evolution of the Gulf of Mexico salt basin, American Association of Petroleum Geologists Bulletin, 97(10), 1683–1710, doi:10.1306/04011312073.

Huffman, A. C., S. A. Kinney, L. R. H. Biewick, H. R. Mitchell, G. L. Gunther (2004), Gulf Coast Geology (GCS) Online—Miocene of Southern Louisiana, USGS Data Series 90-A, 1.0.

Galloway, W. E. (2008), Depositional evolution of the Gulf of Mexico sedimentary basin, in Sedimentary basins of the world 5, edited by A. D. Miall, 505–549, doi:10.1016/s1874-5997(08)00015-4.

Goldhammer, R. K., and C. A. Johnson (2001), Middle Jurassic-Upper Cretaceous paleogeographic evolution and sequence-stratigraphic framework of the northwest Gulf of Mexico rim, in The western Gulf of Mexico Basin: Tectonics, sedimentary basins, and petroleum systems, edited by C. Bartolini, R. T. Buffler, and A. Cantú-Chapa, American Association of Petroleum Geologists Memoir, 75, 45-81, doi: 10.1016/s1874-5997(99)80037-9.

Ibrahim, A., J. Carye, G. Latham, and R. Buffler (1981), Crustal structure in Gulf of Mexico from OBS refraction and multichannel reflection data, American

Association of Petroleum Geologists Bulletin, 65(7), 1207–1229, doi:10.1306/03b5948b-16d1-11d7-8645000102c1865d.

Imbert, P. (2005), The Mesozoic opening of the Gulf of Mexico: Part 1, Evidence for oceanic accretion during and after salt deposition, in Transactions of the 25th Annual GCSSEPM Research Conference: Petroleum Systems of Divergent Continental Margins, edited by P. J. Post et al., SEMP, Tulsa, Okla, 1119–1150, doi:10.5724/gcs.05.25.1119.

Imbert, P., and Y. Philippe (2005), The Mesozoic opening of the Gulf of Mexico: Part 2, integrating seismic and magnetic data into a general opening model, in Transactions of the 25th Annual GCSSEPM Research Conference: Petroleum Systems of Divergent Continental Margins, edited by P. J. Post et al., SEPM, Tulsa, Okla, 1151–1189, doi:10.5724/gcs.05.25.1151.

Klitgord, K.D., P. Popenoe, and H. Schouten (1984), Florida: A Jurassic transform plate boundary, Journal of Geophysical Research: Solid Earth, 89(B9), 7753-7772, doi:10.1029/jb089ib09p07753.

Lord, J. (1986), Seismic stratigraphy and geologic history of the West Florida Basin, eastern Gulf of Mexico, M.A. Thesis, Rice University, Houston, Texas, 207 p.

Lord, J. (1987), Seismic stratigraphic investigation of the West Florida Basin, Gulf Coast Association of Geological Societies Transactions, 37, 123-138, doi:10.1306/703c7f93-1707-11d7-8645000102c1865d.

McBride, J. H. (1991), Constraints on the structure and tectonic development of the early Mesozoic South Georgia rift, southeastern United States: Seismic reflection data processing and interpretation, Tectonics, 10(5), 1065-1083, doi:10.1029/90tc02682.

Marton, G. (1995), Jurassic evolution of the southeastern Gulf of Mexico, Ph.D. Dissertation, University of Texas at Austin, Austin, Texas, 276 p.

Marton, G., and R. Buffler (1993), Application of simple-shear model to the evolution of passive continental margins of the Gulf of Mexico basin, Geology, 21(6), 495-498, doi: 10.1130/0091-7613(1993)021<0495:aossmt>2.3.co;2.

Marton, G., and R. Buffler (1994), Comment on Jurassic reconstruction of the Gulf of Mexico Basin, International Geology Review, 36(6), 545–586, doi:10.1080/00206819409465475.

Marton, G., and R. Buffler (1999), Jurassic-Early Cretaceous tectono-paleogeographic evolution of the southeastern Gulf of Mexico basin, Sedimentary Basins of the World, 4, Elsevier, 63-91, doi:10.1016/s1874-5997(99)80037-9.

Mueller, P.A., A.L. Heatherington, D.A. Foster, W.A. Thomas, and J.L. Wooden (2014), The Suwannee suture: significance for Gondwana-Laurentia terrane transfer and formation of Pangaea, Gondwana Research, 26(1), 365–373, doi:10.1016/j.gr.2013.06.018.

Mueller, P.A., A.L. Heatherington, J.L. Wooden, R.D. Shuster, A.P. Nutman, and I.S. Williams (1994), Precambrian zircons from the Florida basement: a Gondwanan connection, Geology, 22(2), 119–122, doi:10.1130/0091-7613(1994)022<0119:pzftfb>2.3.co;2.

Mueller, P. A., and J. W. Porch (1983), Tectonic implications of Paleozoic and Mesozoic igneous rocks in the subsurface of peninsular Florida, Gulf Coast Association of Geological Societies Transactions, 33, 169-173, doi:10.1306/ad460788-16f7-11d7-8645000102c1865d.

Nance, R. D., G. Gutiérrez-Alonso, J. D. Keppie, U. Linnemann, J. B. Murphy, C. Quesada, R. A. Strachan, and N. H. Woodcock (2012), A brief history of the Rheic Ocean, Geoscience Frontiers, 3(2), 125-135, doi: 10.1016/j.gsf.2011.11.008.

Nguyen, L., and P. Mann (2016), Gravity and magnetic constraints on the Jurassic opening of the oceanic Gulf of Mexico and the location and tectonic history of the Western Main transform fault along the eastern continental margin of Mexico, Interpretation, 4(1), SC23-SC33, doi:10.1190/int-2015-0110.1.

Pascoe, R., P. Nuttall, D. Dunbar, and D. Bird (2016), Constraints on the timing of continental rifting and oceanic spreading for the Mesozoic Gulf of Mexico Basin, in Mesozoic of the Gulf Rim and Beyond: New Progress in Science and Exploration of the Gulf of Mexico Basin, 35th Annual Gulf Coast Section SEPM Foundation Perkins-Rosen Research Conference, GCSSEPM Foundation, Houston, TX, USA, 81–122.

Pindell, J. L. (1985), Alleghenian reconstruction and subsequent evolution of the Gulf of Mexico, Bahamas, and Proto-Caribbean, Tectonics, 4(1), 1-39, doi: 10.1029/tc004i001p00001.

Pindell, J., and L. Kennan (2009), Tectonic evolution of the Gulf of Mexico, Caribbean and northern South America in the mantle reference frame: An update, in The Origin and Evolution of the Caribbean Plate, Geological Society Special Publications, edited by K. H. James, M. A. Lorente, and J. L. Pindell, 328, Geological Society, London, 1–55, doi:10.1144/SP328.1.

Pindell, J., R. Graham, and B. Horn (2014), Rapid, outer marginal collapse at the rift to drift transition of passive margin evolution, with a Gulf of Mexico case study, Basin Research, 26(6), 701–725, doi:10.1111/bre.12059.

Poppe, L.J., and W.P. Dillon (1989), Petrology of some Lower Ordovician-Silurian sedimentary strata from the Southeast Georgia Embayment, U.S. outer continental shelf, Southeastern Geology, 29 (3), 169–194.

Poppe, L.J., P. Popenoe, C.W. Poag, and B.A. Swift (1995), Stratigraphic and paleoenvironmental summary of the south-east Georgia embayment a correlation of exploratory wells, Marine and Petroleum Geology, 12 (6), 677–690, doi:. 10.1016/0264-8172(95)98092-j.

Rowan, M.G. (2018), The South Atlantic and Gulf of Mexico salt basins: Crustal thinning, subsidence and accommodation for salt and presalt strata, Passive Margins, in Tectonics, Sedimentation and Magmatism, edited by K. R. McClay, and J. A. Hammerstein, Geological Society, London, Special Publications, 476, doi:10.1144/SP476.6.

Salvador, A. (1987), Late Triassic-Jurassic paleogeography and origin of Gulf of Mexico Basin, American Association of Petroleum Geologists Bulletin, 71(4), 419-451, doi:10.1306/94886ec5-1704-11d7-8645000102c1865d.

Salvador, A. (1991), Triassic-Jurassic, the Gulf of Mexico Basin, in The Geology of North America J, edited by A. Salvador, Geological Society of America, Boulder, Colorado, 131-180, doi:10.1130/dnag-gna-j.131.

Sandwell, D., R. Müller, W. Smith, E. Garcia, and R. Francis (2014), New global marine gravity model from CryoSat-2 and Jason-1 reveals buried tectonic structure, Science, 346(6205), 65–67, doi:10.1126/science.1258213.

Sanford, J. C., J. W. Snedden, and P. S. Gulick (2016), The Cretaceous-Paleogene boundary deposit in the Gulf of Mexico: Large-scale oceanic basin response to the Chicxulub impact, Journal of Geophysical Research: Solid Earth, 121(3), 1240-1261, doi:10.1002/2015jb012615.

Sawyer, D. S., R. T. Buffler, and R. H. Pilger Jr. (1991), The crust under the Gulf of Mexico Basin, in Gulf of Mexico Basin, Geological Society of America, edited by A. Salvador, The Geology of North America, Boulder, Colorado, 53–72, doi: 10.1130/dnag-gna-j.53.

Schlager, W., R. T. Buffler, D. Angstadt, and R. Phair (1984), Geologic history of the southeastern Gulf of Mexico, Initial reports of the Deep Sea Drilling Project, 77(SEP), 715-738, doi:10.2973/dsdp.proc.77.132.1984.

Seton, M., R. D. Muller, S. Zahirovic, C. Gaina, T. Torsvik, G. Shephard, A. Talsma, M. Gurnis, M. Turner, S. Maus, and M. Chandler (2012), Global continental and ocean basin reconstructions since 200 Ma, Earth-Science Reviews, 113(3-4), 212-270, doi:10.1016/j.earscirev.2012.03.002.

Shaub, E.J. (1983), Origin of the Catoche Tongue, in Seismic Expression of Structural Styles -- A Picture and Work Atlas, edited by A.W. Bally, American Association of Petroleum Geologists Study of Geology, 15 (2), 2.2.3-129, doi:10.4043/5462-ms.

Smith, D. L (1982), Review of the tectonic history of the Florida basement, Tectonophysics, 88(1-2), 1-22, doi: 10.1016/0040-1951(82)90201-3.

Smith, D. L., and K. M. Lord. (1997), Tectonic evolution and geophysics of the Florida basement, in Geology of Florida, edited by A. F. Randazzo, and D. S. Jones, 13–26.

Snedden, J., D. Eddy, G. Christeson, H. Van Avendonk, H. Olson, P. Ganey-Curry, and I. Norton (2013), A new temporal model for eastern Gulf of Mexico Mesozoic deposition, Gulf Coast Association of Geological Societies Transactions, 63, 609-612.

Snedden, J., I. Norton, G. Christeson, and J. Sanford (2014), Interaction of deepwater deposition and a mid-ocean spreading center, eastern Gulf of Mexico Basin, USA, Gulf Coast Association of Geological Societies Transactions, 64, 371-383.

Steier, A. (2018), Jurassic-Cretaceous stratigraphic and structural evolution of the Northern Yucatan margin, Gulf of Mexico Basin, M.S. thesis, University of Houston, Houston, 76 p.

Thomas, W. A. (1991), The Appalachian-Ouachita rifted margin of southeastern North America. Geological Society of America Bulletin, 103(3), 415-431, doi:10.1130/0016-7606(1991)103<0415:taormo>2.3.co;2.

Thomas, W. A. (2004), Genetic relationship of rift-stage crustal structure, terrane accretion, and foreland tectonics along the southern Appalachian-Ouachita orogeny, Journal of Geodynamics, 37(3-5), 549-563, doi:doi.org/10.1016/j.jog.2004.02.020.

Van Houten, F.B. (1977), Triassic-Liassic deposits of Morocco and eastern North America comparison, American Association of Petroleum Geologists Bulletin, 61(1), 79-99, doi:10.1306/c1ea3bfe-16c9-11d7-8645000102c1865d.

Withjack, M. O., R. W. Schlische, and P. E. Olsen (1998), Diachronous rifting, drifting, and inversion on the passive margin of central eastern North America: an analog for other passive margins, American Association of Petroleum Geologists Bulletin, 82(5), 817-835, doi: 10.1306/1d9bc60b-172d-11d7-8645000102c1865d.

CHAPTER III: CRUSTAL STRUCTURE OF AN EXTINCT, LATE JURASSIC SPREADING CENTER AND ITS ADJACENT JURASSIC OCEANIC CRUST IN THE EASTERN GULF MEXICO

3.1 Significance and objectives of this chapter

Satellite-derived gravity data reveals a 490-km-long, short, oceanic spreading ridge-and long fracture zone system in the western GOM, and a 286-km-long, collinear line of extinct and short spreading ridge segments in eastern GOM that are separated by small, but recognizable, left-lateral, northeast-southwest offsets (Sandwell et al., 2014) (Figs 3.1a, 3.1b). In the eastern GOM, localized magnetic anomaly highs are aligned with a northwest-trending, magnetic lineament that is collinear with the spreading ridge segments (Hall and Najmuddin, 1994; Imbert and Philippe, 2005; Nguyen and Mann, 2016).

Using this remotely-imaged, pattern of oceanic, spreading ridge-and-fracture zone geometries and the location of the continent-ocean boundary (COB) interpreted from the tilt derivative of residual Bouguer gravity anomalies, Nguyen and Mann (2016) proposed a 37º counterclockwise rotation of the Yucatan block about a single pole of rotation located near northwestern Cuba (Fig. 3.1a). Prior to the availability of the marine satellite gravity data of Sandwell et al. (2014) - that formed the observational basis for the reconstruction by Nguyen and Mann (2016) several previous studies proposed that the Yucatan block had undergone a Mesozoic counterclockwise rotation through an angle ranging from 40-60° (Hall and Najmuddin, 1994; Marton and Buffler, 1994; Bird et al., 2005; Pindell and Kennan 2009). Such a large block rotation was required to produce the crescent-shaped area of oceanic crust known from previous, refraction studies to underlie most of the deepwater area of the GOM (Ibrahim et al., 1981; Ebeniro et al., 1986) (Figs. 3.1, 3.2). While these previous studies all proposed a single pole of opening in the vicinity of western Cuba, Imbert and Philippe (2005) and Pindell and Kennan (2009) proposed a multi-phase episode of seafloor formation that required multiple poles of rotation.

In this chapter, I improve the mapping of this poorly known, Jurassic, spreading ridge and fracture zone system in the eastern GOM by generating regional maps of the top of Jurassic, oceanic crust and base of oceanic crust (Moho) from the same grid of deep-penetration oil industry data used in chapter 2 of this study (Fig. 2.1). This extinct spreading ridge is also significant in that it is one of the oldest, undeformed, Jurassic spreading ridges on Earth (Müller et al., 2008).

I then integrate my seismic reflection mapping results of the oceanic basement with potential fields and refraction data to improve both the map view orientation and 3-D crustal structure of the extinct, Jurassic oceanic spreading system, which is now deeply buried by 5.5-7-km of early Cretaceous to recent, deep-marine sedimentary rocks (Fig. 3.2). I integrate seismic reflection mapping with 3D gravity inversion to: 1) determine variations in the thickness of the oceanic crust; 2) provide a more precise location of the continent-ocean boundaries on both the Yucatan and Florida conjugate margins; and 3) reveal a more detailed, mapview pattern of the ridge axes and intervening fracture zone offsets that improves upon the previous studies by Sandwell et al. (2014) and Nguyen and Mann (2016) (Fig. 3.1b).

An important conclusion of this study is to further support the extreme asymmetry of oceanic crust of the eastern GOM with 55-60% of the crust located on the northern limb of the extinct, spreading center (Müller et al., 2008). I propose two possible explanations for this asymmetry as a follow up to the global study of spreading ridge asymmetry by Müller et al. (2008).

The availability of the Spectrum datasets from both the Florida and Yucatan margins when combined with regional gravity and magnetic maps allow for a detailed comparison of the early Jurassic fit between the two, continental margins comparing with various single vs. multiple poles of opening and kinematic, opening models (Imbert and Philippe, 2005; Pindell et al., 2014; Pascoe et al. 2016; Nguyen and Mann, 2016).

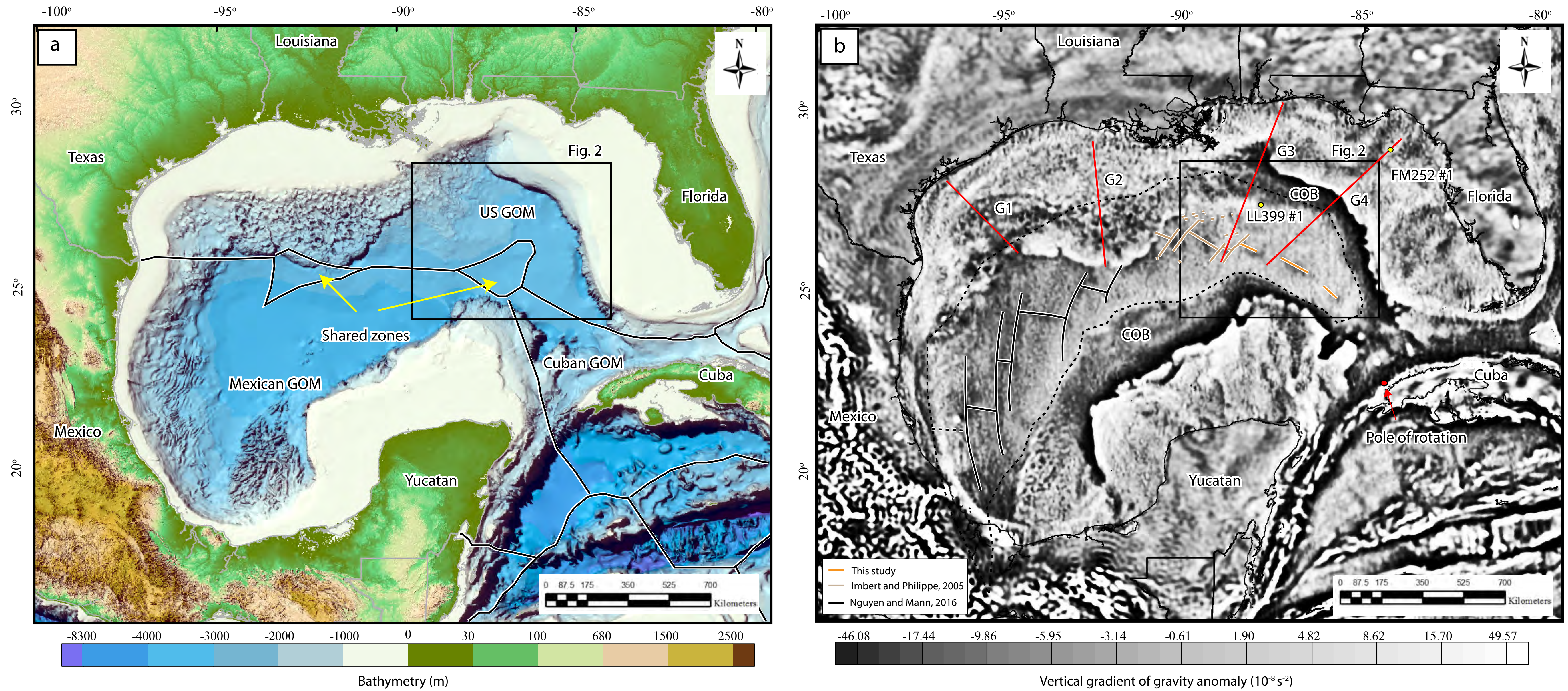

Figure 3.1 (a) Geographic setting of the Gulf of Mexico basin (GOM) with an overlay of the GEBCO bathymetric compilation map (Jakobsson et al., 2012). Box in a and b shows the location of study area discussed in this chapter. (b) Vertical gradient of free-air gravity (VGG) anomalies of the GOM showing a slightly darker, linear expression of the extinct, deeply buried, Jurassic ridge-and-fracture zone system (Sandwell et al., 2014). Solid white and yellow lines represent ridge segments and fracture zones, respectively; less pronounced ridges and fracture zones are shown as dotted lines. The solid, light-blue, pink, and dashed dark blue lines represent ridges, fracture zones, and pseudo-faults, respectively, as interpreted by Imbert and Philippe (2005). Red lines show the locations of refraction profiles from the Gulf of Mexico Opening (GUMBO) project (Christeson et al., 2014; Eddy et al., 2014). The red dot indicates the location of the pole of rotation in northwestern Cuba as determined by using the curvilinear pattern of fracture zones from Nguyen and Mann (2016).

3.2 Geologic setting and opening phases of the Gulf of Mexico

3.2.1 Opening phases of the GOM

As discussed at length in Chapter 2 of this dissertation, most workers now accept a GOM opening history that spans the period from late Triassic through earliest Cretaceous and is divided into two phases of rifting and basin opening. Phase 1, Late Triassic- Middle Jurassic, continental rifting occurs as the Yucatan block-Florida block rifts apart in a northwest-southeast direction during the initial breakup of the Pangean supercontinent (Marton and Buffler, 1994; Pindell and Kennan, 2009; Hudec et al., 2013; Eddy et al., 2014; Nguyen and Mann, 2016) (Fig. 3.2). Phase 1 rifting is characterized by rifts trending to the NE and are distinctive from Phase 2 rifts whose trends are to the southeast and orthogonal in the southeast GOM (Escalona and Yang, 2013).

As Phase 1 rifting ended in the early Jurassic, seawater filled a large, unfaulted, sag basin that overlays a broad zone of rifted, continental crust (Fig. 3.2) (Eddy et al., 2016, 2018). Evaporation of this seawater in an arid setting led to the accumulation of ~5 km of the Callovian, Louann-Campeche salt deposit.

Phase 2 rifting began in the Oxfordian of the late Jurassic as the Yucatan block rotated counterclockwise away from North America in a more southwestward direction. Initial rifting of phase 2 led to the formation of the spreading ridge and the subsequent formation of a 100,000 km^2 area of oceanic crust in the EGOM (Figs. 3.1, 3.2).

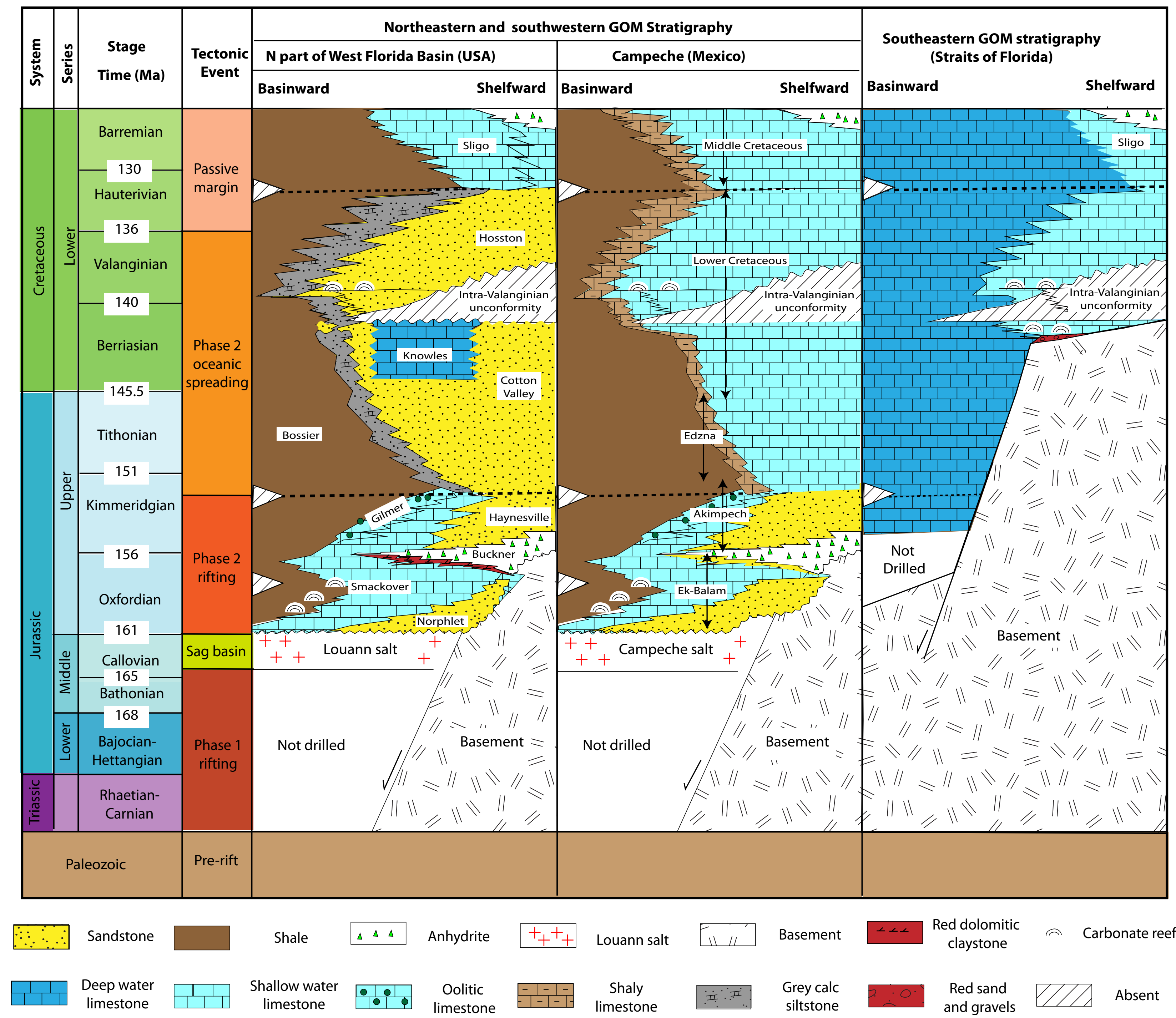

Figure 3.2 Stratigraphy of the northeastern and southwestern EGOM correlated with six, tectonic phases for GOM basin history including 1) **pre-Triassic, pre-rift**; 2) **Triassic-middle Jurassic Phase 1 rifting**; 3) **Callovian sag basin (Louann-Campeche salt)**; 4) **Oxfordian-Kimmeridgian Phase 2 rifting**; 5) **Late Jurassic-early Cretaceous Phase 2 oceanic spreading**; and 6) **early-late Cretaceous passive margin**. The chronostratigraphic chart for northern part of the West Florida Basin is modified from Dobson and Buffler (1997), Goldhammer and Johnson (2001), and Snedden et al. (2014). The chronostratigraphic chart for the Campeche area of Mexico in the southwestern GOM is modified from Angeles-Aquino, and Cantú-Chapa (2001). The southeastern GOM stratigraphy is modified from Marton and Buffler (1999).

Late Jurassic, seafloor spreading separated the thick salt deposits into two regions separated by oceanic crust: the Louann salt in the US sector of the GOM and the Campeche salt in the Mexico sector (Fig. 3.1b, 3.2). The cessation of seafloor spreading is indicated by synrift, sedimentary filling of the southeastern GOM by the earliest Cretaceous (late Berriasian) (Marton and Buffler, 1994) (Fig. 3.2).

3.2.2 Age of seafloor spreading following Phase 2 rifting

The initiation and cessation of seafloor accretion in the GOM was related to the rotation of the Yucatan block but is not well dated because seafloor spreading anomalies have not been recognized - likely as the result of the formation of the oceanic spreading during the "Jurassic Magnetic Quiet Zone" (Bird et al., 2005; Christeson et al., 2014). Proposed age correlations of observed anomalies in the eastern GOM range from Tithonian (151 Ma) (Hall and Najmuddin, 1994) to Berriasian (142 Ma) (Eskamani, 2014).

Four long-offset, wide-angle seismic reflection and refraction profiles were acquired in the GUMBO project by Christeson et al. (2014), and Eddy et al. (2014, 2018) to understand the crustal structure and opening history of the GOM (Fig. 3.1). Two of these GUMBO profiles in the EGOM traverse the late Jurassic spreading center and allow an estimate for the timing of seafloor accretion based on the stratigraphic ages of the overlying basal Jurassic sedimentary horizons (Snedden et al., 2013, 2014) (Fig. 3.2). Based on the age of horizons correlated from exploration well LL #399 in the northeastern GOM, Snedden et al. (2013), and Eddy et al. (2014) estimated seafloor spreading rate along GUMBO 3 to be ~2.4 cm/yr. Christeson et al. (2014), and Snedden et al. (2014) calculated that seafloor spreading rate along GUMBO 4 decreased to ~2.2 cm/yr because GUMBO 4 is located to the east of GUMBO lines 1-3 and is closer to the proposed pole of GOM opening located near western Cuba (Fig. 3.1).

3.2.3 Geometry of ridges and fracture zones in the GOM

In the EGOM, a line of isolated and extinct spreading ridge segments is observed but these ridges are separated by small but recognizable transforms (Sandwell et al., 2014; Nguyen and Mann, 2016) (Fig. 3.1b). Several industry, deep-penetration reflection surveys are extended to the deepwater EGOM which partially imaged the spreading center using 2-D and 3-D seismic reflection data acquired in the deepwater area (Stephens, 2001; Imbert and Philippe, 2005; Snedden et al., 2013, 2014; Kegel et al., 2017). Buried “abyssal hill topography” and “mini-basins” associated with the rough, upper surface of the Jurassic oceanic crust in the northwestern GOM were described by Stephens (2001) using interpretations from seismic reflection 2D industry and seismic surveys in the northwestern part of the EGOM (Fig. 3.1a). These buried abyssal hills were interpreted by Stephens (2001) as large seamounts formed within transform fault valleys which in turn led this author to propose a map pattern of Jurassic, northeast-trending, spreading ridges connected by northwest-trending transform faults.

Using the same 2D seismic dataset, Imbert and Philippe (2005) used a different grid of 2D seismic reflection data to propose an orthogonal spreading direction from that proposed by Stephens (2001) with northwest-oriented, spreading ridges connected by northeast-trending transforms (Fig. 3.1a). Several previous studies have noted close alignments between seamounts and magnetic anomaly highs (Hall and Najmuddin, 1994; Imbert and Philippe, 2005; Nguyen and Mann, 2016; Chapter 2, this dissertation).

Snedden et al. (2014) interpreted industry, 2D seismic data over the extinct spreading ridge and a larger area of the eastern GOM and mapped discontinuous axial valleys within the basement that they interpreted to be discrete sections of a northwestern-trending Jurassic spreading center. Snedden et al. (2014) proposed that basement highs along the spreading axis correspond to axial spreading ridge seamounts that probably were related to local variations in magma supply as commonly observed along active, slow-spreading ridges worldwide (Fig. 3.3). More recently, Deighton et al. (2017) mapped a long fracture zone in the western GOM using 3D seismic data. The curved, fracture zone is characterized by an 8-10 km wide troughs filled with 200-400 ms (300-600 m) of sediments.

3.3 Data and Methods

3.3.1 Gravity and magnetic data

The US maritime sector of my study area in the eastern GOM is covered by 2D reflection data acquired by industry seismic vessel GeoArctic in 2007 and covers an area of 120,000 km^2 (Chapter 2, this dissertation) (Fig. 3.3a). The shot point interval and time record length for this seismic grid are 37.5 m and 13-14 seconds, respectively. The seismic data were processed using Kirchoff pre-stack depth migration (PSDM) commonly used for moderately-complex, geologic settings. The Mexico maritime sector of the study area is covered by 2-D reflection data acquired by Spectrum Geo in

2015. These reflection data were made available to me only as two-way travel time sections (Fig. 3.3a).

Gridded, ship-track bathymetry was used in the US sector of the EGOM, and TerrainBase bathymetry (Row et al., 1995) was used for the Mexico sector (Fig. 3.3a). I used the ship-track gravity for the US and Mexico parts of the EGOM along with satellite-derived, free-air gravity (Sandwell et al., 2014) (Fig. 3.3b). I calculated Bouguer anomalies by assuming the density beneath the water bottom is 2.0 g/cm^3, then added 0.97 g/cm^3 density for the water layer (Fig. 3.4a). I calculated residual Bouguer gravity anomalies by subtracting a 3-km-upward continuation of Bouguer anomalies from the original Bouguer gravity grid (Fig. 3.4b) because residual gravity anomalies enhance short wavelengths at the expense of long wavelengths and allow subtle anomalies to be more confidently interpreted.

I used the ship-track magnetic grids for the US and Mexico sectors of the EGOM and satellite-derived Decade of North American Geology magnetic (Finn et al., 2001) grids for the Cuban EGOM (Fig. 3.5a). Following Besse and Courtillot (2002) true polar wander path for the Jurassic age EGOM (140 Ma), I calculated reduced-to-pole magnetic anomalies using paleo-magnetic field inclination and declination values of 48.2° and - 24.5°, respectively (Fig. 3.5b).

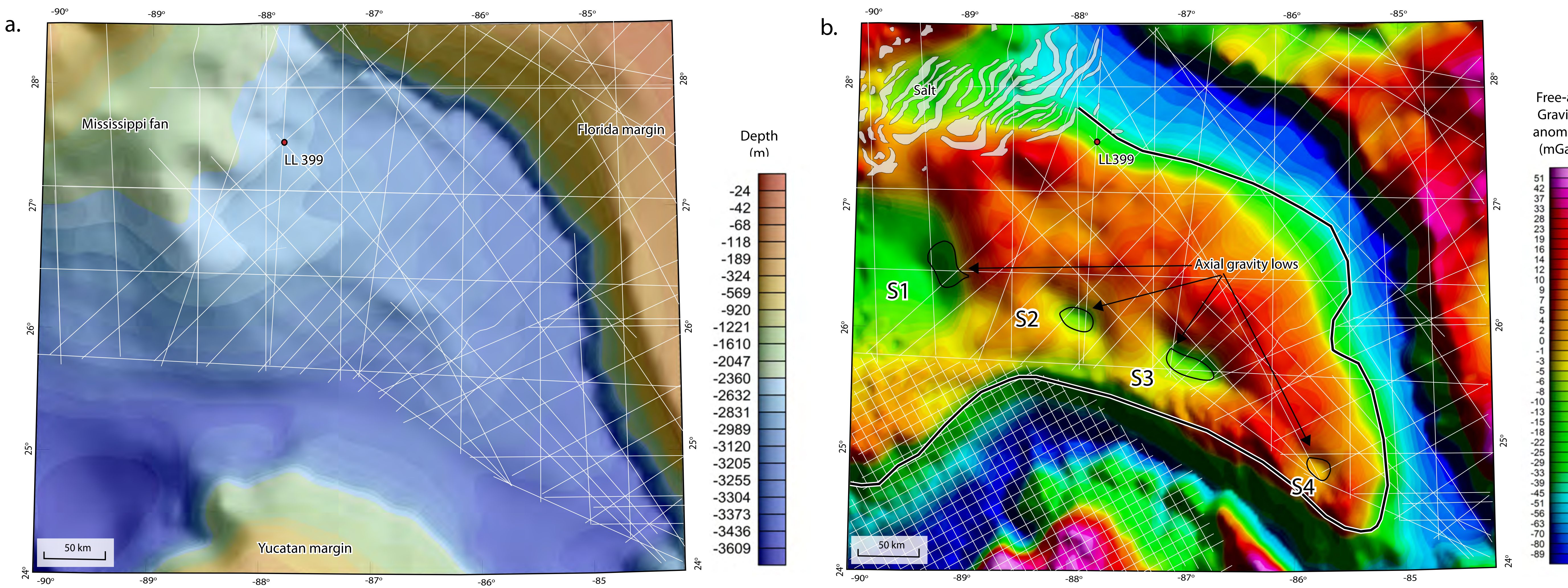

Figure 3.3 (a) Bathymetric map with the Spectrum Big Wave, the 2D seismic survey used in this study shown as white lines. All the lines made available for my study were depth-converted. (b) Ship-based, free-air gravity map of the same area shown in Fig. 3.3a. The pink line is the continent-ocean boundary (COB) identified from my gravity inversion used to map crustal thickness. The white lines are the ship tracks for the gravity and magnetic data. Sub-circular, gravity lows along four, extinct, Jurassic spreading ridge segments are labeled S1, S2, S3, and S4.

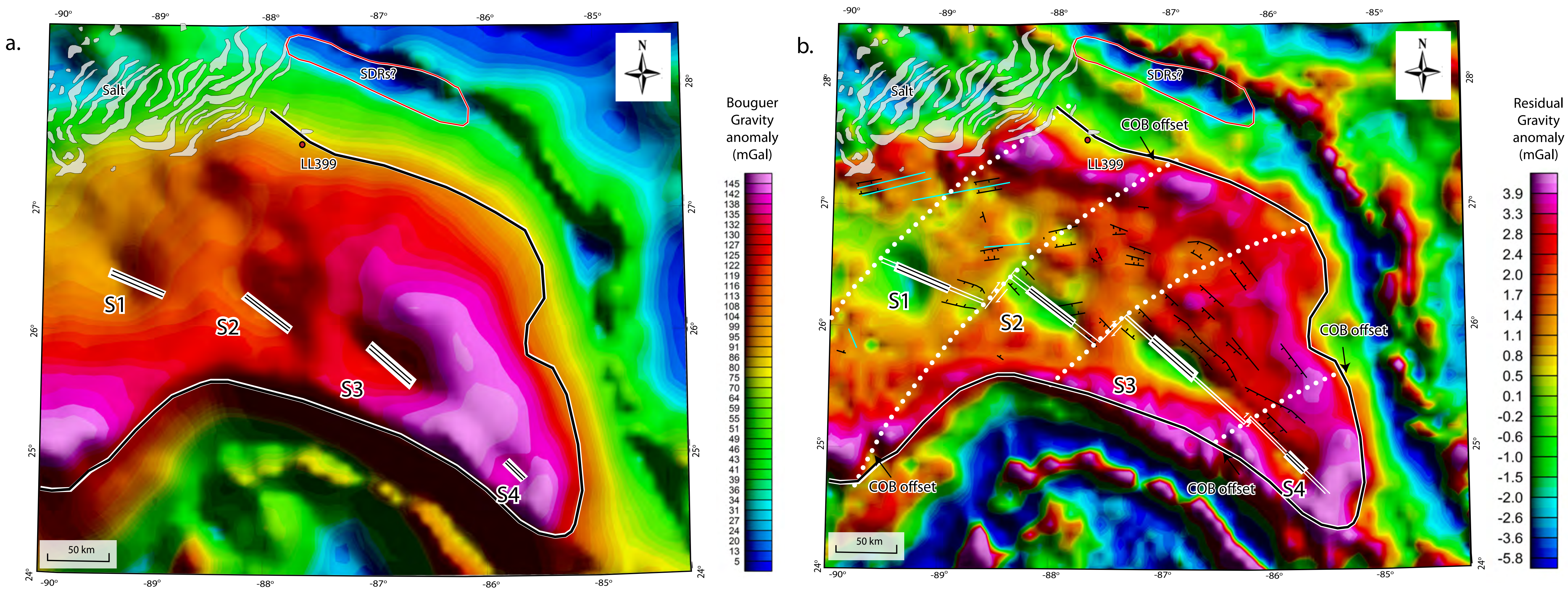

Figure 3.4 (a) Residual Bouguer gravity anomalies of the study area. White circles are locations of breaks in residual Bouguer gravity anomaly trends along my proposed COB and indicate continentward projections and marginal offsets along fracture zones. (b) 3-km upward continuation of residual Bouguer gravity anomalies. Short, white bars indicate spreading-ridge segments. Normal faults mapped in the 2D seismic grid and areas of major salt bodies are indicated.

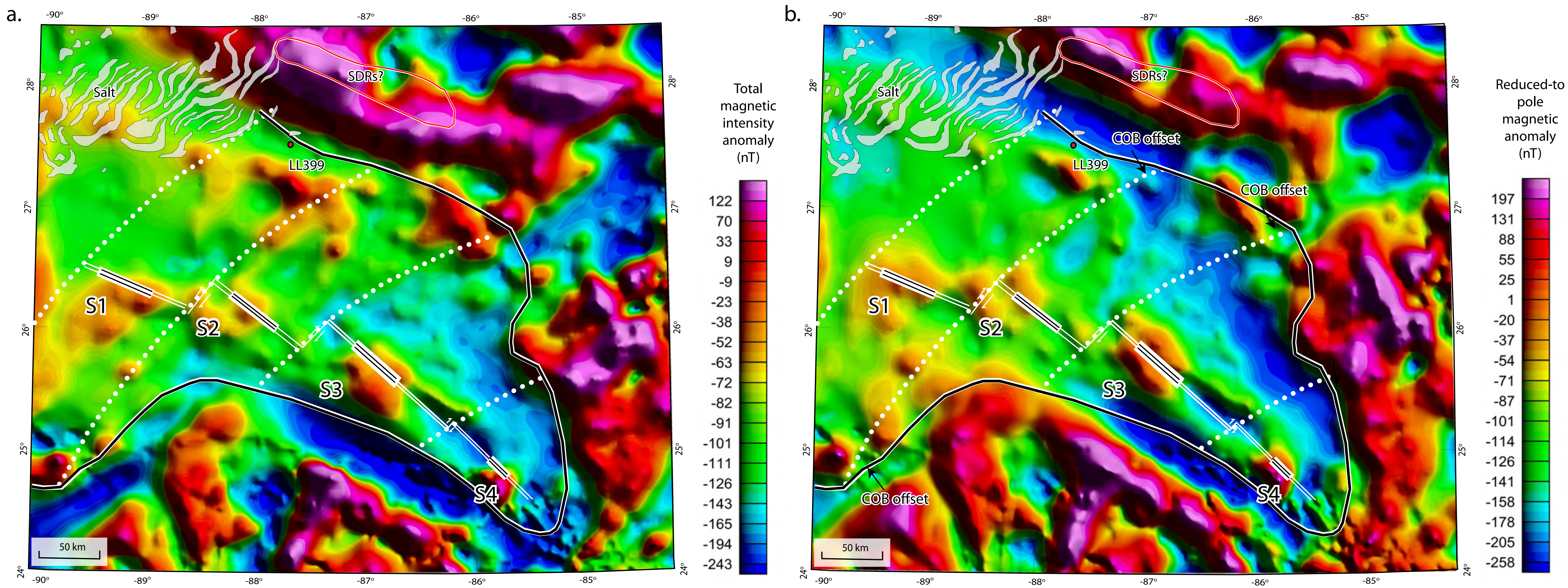

Figure 3.5 (a) Total magnetic anomalies of the study area. Thinner, white bars are the inferred prolongations of the known spreading ridge (short, white bars) based on basement mapping and gravity data shown in Figs. 3.4 a, 3.4b. White, dotted lines are small circle flowlines calculated from GOM opening pole located by Nguyen and Mann (2016) near northwestern Cuba (22.41°, -84.33°). (b) Reduced-to-pole magnetic anomalies for the study area.

3.3.2 Seismic reflection and well data

Two interpreted horizons were critical as constraints for the gravity-modeling study: 1) the top basement and base of the crystalline crust (Moho). I integrated seismic reflection data with seismic refraction and gravity data by comparing layer thicknesses and velocities from the refraction data with my reflection interpretation (Ibrahim et al., 1981; Christeson et al., 2014; Eddy et al., 2014). I then imported these horizons into a regional 3-D gravity model to perform a structural inversion of the Moho. Finally, I compared these results with the interpreted Moho from reflection data and Moho depths reported from the refraction studies.

Jurassic to Tertiary horizons were correlated from well LL399 #1 and following chronostratigraphically-defined horizons from Galloway et al. (2000), and Snedden et al. (2013). These horizons that are tied from the seismic grid to the LL399#1 well include: the Paleocene-Eocene boundary (PEB) (56Ma); the Cretaceous-Tertiary boundary (KTB) (66 Ma); the top of Sligo-Hosston (SH) (123.9 Ma); and the top of Cotton Valley-Knowles (CVK) (138.2 Ma) (Fig. 3.6). I converted the major time horizons in the Yucatan into depth by a water velocity of 1500 m/s, Tertiary sediment velocity of 2700 m/s, Sligo-Hosston sediment with a velocity of 3000 m/s, and underlying sediment with a velocity of 3400 m/s.

a.

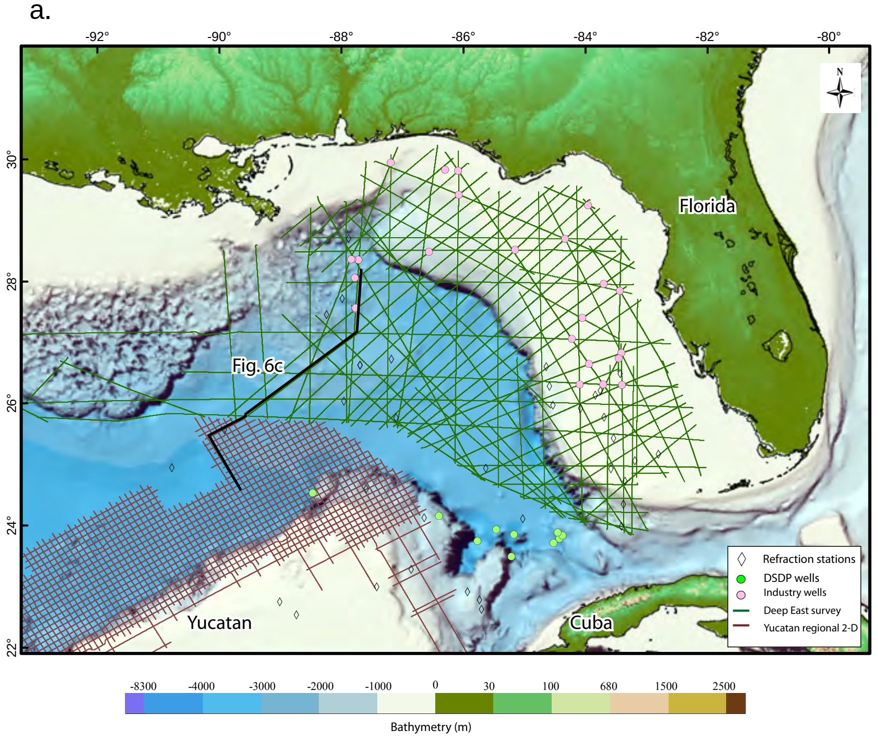

b.

Top Chronostratigraphic Surface	Top Seismic Unit	Supersequence
Ma4_700mfs (66.0 Ma)	KTB	Navarro-Taylor
Ap3_ssb (122.9 Ma)	SH	Sligo-Hosston
Va2_ssb (138.2 Ma)	CVK	Cotton Valley-Knowles
Be5_sb (141.9 Ma)	CVB	Cotton Valley-Bossier
Kim4_mfs (152.4 Ma)	HVB	Haynesville-Buckner

c.

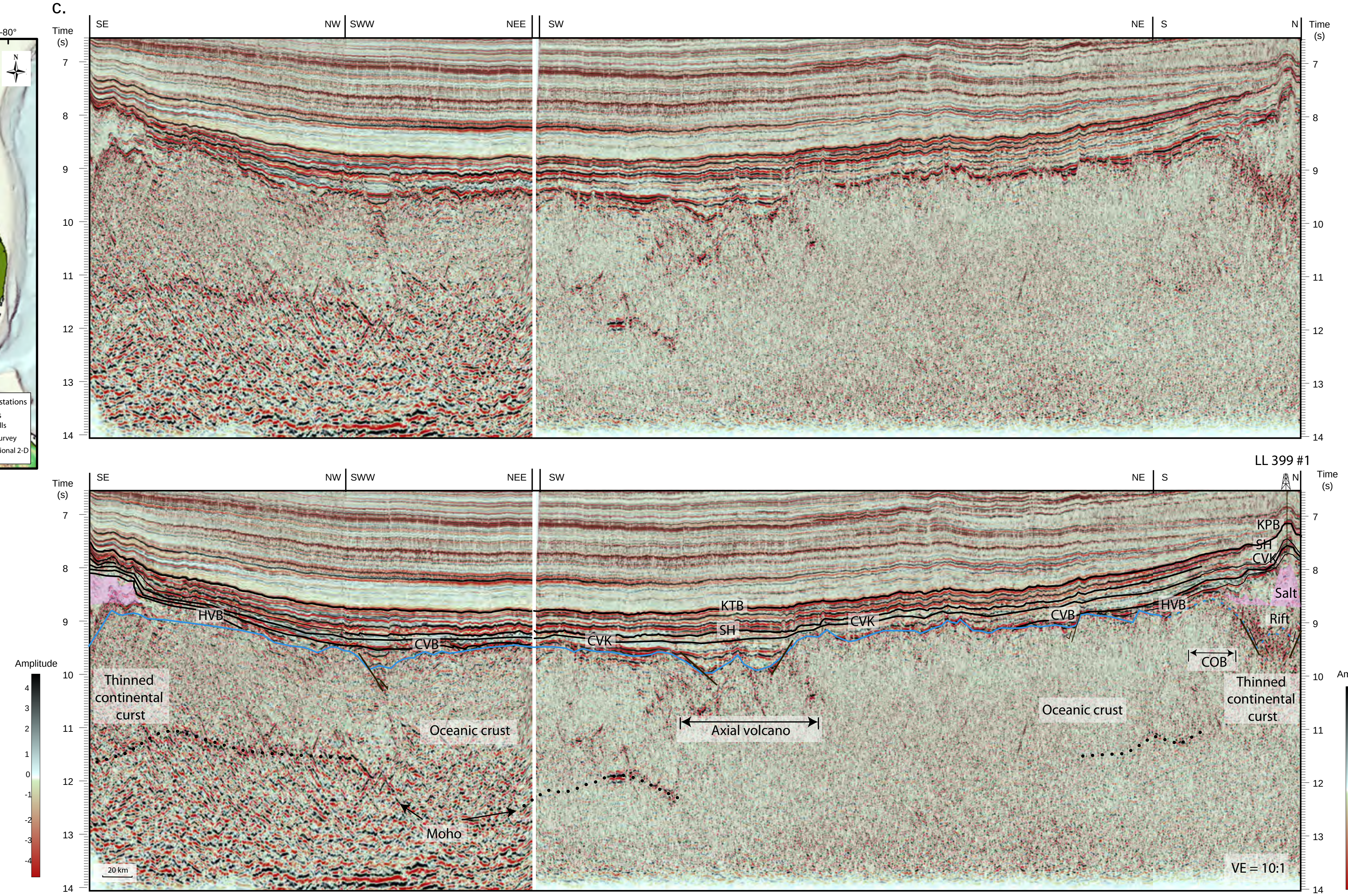

Figure 3.6 (a) Location map of seismic grids used to correlate between the Florida and Yucatan conjugate margins. Heavy line indicates the location of the seismic line shown in Fig. 3.6c. (b) Chronostratigraphy of seismic reflection units modified from Snedden et al. (2014). (c) 69-km-long, time-migrated seismic section showing seismic correlations between the Florida and Yucatan conjugate margins at 10 to 1 vertical exaggeration (located on the map in Fig. 3.6a). The blue horizon represents the interpreted top of Jurassic, oceanic basement. Labeled horizons include the following stratigraphic horizons defined by Snedden et al. (2014): Paleocene-Eocene boundary (PEB); Cretaceous-Tertiary boundary (KTB); top of Sligo-Hosston Formations (SH); top of Cotton Valley-Knowles Formations (CVK), top of Cotton Valley-Bossier Formations (CVB), and top of Haynesville Formation (HVB). The black horizon is the interpreted Moho from seismic data and is shown as a solid, black line where it is a high-amplitude and continuous reflector; reflectors are shown as dotted lines where the reflectors are less apparent.

3.3.3. Gravity modeling

The 3-D gravity model includes five layers separated by four horizons: sea surface, bathymetry, basement, and Moho. For the US sector of the EGOM, I interpreted basement and Moho from the grid of Spectrum's Deep East seismic reflection survey. For the Mexican and Cuban sectors of the EGOM, the basement grid was calculated by subtracting NOAA's sediment thickness grid (Whittaker et al., 2013) from the bathymetry. My initial Moho grid was derived from an isostatic calculation (Blakely, 1995).

$$d_m = h\ (\rho_t/\Delta\rho) + d_s$$

In this equation, all depths are in km, d_m and ds are the Moho depth with the compensation depth (33 km) at the shoreline, h is elevation, ρ_t is the average crustal density, and $\Delta\rho$ is the density contrast at the base of the crust.

Due to a low signal-to-noise ratio in the deep sections of the seismic reflection data, a single velocity of 7 km/s was applied to the depth conversion of the deeper parts of the seismic sections. I adjusted the Moho interpreted from reflection data by 500 m by comparing these deep velocities with seismic refraction velocities (Ibrahim et al., 1981; Christeson et al., 2014; Eddy et al., 2014). The density of water, crystalline crust, and upper mantle used in my model were 1.03, 2.85, 3.3 g/cm^3 respectively. These values are similar to values used for previous gravity model studies in the GOM (Bird et al., 2005; Nguyen and Mann, 2016).

Sedimentary rock densities were gridded as a function of the thickness of the entire section by integrating each grid node over an exponential decay function that simulates clastic compaction of sedimentary rocks (Cordell, 1973). Structural inversion of the Moho in my 3-D gravity model was performed using a method described by Parker (1973), which established a Fourier transform technique for calculating potential field anomalies that are produced by uneven layers. I set the convergence limit of the inversion to 1 mGal, and after six iterations the algorithm converged, which is an excellent test result.

3.4 Results

3.4.1 Gravity and magnetic anomalies of the spreading ridge and oceanic crust of the EGOM

3.4.1.1 Gravity lows along the ridge crest

Four isolated, circular to elliptical, free-air gravity lows with an amplitude of 4 mGal can be observed trending to the northwest across the eastern GOM (Fig. 3.3b). The axial gravity low observed over active, slowly-spreading ridges is generally related to the partial melting beneath the spreading axis (Jonas et al., 1991). For extinct, slow-spreading ridges, Hall et al. (1986) proposed that the density of the upper mantle was altered during this final phase of upwelling along the spreading ridge and became preserved in place as long-lived, low-density bodies.

For extinct, slow-spreading ridges, the axial valley depth and the length of the low-density root are assumed to decrease as the spreading velocity increases (Hall et al., 1986). Therefore, the magnitude of negative gravity anomalies would also tend to decrease as the spreading rate increases. Low, P-wave velocities observed in the upper mantle of other, extinct, slow-spreading ridge (e.g. Labrador Sea – Osler and Louden

1995) support the presence of a low-density, serpentinized mantle root beneath extinct, spreading ridges. Therefore, I attribute the presence of an axial negative gravity anomaly to the presence of a preserved, low-density root formed during the early Cretaceous (~140 Ma), waning period of GOM seafloor spreading (Chapter 2, this dissertation).

3.4.1.2 Basement structures from residual gravity

The residual gravity anomaly in the eastern GOM becomes a more linear feature if the effect of the deeper part of low-density root centered on the spreading ridge is removed (Fig. 3.4b). The residual gravity map can also be used to map faults in the oceanic basement especially in areas of sparse, 2-D seismic data coverage (Fig. 3.4b). A comparison of the residual gravity map to the proposed location of pseudo faults proposed by Imbert and Phillipe (2005) is shown as the blue lines on Fig. 3.4b. No apparent gravity signature exhibits related to these proposed pseudo faults.

3.4.1.3 Apparent offsets of the conjugate, continent-ocean boundaries

Basin-opening, flowlines were generated using the pole of rotation proposed by Nguyen and Mann (2016) (Figs. 3.5a, 3.5b). The flowlines shown on Figs. 3.5a and 3.5b align with 1) apparent offsets of the ridge crest; 2) lineaments in the adjacent oceanic crust that also align with the ridge-crest offsets; and 3) apparent offsets in the continent- ocean boundary - such as the flowline between ridge discontinuities S1 and S2 which both align with offsets of the Florida and Yucatan, continent-ocean boundary (Figs. 3.5a, 3.5b). Minor offsets are also observed along the flowline separating S3 and S4 (Figs. 3.5a, 3.5b). Similar, small offsets of the continent-ocean boundary have been described from other small, obliquely-opening, oceanic basins like the Woodlark basin of Papua New Guinea (Taylor et al., 1999) and the Okinawa backarc basin (Liu et al., 2017) of the western Pacific Ocean.

3.4.1.4 Volcanic features identified from magnetic data

The magnetic anomaly map shows a positive anomaly over central of EGOM (Fig. 3.5a). The bold, white lines represent the center points of the short, spreading ridge segments which correspond to large volcanoes mapped from 2D seismic lines (Fig. 3.7).

The magnetic highs show an improved correlation to volcanic features with a reduced-to-pole, Jurassic pole correction (Fig. 3.5b). The red shaded area corresponds to seaward-dipping reflectors as mapped by Imbert (2005). The pole correction also reveals that the area of seaward-dipping reflectors coincides with an area of a large magnetic high that is consistent with this area being a rift zone with a voluminous, volcanic output. Neither the free air nor residual gravity shows a similar gravity high that might be related to a large area of volcanic rocks (Fig. 3.4).

3.4.2 Structure of the oceanic basement in the EGOM

3.4.2.1 Seismic reflection expression

The top of oceanic basement was defined within my seismic reflection grid as a high-amplitude, rugose, but continuous reflector that separates Mesozoic sediments from the underlying, oceanic crust (Figs. 3.8, 3.9). For areas of continental crust, the top basement was picked at the base of rifted, Mesozoic sediments (Fig. 3.8). The base salt horizon is marked by a moderate-to-strong amplitude, reflector with a velocity pull-up beneath the thicker areas of salt (Fig. 3.8).

My interpretation of the top of oceanic basement - based on my integration of seismic reflection and gravity data - indicates that northwest-elongated, negative gravity anomalies are correlative with a set of buried, northwest-elongated, submarine volcanoes that occupy the center points of the four, 30-60-km-long, axial rift valley segments observed in the eastern GOM (Fig. 3.10). These axial volcanoes reach maximum heights of 1-2 km in the centers of the ridge segments (labeled as R1 through R4 on Fig. 3.10) and decrease in size and elevation towards the ends of each spreading segment.

Examples of volcanoes that decrease in height and width as they approach the end of spreading ridge are shown on the 2D seismic lines in Figs. 3.10a, 3.10c, and 3.10e. Wide, axial valleys were mapped where ridges and fracture zones intersect, which are known as “nodal basins” (Fox and Gallo, 1984). Ridge axis volcanoes range from 10-30 km in width and 1- 2-km in depth. Nodal basins are common along slow

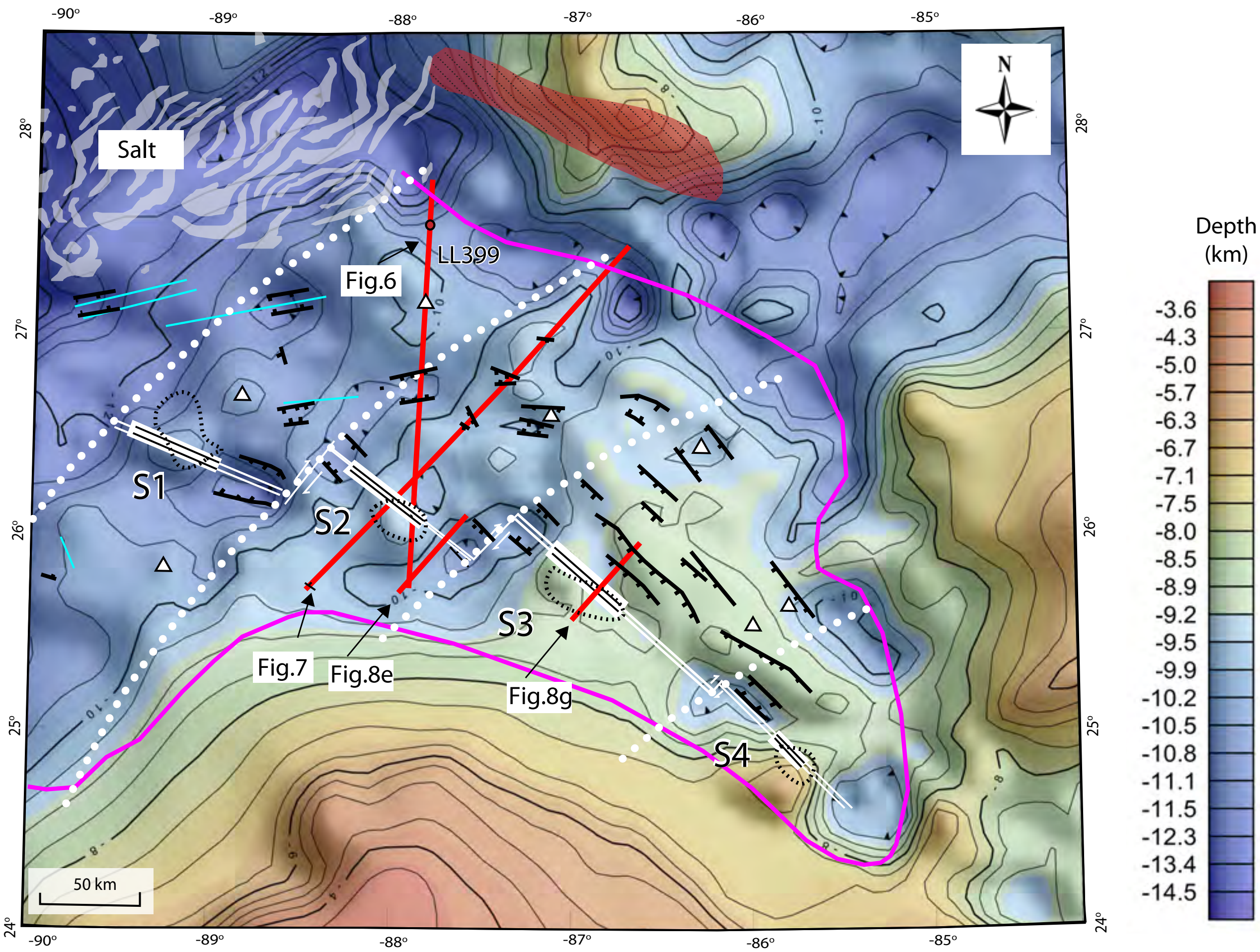

Figure 3.7 Structure map of the top of Jurassic oceanic basement and top of thinned, Paleozoic basement interpreted from the study area using the Spectrum Big Wave, 2D grid of industry seismic reflection data with a contour interval of 0.5 km. Symbols are the same as used in Fig. 4b. Red lines are locations of 2D seismic lines in Figs 3.8, 3.9, 3.10e, 3.10g.

spreading centers with the length and depth of the nodal basins increasing as the pole of rotation is approached (Fox and Gallo, 1984).

3.4.2.2 Expression of secondary discontinuities along the ridge axis

Slow spreading centers are characterized by different scales of discontinuity gaps. A first-order discontinuity is a transform fault that connects spreading centers offset by as much as several hundred kilometers (Fox and Gallo, 1984). Secondary discontinuities are less well developed and exhibit much shorter (20-80 km) ridge offsets (Macdonald et al., 1993). Globally, fracture zones along active and extinct ridges range in width from 20 to 50 km, but those GOM fracture zones described by Stephens (2001) using 3D seismic data in the northeast GOM were less than 5 km wide.

In my study area, 30-60 km long ridge segments are separated by 5-30 km inter-volcanic gaps that I propose to be second-order discontinuities as defined by Macdonald et al. (1993) (Fig. 3.7). I extended the interpreted ridge segments beneath the residual gravity lows to approximate the extinct ridge and fracture zone geometry of the EGOM (Fig. 3.7).

Small-circle flowlines through the proposed fracture zone locations were generated using Nguyen and Mann's (2016) pole of rotation for the Yucatan block. These flowlines roughly correlate with broad, arcuate gravity lows (Fig. 3.4b), suggesting that four main spreading segments developed in the EGOM as the Jurassic ocean basin began to open. Several map view offsets of the edge of the continent-ocean boundary on both conjugate margins coincide with flowline intersections with the continental margins and are inferred to represent the earliest accretion of oceanic crust.

3.4.2.3 Structural and volcanic features of the ridge axis and adjacent oceanic crust

The overall basement fabric of the study area - interpreted from seismic reflection data and correlated with the residual gravity map - consists of northwest-trending basement faults that dip inwards towards the extinct spreading center as is commonly observed along active, slow-spreading ridges (Fox and Gallo, 1984) (Fig. 3.7). These normal faults have relatively small offsets that vary from 0.2-1 km (Fig. 3.9). In the north-trending, regional 2D seismic line that intersects well LL 399, a 15-km-wide 2-km-deep valley is bounded by east-striking and inwardly-dipping normal faults (Fig. 3.8). These basement faults follow the general trend of pseudo faults proposed by Imbert and Philippe (2005) in the northeastern EGOM (Fig. 3.7). However, I interpret these proposed pseudo faults as transform fault valleys that parallel the flow-line parallel fracture zones.

In addition to the large volcanoes located in the centers of spreading segments, off-axis volcanos are widely distributed on the Jurassic oceanic crust that flank the spreading ridge (Fig. 3.7). Several of these off-axis volcanoes formed near basement faults, or within basement depressions.

Seismic reflection data through ridge segment 2 reveals the largest buried volcano in the study area, which is surrounded by several, smaller volcanoes (Fig. 3.9). This central, large and buried volcano rises 2.2 km over the basement and is 13.5 km wide with very steep slopes (~12°). Cretaceous to Tertiary, post-spreading, strata onlap this ocean floor and are deformed by differential compaction arching over volcanoes of various sizes. Based on the horizon correlated from well 399 #1, I suggest that the peak of the 2-km-high volcano in this ridge center was not completely buried by sediment until the Late Oligocene (Fig. 3.9).

Minor extensional normal faults and compaction folds on and above the crest of the ridge volcano are shown in Fig. 3.10. Sediment horizons below the axial volcanoes in Figs. 3.10e, 3.10g indicate that the volcanic topography formed during the final stages - or immediately after – the end of seafloor spreading.

Volcanism in the spreading center could be related to fertile mantle material that erupted as the spreading rate decreased, or soon after seafloor spreading had ceased (Haase et al., 2011; Barckhausen et al., 2014). These large volcanoes are the likely origin for the localized magnetic anomaly highs that were noted by previous studies along the spreading ridge segments in the EGOM (Hall and Najmuddin, 1994; Imbert and Philippe, 2005; Nguyen and Mann, 2016). Similar post-spreading volcanism has been observed along an extinct, Oligocene spreading center in the South China Sea (Zhao et al., 2016).

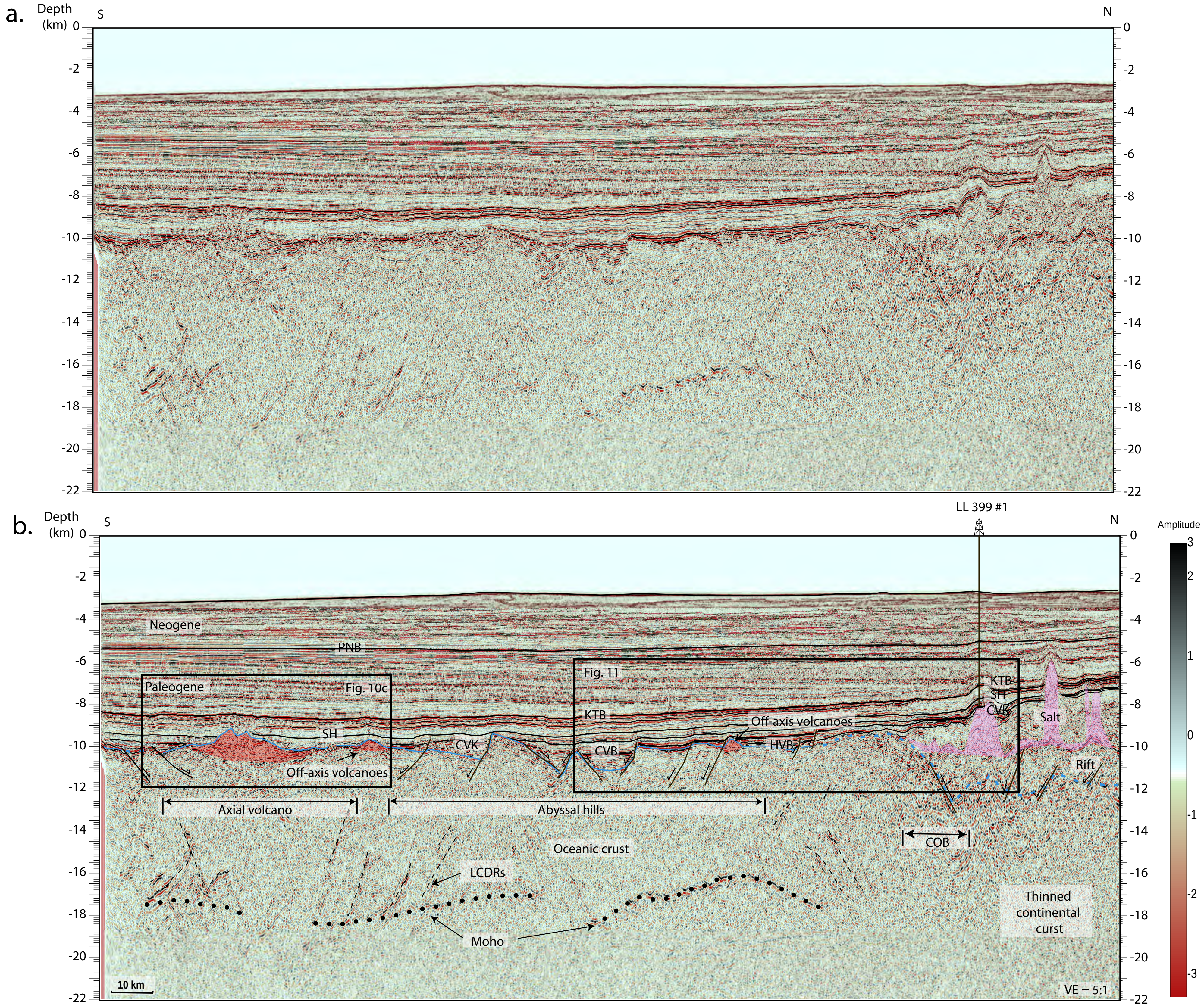

Figure 3.8 (a) Uninterpreted, depth-migrated, 2D seismic line crossing the extinct spreading ridge, the oceanic crust northeast of the spreading ridge, and the marginal rift marking the continent-ocean boundary. (b) Interpreted depth-migrated seismic section showing large volcano occupying the axial valley of the extinct, spreading ridge and rifted oceanic crust forming the abyssal hills northeast of the spreading center. Near-vertical black dashed lines indicate lower crustal, dipping reflectors (LCDR) within the oceanic crust. The marginal rift is formed on thinned, continental crust and localizes thicker salt deposits. Industry well LL-399#1 is located on one of these salt diapirs and was used here and by Snedden et al. (2013) to correlate sedimentary formations shown annotated in Fig. 3.2 across the top of the late Jurassic oceanic basement. The black rectangle in the left is a zoom of the spreading ridge shown on the 2D seismic line in Fig. 3.10d. The black rectangle in the right is a zoom of the seismic well correlation shown on the 2D seismic line in Fig. 3.11. Vertical exaggeration is 5.

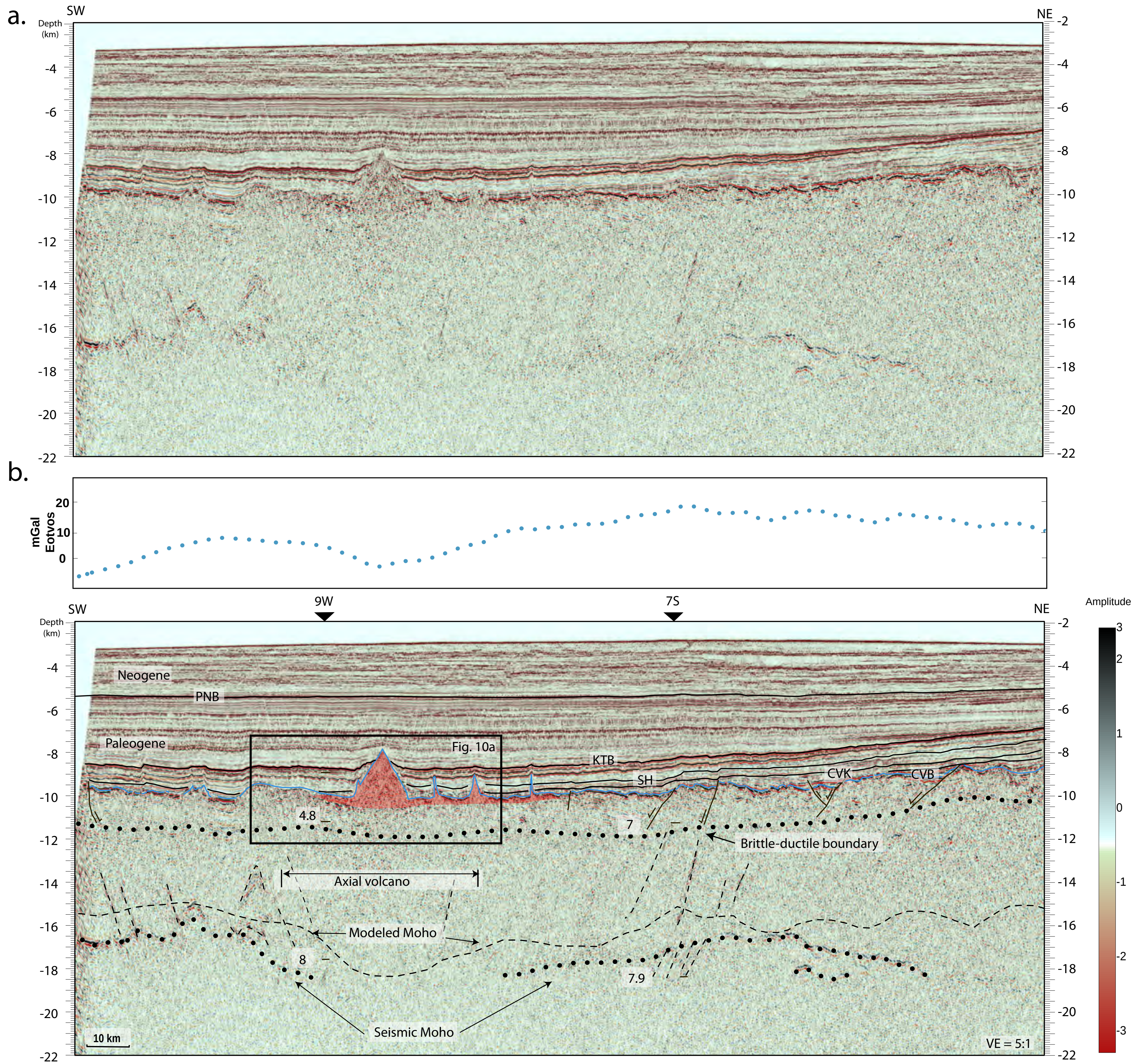

Figure 3.9 (a) The uninterpreted depth-migrated seismic section located on the map in Fig. 3.7 and showing a large volcano occupying axial valley of spreading segment 2 (this seismic line is located on the map in Fig. 3.7). (b) The interpreted depth-migrated seismic section with the dotted, grey line showing the brittle-ductile boundary interpreted from the integration of refraction and reflection data. The dashed black line is the Moho generated in this study from a 3-D gravity inversion. The gravity profile at the top of the seismic line is extracted from the free-air gravity grid shown in Fig. 3.3b. Vertical exaggeration is 5.

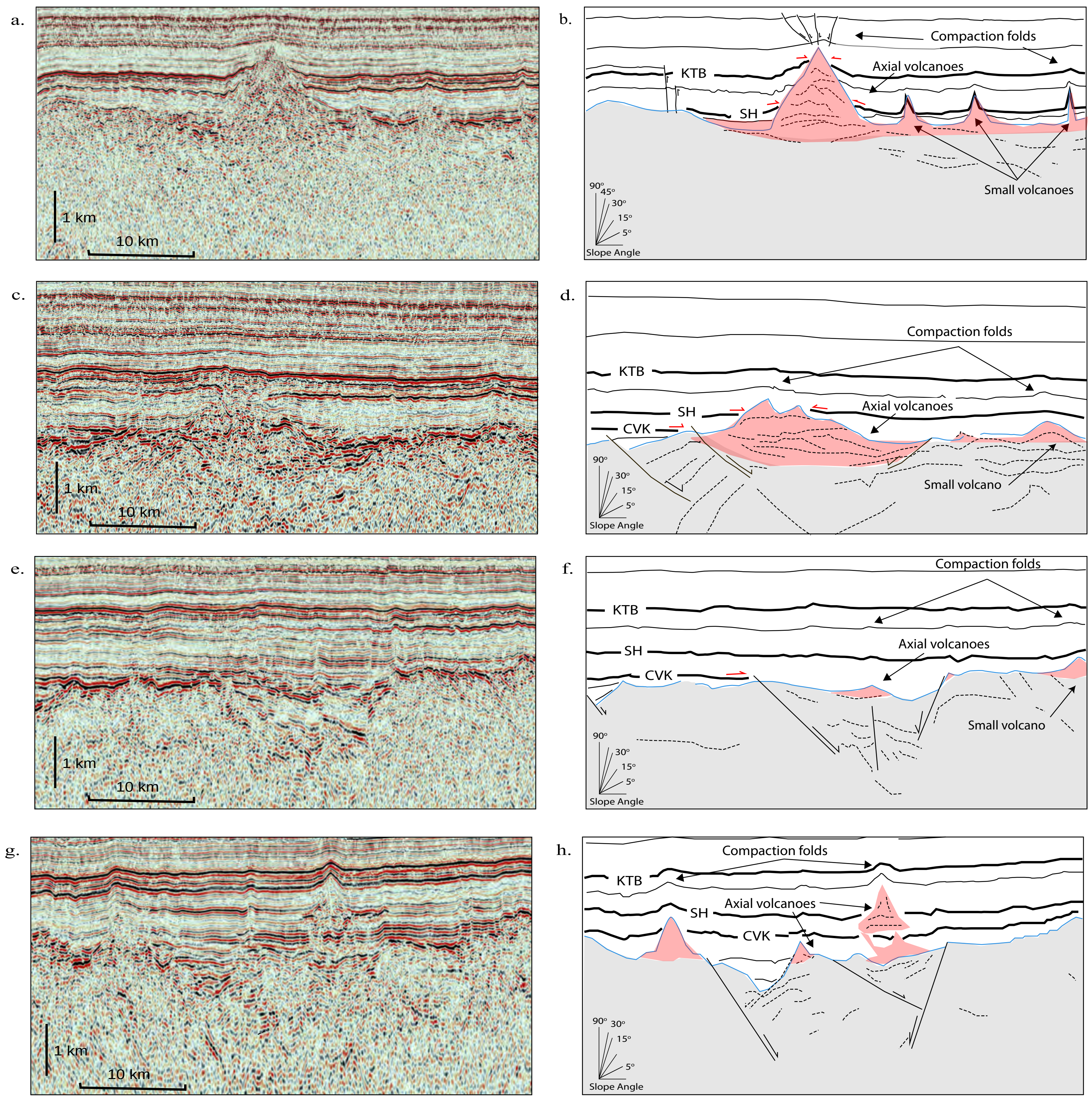

Figure 3.10 (a) Uninterpreted depth-migrated seismic section across the center of mid-ocean ridge segment 2 (S2). Location is shown in Figs. 3.7 and 3.9. The axial volcano is about 2-km high. (b) Schematic illustration interpreted from the seismic line in Fig. 3.10a. Folds and minor faults are compaction effects formed over the top of the large, axial volcanoes. Black lines show stronger reflectors within sedimentary units. Bold black lines are horizons identified in Fig. 3.6b. The black, dashed lines show internal reflectors within the volcano and other, weak reflectors within the upper, oceanic crust. (c) Uninterpreted depth-migrated seismic section 15 km southeast of Fig. 3.10a. Location is shown on Figs. 3.7 and 3.8. The vertical relief of the axial volcano decreases in this area to less than 1 km. (d) Schematic illustration interpreted from the seismic line in Fig. 3.10c. As the vertical relief on the axial volcano diminishes, the axial valley marking the Jurassic spreading ridge becomes more apparent. (e) Uninterpreted depth-migrated seismic section across the southeast end of mid-ocean ridge segment 2 (S2). Location of this 2D seismic section is shown in Fig. 3.7. The spreading ridge is well defined in this area by a 1-km-deep axial valley, although a series of small volcanoes are visible on the seismic section. (f) Uninterpreted depth-migrated seismic section located on Fig. 3.7 showing ridge segment 3 (S3) with volcanoes adjacent to the axial valley. (g) Interpretation of the 2D seismic line in Fig. 3.10f. Note that the base of the volcano adjacent to the axial valley overlies the top of Cotton Valley-Knowles Formation as also observed on the 2D seismic lines in Fig. 3.10d and 3.10f. Deposition of the Berriasian Cotton Valley Formation marked the end of seafloor spreading in the range of 141.9-138.2 Ma.

3.4.2.4 Age of oceanic crust in the EGOM

Based on the horizons correlated from well 399 #1, the termination of the mapped horizons on the oceanic crust could represent the relative evolution of the oceanic crust (Figs. 3.11, 3.12). The structure maps in the Florida and Yucatan margin show the development of oceanic crust of EGOM (Figs. 3.12a, 3.12b, 3.12c). The irregularity of the surface formed by volcanic-related, basement highs along the spreading ridge explains the local irregularity of the Cretaceous isopachs (Figs. 3.12d, 3.12e). The plate model and ages of oceanic crust was modified from Snedden et al. (2013) (Fig 3.12f).

The highly, asymmetrical, oceanic crust geometry during deposition of the Haynesville Formation suggests two, possible explanations. The first explanation is a ridge jump during the early stages of seafloor spreading. Based on the near north-south trending normal faults (pseudo faults) in the northeastern GOM, Imbert and Philippe (2005), and Pindell et al. (2009, 2016) all proposed an early stage of near north-south seafloor spreading in the oceanic crust that was accompanied by the thicker deposition of Jurassic salt. My mapping of Jurassic and Cretaceous, sedimentary isopachs in Fig. 3.11 during seafloor spreading and COB offset suggest a faint, but possible, northwest-southeast spreading ridge northeast of the single, pole of rotation in northwest Cuba shown as a black dash line in Fig. 3.12f.

Morphological expression of an extinct, spreading ridge has been described from other oceanic basins, such as from the Mathematician ridge, formed in the Pliocene (4 Ma) in the eastern equatorial Pacific (Mammerickx et al., 1988). This extinct ridge is marked by linear troughs formed during rapid, thermal subsidence following a ridge jump that is recorded by magnetic anomalies (Mammerickx and Sandwell, 1986). In this study, the lack of magnetic anomalies combined with deep burial following Jurassic spreading makes it difficult to identify the exact location of the abandoned ridge in the northeastern GOM.

3.4.2.5 Possible explanations for crustal asymmetry in the eastern GOM

A possible tectonic mechanism for the asymmetry of the oceanic crust in the eastern GOM was proposed by Müller et al. (2008) who noted that areas of asymmetrical, oceanic crust appear to be frequently related to asthenospheric flow from mantle plumes to spreading ridges and result in ridge jumps (Table 3.1). A late Jurassic mantle plume (150 Ma) in the central GOM identified from basement and gravity highs (Bird et al., 2005) could result to a westward jump of the spreading ridge in the early stage of seafloor spreading. However, the most well-studied plume, the Central Atlantic Magmatic Province (CAMP) (190-165 Ma), in the study area is located closer to excess (northeastern) spreading plate near the state of Georgia in the southeastern USA. The center point of the CAMP plume is indicated by the radial dike swarms of 190-165 Ma age (201 Ma) (Byerly, 1991; McHone, 2003).

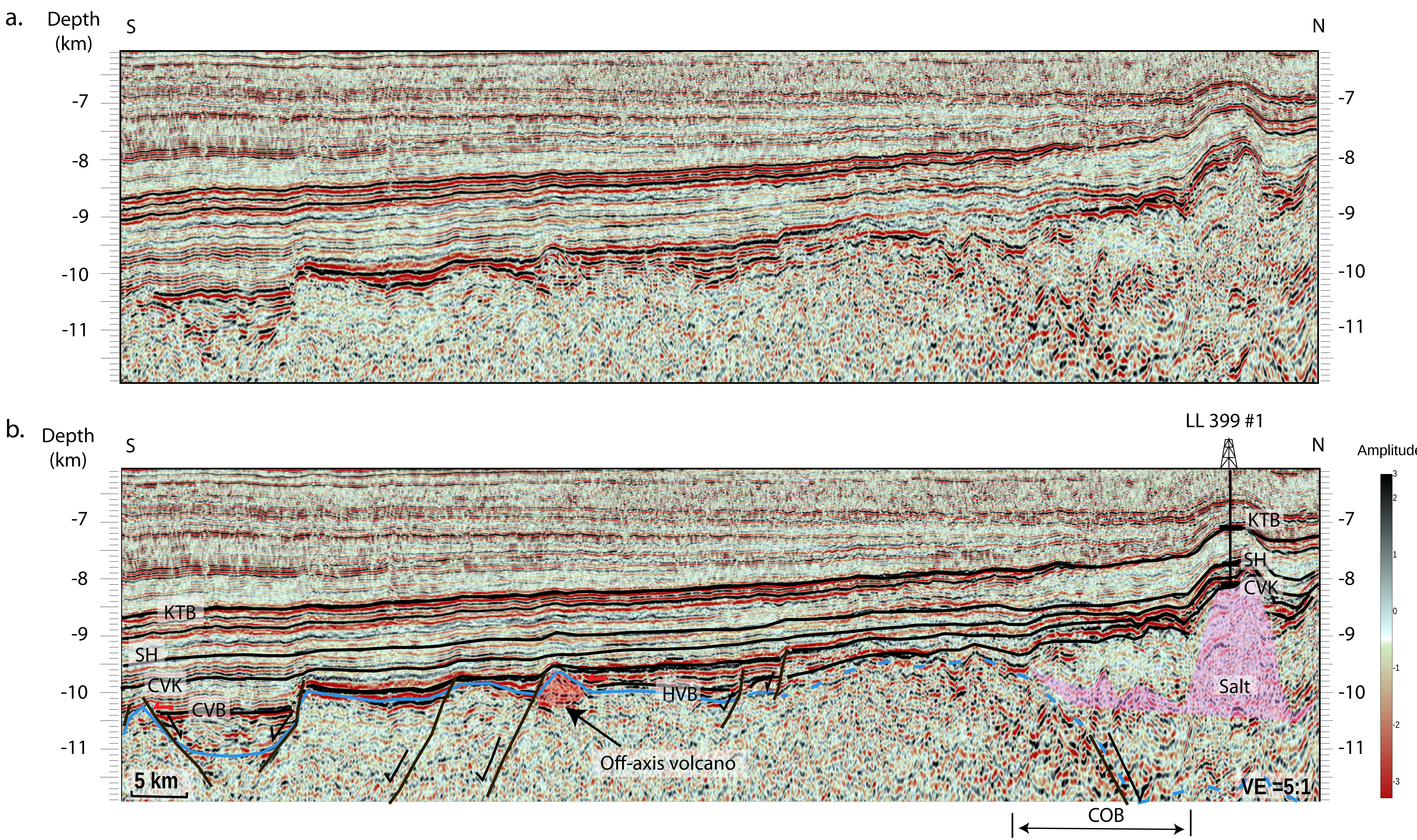

Figure 3.11 (a) Zoom of the seismic line shown in Fig. 3.8a with the same vertical exaggeration. (b) Zoom of the seismic line shown in Fig. 3.8b to show the seismic well correlation from LL 399 #1 around COB to the oceanic crust. Red arrows show the onlap of the CVB and HVB correlated from LL 399 #1.

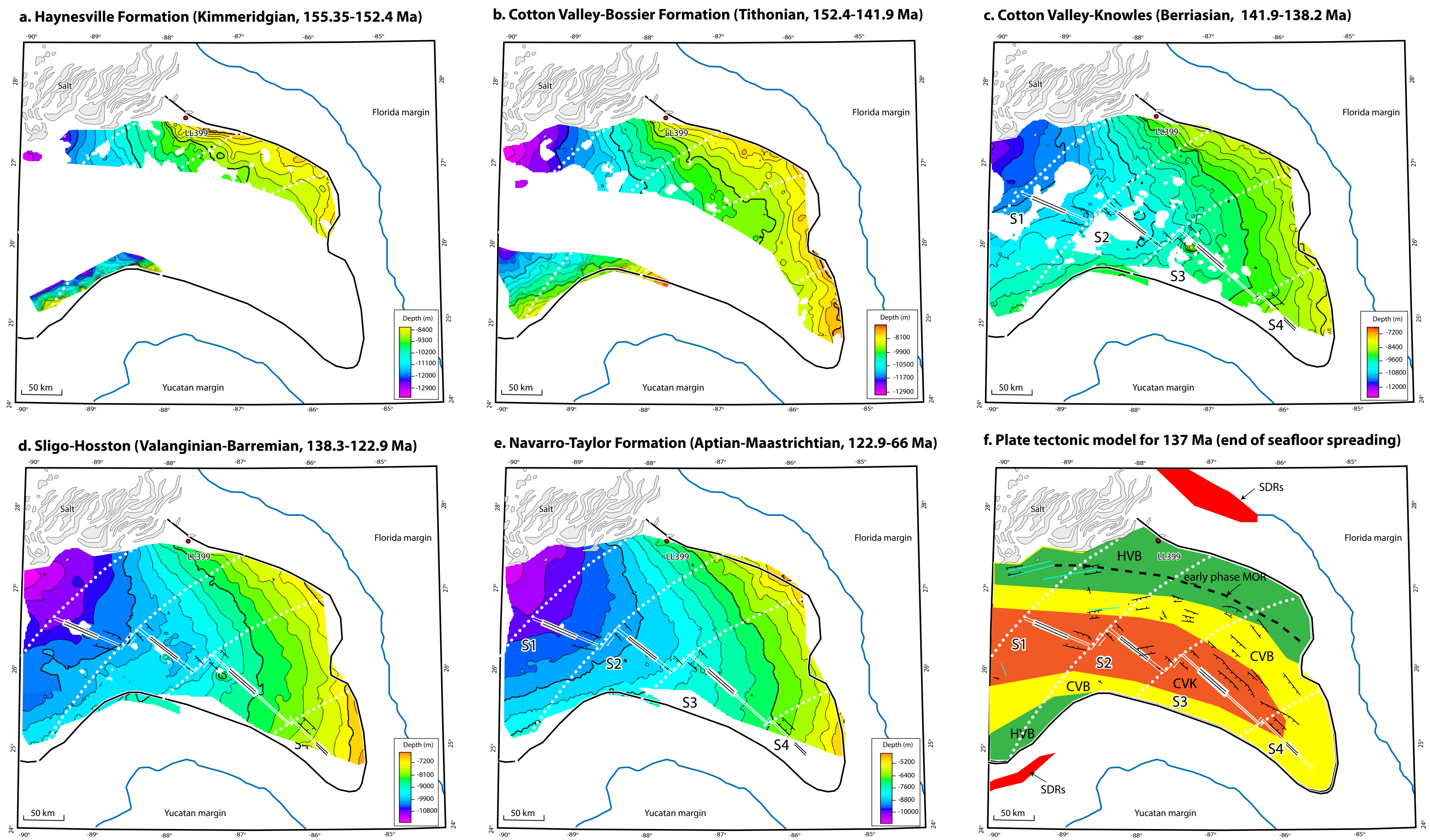

Figure 3.12 (a) The structural map in depth of the top of Haynesville Formation (HVB) of Kimmeridgian age (155.35-152.4 Ma). During this period, the oceanic crust had only formed along the northeastern and southwestern edges of the EGOM. (b) The structural map in depth of the top of Cotton Valley-Bossier Formation (CVB) of Tithonian age (152.4-141.9 Ma). During this period, the newly-formed, oceanic crust increased the width of northeastern and southwestern EGOM and extended towards the southeast. (c) The structural map in depth of the top of Cotton Valley-Knowles Formation (CVK) of Berriasian age (141.9-138.2 Ma). During this period, the oceanic crust ceased spreading and attained its present-day width. (d) The structural map in depth of the top of Sligo-Hosston Formation (SH) of Valanginian-Barremian age (138.3-122.9 Ma). The top of Sligo-Hosston Formation is the first stratigraphic horizon to bury most of the GOM Jurassic oceanic crust with the exception of several, prominent seamounts aligned along the extinct, spreading axis.. (e) Structural map in depth of the top of the Cretaceous-Tertiary boundary (KTB). The Cretaceous-Tertiary boundary is a widespread, unconformity identified in many areas of the GOM (Ibrahim et al. 1981). (f) Plate tectonic model for 137 Ma (end of seafloor spreading) based on compiling the lateral extends of the of the top of Haynesville Formation (HVB), top of Cotton Valley-Bossier Formation (CVB), and top of Cotton Valley-Knowles Formation (CVK) as shown on Figs. 3.12a, 3.12b, and 3.12c.

MOR location	Excess plate	Crustal accretion value	Excess accretion rate	Asymmetric spreading Age	Related hot spot	Hot spot age
Central North Atlantic Ocean	Newfoundland	53%	3%	last 130 Ma	NA	NA
Central North Atlantic Ocean	U.S East Coast	51%	1%	last 130 Ma	NA	NA
Gulf of Mexico	Gulf of Mexico	55-60%	5-10%	158-138 Ma	NA	NA
Equatorial Atlantic Ocean	Demerara Abyssal Plain	55-65%	5-15%	last 80 Ma	NA	NA
Souhtern South Atlantic Ocean	Argentine basin	53-54%	3-4%	last 30 Ma	Tristan Da Cunha hot spot	125 Ma
Central Indian Ocean	Bay of Bengal	55-65%	5-15%	100-80 Ma	NA	NA
West Pacific Ocean	Southwest of the Philippine Sea	60-70%	10-20%	last 70 Ma	NA	NA
Australian Antarctic Discordant Zone	Australian plate	52-70%	2-20%	60-30 Ma	Balleny hot spot	36 Ma
East Pacific Rise	Nazca plate	70%	20%	last 20 Ma	Pacific hot spot	NA

Table 3.1 Summary of asymmetric oceanic crust, and excess accretion rate compiled from Muller et al. (2018). The GOM has a relatively high excess accretion rate of about 5-10%. The age of hot spot is from Steinberger (2000).

3.4.2.6 Inferring age of oceanic crust and subsidence history from patterns of regional, sedimentary isopachs

Jurassic-Cretaceous sediment thickness variations from isopach maps in the Florida and Yucatan margins (Fig. 3.13) are mainly controlled by the oceanic basement structure and sediment supply. In the Kimmeridgian, a thin Haynesville sequence (200-600 m) was deposited on the V-shaped area of oceanic crust in the northeastern GOM (Fig. 3.13a). In the Tithonian, 1000-1300 m thick Cotton-Valley-Bossier fluvial-deltaic sequence was deposited on the newly formed oceanic crust in the southeast, with clastic, sedimentary sources created by the rifts formed during ridge propagation into the southeastern GOM (Fig. 3.13b).

In the Berriasian, the oceanic crust finally achieved the present-day geometry, and rifting in the southeastern GOM ceased (Marton, 1995; Marton and Buffler, 1999). The Knowles limestone was deposited following a short transgression near the end of Cotton Valley deposition (Cregg and Ahr, 1984; Dobson and Buffler, 1997). The Cotton Valley sequence is thickest (1000-1300 m) in the nodal basins at the ends of spreading ridges and thins onto the axial volcanoes along the spreading ridge (Fig. 3.13d). In the Valanginian-Barremian, Sligo-Hosston sequence sediments buried most of the structural relief on the oceanic crust - with except for the 1-2-km highs formed by the axial volcanoes (Fig. 3.13d). In the Aptian-Maastrichtian, the Navarro-Taylor sequence was more uniformly distributed and thickest (1000-1200 m) in the northeastern GOM (Fig. 3.13e).

Tertiary, clastic sediments are thickest (7600 m) in the northeastern GOM, and thinnest (2000 m) towards the southeast (Fig. 3.13f). From Kimmeridgian to Maastrichtian, relative thinner (1000-1500 m), Late Jurassic deepwater sediments were deposited in the Yucatan margin compared to the Florida conjugate margin (2000-2500 m) (Figs. 3.13a, 3.13b, 3.13c, 3.13d, 3.13e).

The 1000-1300-m, thick Haynesville, Cotton Valley-Bossier sequences were deposited during seafloor spreading in the southeastern GOM (Figs. 3.13a, 3.13b, 3.13c) and represent the combined effect of: 1) a slowing spreading rate close to the pole of rotation in northwestern Cuba; and 2) the proximity to terrigenous, clastic sources in the southeastern GOM.

The 800-1000-m-thick Cotton Valley-Knowles and 600-1000-m Sligo-Hosston sequences in the northeast EGOM both reflect a rapidly subsided oceanic crust following the cessation of seafloor spreading around Berriasian time (Figs. 3.13d, 3.13e). Thick, Tertiary sediments in the northwestern EGOM were sourced by the fluvial systems along GOM coastal plain (Galloway, 2008). Thin (1000-1500 m) Kimmeridgian to Maastrichtian sediments deposition are related to the lack of fluvial sources in the Yucatan margin.

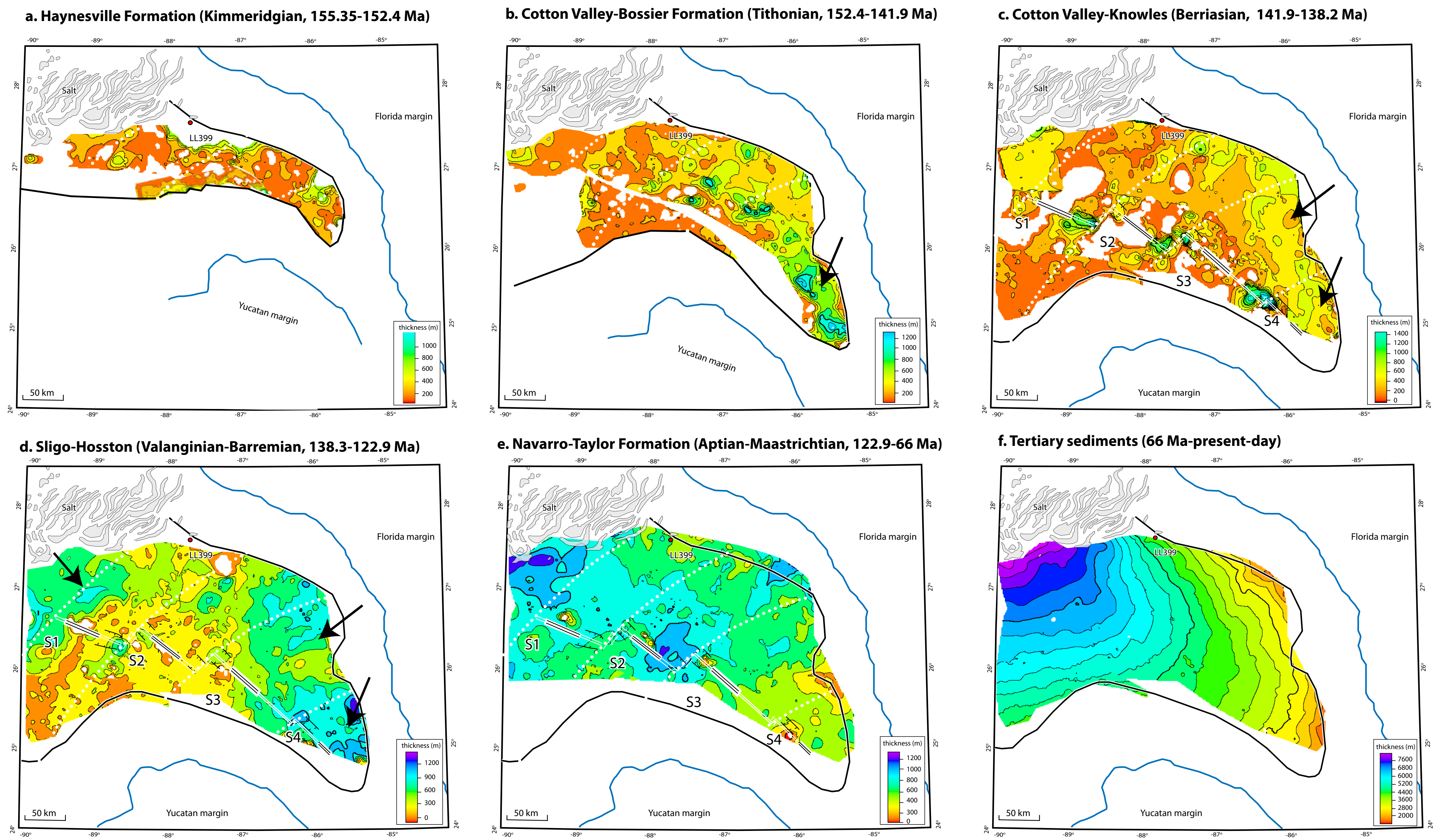

Figure 3.13 (a) Isopach map for the late Kimmeridgian stratigraphic interval (155.35-152.4 Ma) between the top of Jurassic oceanic basement and the top of Haynesville (HVB). Reconstructed map bases shown in Figures 3.13a, 3.13b, and 3.13c are all based on the pole of rotation in northwestern Cuba by Nguyen and Mann (2016). (b) Isopach map of the Cotton Valley-Bossier Formation (CVB) of Tithonian age (152.4-141.9 Ma). Black arrow shows a prominent CVB depocenter located in the southeastern GOM. (c) Isopach map of the Cotton Valley-Knowles Formation (CVK) during the Berriasian (141.9-138.2 Ma). Note that the CVK depocenter extends in a northwesterly direction. (d) Isopach map of the Sligo-Hosston Formation (SH) of Valanginian-Barremian age (138.3-122.9 Ma). As seafloor spreading ceases, the Jurassic-Cretaceous sedimentary section is evenly distributed in the EGOM with the thinnest sediments along the ridge axis. (e) Isopach map of the Navarro-Taylor Formation (NT) of Aptian-Maastrichtian (122.9-66 Ma) between the top of Sligo-Housston Formation (SH) and the Cretaceous-Tertiary boundary (KTB) (65 Ma). The thickness of between SH and KTB show abrupt thickness changes along the same trends as the small circles about the pole in northwestern Cuba. (f) Isopach map of the Tertiary passive margin stage. The rapid thickness increase towards the northwest reflects the southward progradation of the Mississippi fan.

3.4.3 Crustal structure of oceanic crust of the EGOM

3.4.3.1 Depth to the Moho from 3D gravity inversion

The seismic Moho (Fig. 3.14) was interpreted from deep, high-amplitude, and continuous horizons underlying basement. The gap in depth between the Moho interpreted from seismic data, and the Moho derived from gravity inversion (Fig. 3.9) is related to the low velocities (7 km/s) used for depth conversion by Spectrum of the seismic reflection beneath basement. The Moho inverted from integrated 3-D gravity inversion reveals its deep root beneath the spreading ridge (Fig. 3.15a). The RMS difference between observed and calculated gravity after the inversion is less than one mGal for the oceanic crust, and around ±6 mGal in the continent-ocean boundary (COB) and in the carbonate bank on the Yucatan conjugate margin (Fig. 3.15b).

3.4.3.2 Origin of lower-crustal dipping reflectors

Lower-crustal, dipping reflectors (LCDRs) observed in the upper and lower, oceanic crust in areas of fast spreading centers are thought to be related to either: 1) hydrothermal circulation at the base of sheeted dikes (Ranero et al., 1997b); or 2) shear zones characterized by interstitial melt or mylontization (Bécel et al., 2015). For slow-spreading ridges, LCDRs observed in other, oceanic basins have been interpreted as: 1) thermal changes caused either by variable spreading rates or presence of a mantle plume (Ranero et al., 1997a); 2) fault systems that rupture the entire thickness of oceanic crust (White et al., 1990; Morris et al., 1992); and 3) shear zones related to brittle-ductile deformation (Mutter and Karson, 1992).

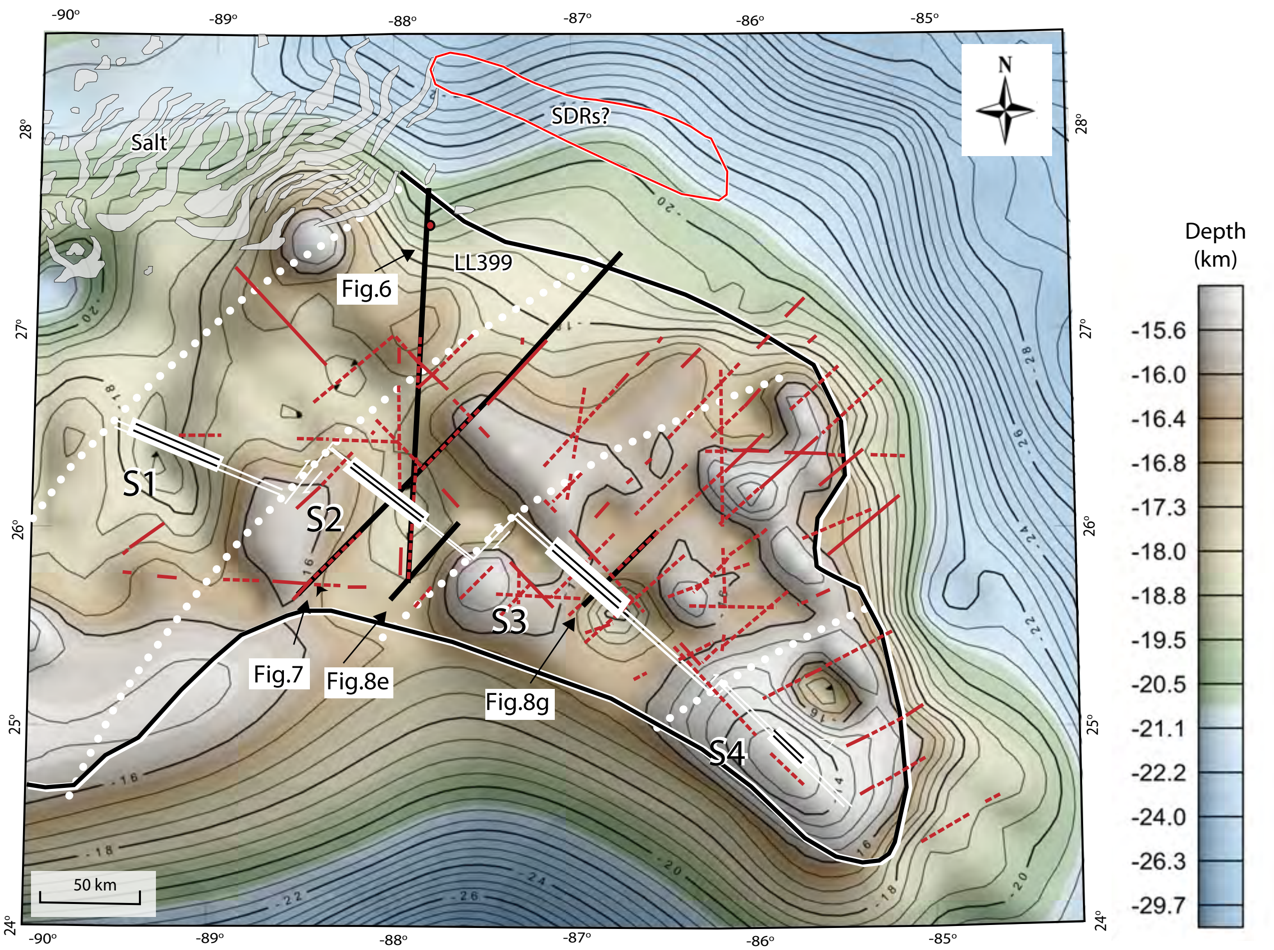

Figure 3.14 Map of the seismic Moho interpreted from the industry, 2-D seismic reflection grid shown in Fig. 3.3a. To complete the map in areas where there is no industry seismic coverage, the isostatic Moho was used to complete these parts of the Moho map. Solid black lines show seismic Moho picked with confidence and dashed lines show picks with less confidence. Note the seismic Moho is absent around the mid-ocean ridge (MOR) and in the northwestern EGOM. The contour interval is 0.5 km.

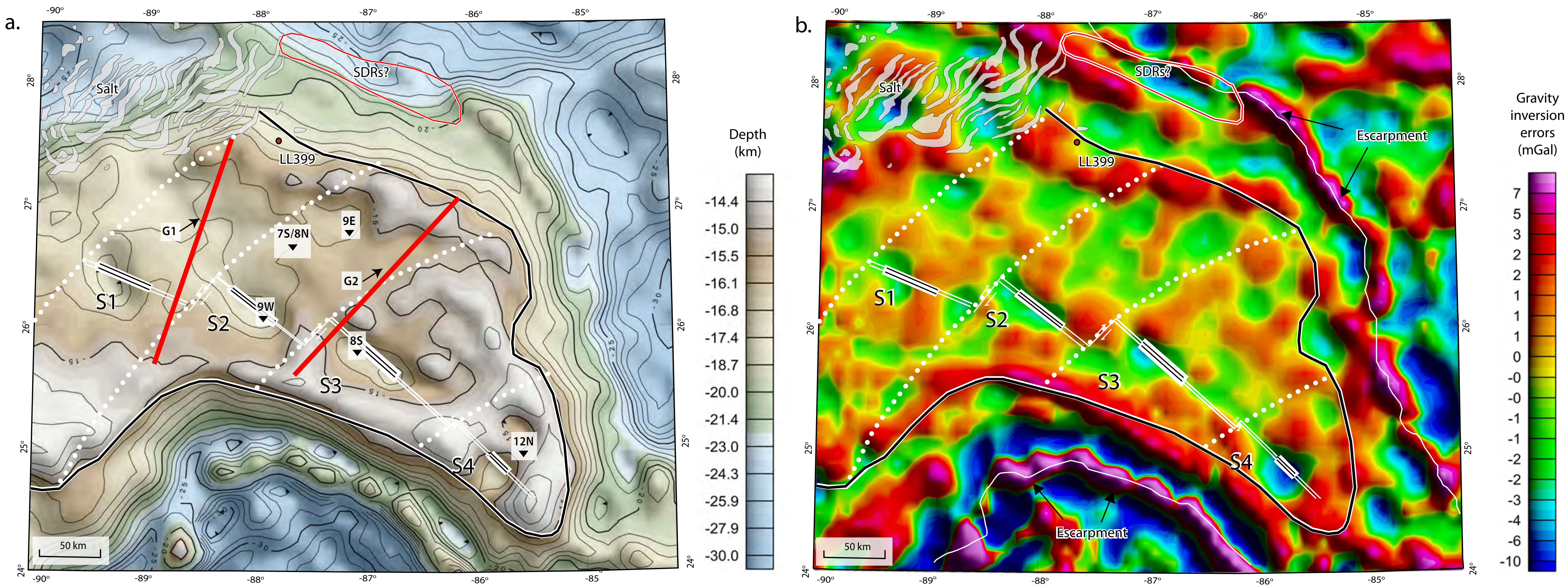

Figure 3.15 (a) Moho surface derived from 3-D gravity structural inversion and contoured at an interval of 1 km. Inverted black triangles are refraction station locations used for Moho corrections. The gravity inversion reveals a deep Moho depression parallel to the trend of the mid-ocean ridge segments. (b) Map of the gravity inversion error grid. Most of the inversion error occurs along abrupt, bathymetric scarps formed along the carbonate margins of the Florida and Yucatan margins.

Based on the relationship between maximum displacement and fault length by (Schultz et al., 2006), small offsets of tens to hundreds of meters do not support the second interpretation that reflectors are fault-plane reflections of normal faults extending at depth into the lower crust (Figs. 3.8, 3.9). I propose a third explanation that involves deformation of the brittle upper crust by normal faulting during slow, seafloor spreading and deformation of the lower crust along ductile shear zones. The boundary of brittle- ductile deformation correlates with a refraction boundary where velocities increase from 6.3 to 7.0 km/sec (Ibrahim et al., 1981) (Fig. 3.9).

3.4.3.3 Variations in the thickness of the oceanic crust

White et al. (1992) found that the global average thickness of oceanic crystalline crust is 7.1 ± 0.8 km, while Reid and Jackson (1981) reported that the thickness of oceanic crust ranges from 5-6.6 km for crust produced at active, slow spreading centers. Van Avendonk et al. (2016) calculated that the average crystalline thickness of Jurassic oceanic crust in the Indian and Pacific is around 7.1 km, or 1.2 km thicker than present-day, oceanic crust. They attribute these variations to decreasing mantle temperatures following the breakup of Pangaea. The average thickness of the oceanic crust derived from the basement and modeled Moho in this study (Fig. 3.16) is 6.1 km, which is a typical thickness for Jurassic slow spreading centers (Reid and Jackson, 1981; Van Avendonk et al., 2016).

In addition to its greater width, the northwestern flank of the ocean floor in the EGOM is slightly thicker (average 6.4 km) than the southeastern flank (average 5.5 km). Each of the four ridge segments is separated by relatively thin crust (5 km) at secondary discontinuities. However, the crust is thickest in the center of each of the four, spreading ridge segments. The thickened crust (6.4-8.6 km) underlying the centers of the four, ridge segments produces negative residual Bouguer gravity anomalies (Fig. 3.3b). I used the 6.1 km-thickness contour of the crystalline crust as a guide to map the continent-ocean boundary in the EGOM (Fig. 3.15a).

My integrated 3-D crustal model is based on the integration of seismic reflection and gravity data and is summarized as a schematic, block diagram where crustal sections are drawn both parallel and perpendicular to the extinct ridge of the EGOM (Fig. 3.16b). My crustal model is consistent with previous, GUMBO seismic refraction results of Christeson et al. (2014), and Eddy et al. (2014, 2018). Both these groups reported that the thickness of oceanic crystalline crust changes from 8 km in northwestern EGOM to 5.6-5.7 km in the central EGOM, suggesting increased volcanism in the northwestern EGOM during seafloor spreading (Eddy et al., 2014). The excess magma supply in the northwest EGOM is also supported by high-velocity thick oceanic crust, and the existence of SDRs near the COB imaged on GUMBO Line 3 (Imbert, 2005; Eddy et al., 2014).

a.

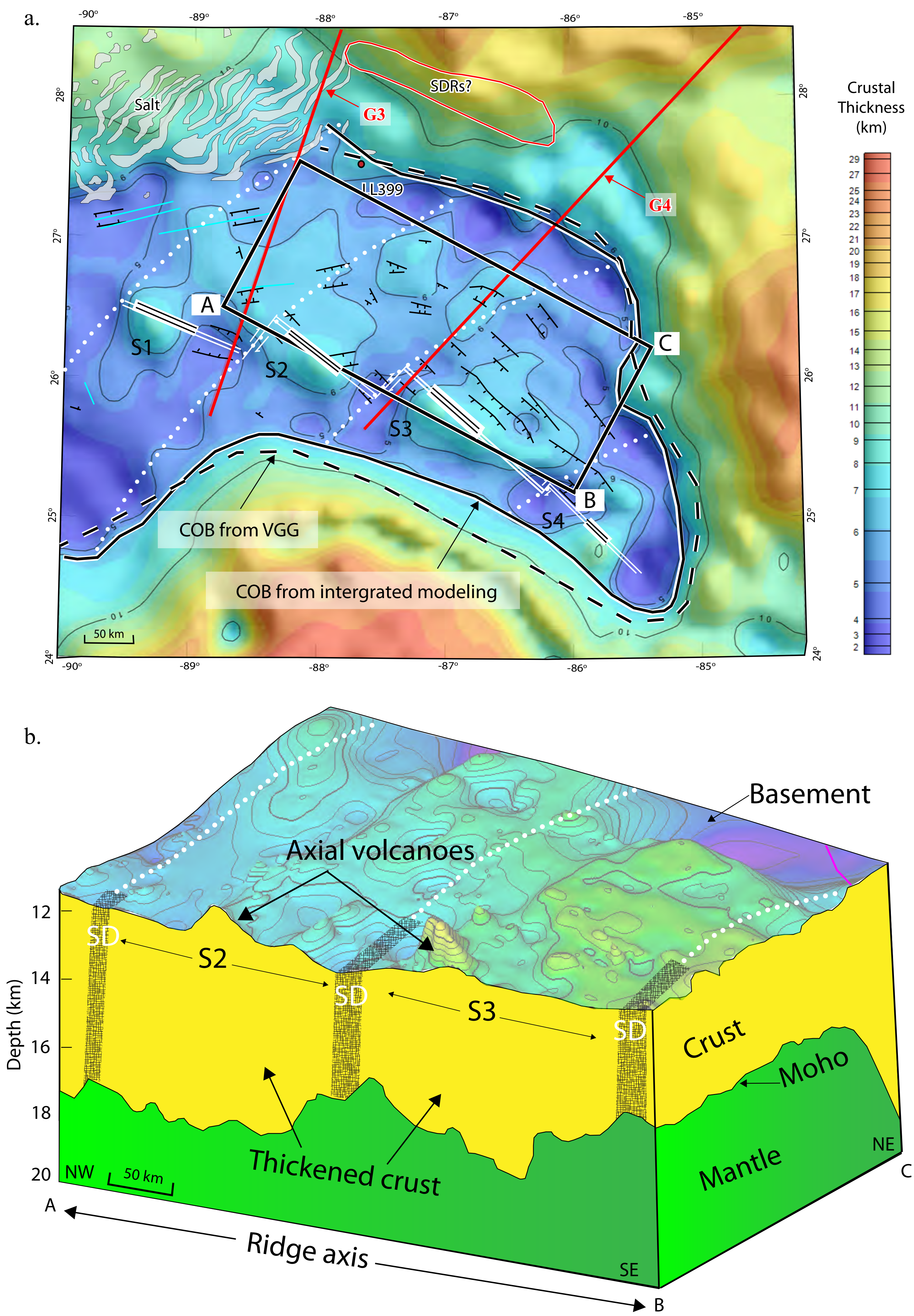

Figure 3.16 (a) Crustal thickness map of the eastern Gulf of Mexico (EGOM) based on my basement interpretation and Moho modeled from the 3D gravity inversion. The red lines are locations of seismic refraction profiles GUMBO 3 (G3) and GUMBO 4 (G4). The orange dashed line is the continent-ocean boundary (COB) from the VGG map (Fig. 3.1b), and the pink line is the COB from my 3D gravity inversion. The black rectangle is the location of the area shown schematically in the block diagram in Fig. 3.16b. (b) The 3-D block diagram shows thicker oceanic crust (6.5-8.6 km) beneath the spreading centers and the off-axis volcanoes northwest of the spreading center. Second-order discontinuities (SD) separate the two ridge segments and exhibit thinner crust typical for areas of secondary discontinuities (White et al., 1992).

3.5 Discussion and Conclusions

In this chapter, I have generated regional maps of the top and base of Jurassic oceanic crust (basement and Moho) using a grid of deep-penetration oil industry data from a 120,000 km^2 area of the eastern Gulf of Mexico (Fig. 3.6a). I have integrated my seismic reflection mapping results of oceanic basement with potential fields and refraction data to reveal an extinct Jurassic oceanic spreading system, which is now buried by 5.5-7-km of early Cretaceous to recent sediments. The central conclusions of my study of the ridge and its adjacent areas of oceanic crust include the following:

1) The morphology of 30-60-km-long, northwest-trending ridge segments is characterized by ridge-axes volcanoes located near the centers of inwardly-dipping, normal-fault-bounded, axial valleys. Ridge segments are truncated by northeast-trending, second-order discontinuities with ridge offsets of 5-30 m as defined by Macdonald et al. (1993) (Fig. 3.7). The COB offsets ranging from 5 to 25 km are interpreted from residual gravity data and correlate with fracture zone terminations at the continental crust boundary (Fig. 3.4b). These continental lineaments may reflect a structural grain in the Paleozoic crust that controlled the locations of the second-order, discontinuities.

2) My integration of residual gravity anomalies with detailed basement mapping from seismic reflection data shows that major basement faults strike northwest and are subparallel to the ridge segments S1 to S4. Several northeast-striking, normal faults are related to the fracture zones (Fig. 3.7). Both trends indicate a continuous northwest opening of EGOM as proposed by previous workers (Marton and Buffler, 1994; Pindell and Kennan, 2009; Hudec et al., 2013; Eddy et al., 2014; Nguyen and Mann, 2016).

3) Based on sedimentary layering inferred beneath prominent axial volcanoes erupted at the spreading ridge (Fig. 3.10), I propose that these large volcanoes formed near the end, or soon after, the cessation of late Jurassic seafloor spreading and reflect an excess magma supply produced by a fertile mantle (Fig. 3.10).

4) Asymmetry of the oceanic crust with the wider (55-60%) limb located to the northwest of the spreading center can be explained by the presence of an earlier, unrecognized, spreading ridge. This ridge is not well displayed on any of my data including the 2D seismic, gravity, and magnetic data. If this ridge is, in fact, present, one possible tectonic mechanism is that the proximity of a hotspot in the central GOM area (west of the spreading axis) that led to asthenospheric flow from the hotspot and mantle plumes to the early spreading ridge and promoted the southwestward, ridge jump.

5) Using high-resolution seismic reflection data, I identified a Lower Crustal Dipping Reflector (LCDR), and a velocity sublayer within the crust defined from refraction data. The distribution of basement faults and LCDR may indicate that this sublayer is a brittle-ductile boundary within the oceanic crust (Fig. 3.9).

6) The integrated 3-D structural gravity inversion, controlled by seismic refraction data from published sources and the results of seismic reflection interpretation show a thicker crust (6.4 km) in the northwestern GOM is supported by the thicker (>8 km) oceanic crust observed in the GUMBO 3 refraction profile (Eddy et al., 2014), and suggests increased magma supply during seafloor spreading (Fig. 3.16).

7) Modeled thicknesses of the crystalline crust in the extinct spreading ridge segments (6.4-8.6-km) are greater in the centers of 30-60-km-long ridge segments, possibly indicating a low-density gabbro root (Fig. 3.16).

REFERENCES

Ángeles-Aquino, F. J. (2006), Monografía petrolera de la Zona Marina: Asociación Mexicana de Geólogos Petroleros, 71, 77 p.

Ángeles-Aquino, F. J., and A. Cantú (2001), Chapter 14: Subsurface Upper Jurassic stratigraphy in the Campeche Shelf, Gulf of Mexico, in The western Gulf of Mexico Basin: Tectonics, sedimentary basins, and petroleum systems, edited by C. Bartolini, R. T. Buffler, and A. Cantú-Chapa, American Association of Petroleum Geologists Memoir, 75, Tulsa, Oklahoma, 343-352.

Barckhausen, U., M. Engels, D. Franke, S. Ladage, and M. Pubellier (2014), Evolution of the South China Sea: Revised ages for breakup and seafloor spreading, Marine and Petroleum Geology, 58, 599-611, doi:10.1016/j.marpetgeo.2014.02.022.

Bécel, A., D. J. Shillington, M. R. Nedimović, S. C. Webb, and H. Kuehn (2015), Origin of dipping structures in fast-spreading oceanic lower crust offshore Alaska imaged by multichannel seismic data, Earth and Planetary Science Letters, 424, 26-37, doi:10.1016/j.epsl.2015.05.016.

Besse, J., and V. Courtillot (2002), Apparent and true polar wander and the geometry of the geomagnetic field over the last 200 Myr, Journal of Geophysical Research: Solid Earth, 107 (B11), 2300, doi:1029/2000JB000050.

Bird, D., K. Burke, S. Hall, and J. Casey (2005), Gulf of Mexico tectonic history: Hotspot tracks, crustal boundaries, and early salt distribution, American Association of Petroleum Geologists Bulletin, 89(3), 311–328, doi:10.1306/10280404026.

Blakely, R. (1995), Potential Theory in Gravity and Magnetic Applications: Cambridge University Press, 441 p.

Byerly, G. R. (1991), Igneous activity, the Gulf of Mexico Basin, in The Geology of North America J, edited by A. Salvador, Geological Society of America, Boulder, Colorado, J, 91-108, doi:10.1130/dnag-gna-j.91.

Cordell, L. (1973), Gravity analysis using an exponential density-depth function: San Jacinto graben, California, Geophysics, 38(4), 684-690, doi:10.1190/1.1440367.

Cregg, A. K., and W. M. Ahr (1984), Paleoenvironment of an upper Cotton Valley (Knowles Limestone) patch reef, Milam County, Texas, in The Jurassic of the Gulf rim: Gulf Coast Section, SEPM, Proceedings of the Third Annual Research

Conference, edited by W. P. S. Ventress, D. G. Bebout, B. F. Perkins, and C. H. Moore, 41–56.

Christeson, G., H. Van Avendonk, I. Norton, J. Snedden, D. Eddy, G. Karner, and C. Johnson (2014), Deep crustal structure in the eastern Gulf of Mexico, Journal of Geophysics Research: Solid Earth, 119(9), 6782–6801, doi:10.1002/2014JB011045.

Deighton, I. C., F. Winter, and D. Chisari (2017), Recent high-resolution seismic, magnetic and gravity data throws new light on the early development of the Gulf of Mexico, in American Association of Petroleum Geologists Annual Meeting Abstracts, Houston.

Dobson, L.M. and R. T. Buffler (1997), Seismic stratigraphy and geological history of Jurassic rocks, northeastern Gulf of Mexico, American Association of Petroleum Geologists Bulletin, 81(1), 100-120, doi:10.1306/522b42a3-1727-11d7-8645000102c1865d.

Ebeniro, J. O., W. P. O'Brien, and F. J. Shaub (1986), Crustal structure of the south Florida platform, eastern Gulf of Mexico: An ocean-bottom seismograph refraction study, Marine Geophysical Researches, 8(4), 363-382, doi:10.1007/bf02084019.

Eddy, D., H. Van Avendonk, G. Christeson, I. Norton, G. Karner, C. Johnson, and J. Snedden (2014), Deep crustal structure of the northeastern Gulf of Mexico: Implications for rift evolution and seafloor spreading, Journal of Geophysical Research: Solid Earth, 119(9), 6802–6822, doi:10.1002/2014JB011311.

Eddy, D., H. Van Avendonk, G. Christeson, I. Norton (2018), Structure and origin of the rifted margin of the northern Gulf of Mexico, Geosphere, 14(4), 1-14, doi:10.1130/GES01662.1.

Escalona, A., and W. Yang (2013), Subsidence controls on foreland basin development of northwestern offshore Cuba, southeastern Gulf of Mexico subsidence controls, northwestern Offshore Cuba, American Association of Petroleum Geologists Bulletin, 97(1), 1-25, doi:10.1306/06111212002.

Eskamani, P. K. (2014), Seafloor spreading in the eastern Gulf of Mexico: New Evidence for marine magnetic anomalies, M.S. thesis, Colorado State University, 58 p.

Finn, C., M. Pilkington, A. Cuevas, I. Hernandez, and J. Urrutia (2001), New digital magnetic anomaly database for North America, The Leading Edge, 20(8), 870-872, doi:10.1190/1.1487297.

Fox, P. J., and D. G. Gallo (1984), A tectonic model for ridge-transform-ridge plate boundaries: Implications for the structure of oceanic lithosphere, Tectonophysics, 104(3-4), 205-242, doi:10.1016/0040-1951(84)90124-0.

Galloway, W., P. Ganey-Curry, X. Li, and R.T. Buffler (2000), Cenozoic depositional history of the Gulf of Mexico basin, American Association of Petroleum Geologists Bulletin, 84(11), 1743-1774, doi:10.1306/8626c37f-173b-11d7-8645000102c1865d.

Galloway, W. E. (2008), Depositional evolution of the Gulf of Mexico sedimentary basin, in Sedimentary basins of the world 5, edited by A. D. Miall, 505–549, doi:10.1016/s1874-5997(08)00015-4.

Goldhammer, R. K., and C. A. Johnson (2001), Middle Jurassic-Upper Cretaceous paleogeographic evolution and sequence-stratigraphic framework of the northwest Gulf of Mexico rim, in The western Gulf of Mexico Basin: Tectonics, sedimentary basins, and petroleum systems, edited by C. Bartolini, R. T. Buffler, and A. Cantú-Chapa, American Association of Petroleum Geologists Memoir, 75, 45-81, doi: 10.1016/s1874-5997(99)80037-9.

Haase, K., M. Regelous, R. Duncan, P. Brandl, N. Stroncik, and I. Grevemeyer (2011), Insights into mantle composition and mantle melting beneath midocean ridges from post-spreading volcanism on the fossil Galapagos Rise, Geochemistry, Geophysics, Geosystems, 12(5), 1-21, doi:10.1029/2010GC003482.

Hall, S., J. Casey, and D. Elthon (1986), A possible explanation of gravity anomalies over mid-ocean ridges, Journal of Geophysical Research: Solid Earth, 91(B3), 3724-3738, doi:10.1029/jb091ib03p03724.

Hall, S., and I. J. Najmuddin (1994), Constraints on the tectonic development of the eastern Gulf of Mexico provided by magnetic anomaly data, Journal of Geophysical Research, 99(B4), 7161-7175, doi: 10.1029/93jb02570.

Hudec, M., I. Norton, M. Jackson, and F. Peel (2013), Jurassic evolution of the Gulf of Mexico salt basin, American Association of Petroleum Geologists Bulletin, 97(10), 1683–1710, doi:10.1306/04011312073.

Ibrahim, A., J. Carye, G. Latham, and R. Buffler (1981), Crustal structure in Gulf of Mexico from OBS refraction and multichannel reflection data, American Association of Petroleum Geologists Bulletin, 65(7), 1207–1229, doi:10.1306/03b5948b-16d1-11d7-8645000102c1865d.

Imbert, P. (2005), The Mesozoic opening of the Gulf of Mexico: Part 1, Evidence for oceanic accretion during and after salt deposition, in Transactions of the 25th Annual GCSSEPM Research Conference: Petroleum Systems of Divergent

Continental Margins, edited by P. J. Post et al., SEMP, Tulsa, Okla, 1119–1150, doi:10.5724/gcs.05.25.1119.

Imbert, P., and Y. Philippe (2005), The Mesozoic opening of the Gulf of Mexico: Part 2, Integrating seismic and magnetic data into a general opening model, in Transactions of the 25th Annual GCSSEPM Research Conference: Petroleum Systems of Divergent Continental Margins, edited by P. J. Post et al., SEPM, Tulsa, Okla, 1151–1189, doi:10.5724/gcs.05.25.1151.

Jakobsson, M., L. A. Mayer, B. Coakley, J. A. Dowdeswell, S. Forbes, B. Fridman, H. Hodnesdal, R. Noormets, R. Pedersen, M. Rebesco, H.-W. Schenke, Y. Zarayskaya A, D. Accettella, A. Armstrong, R. M. Anderson, P. Bienhoff, A. Camerlenghi, I. Church, M. Edwards, J. V. Gardner, J. K. Hall, B. Hell, O. B. Hestvik, Y. Kristoffersen, C. Marcussen, R. Mohammad, D. Mosher, S. V. Nghiem, M. T. Pedrosa, P. G. Travaglini, and P. Weatherall (2012), The International Bathymetric Chart of the Arctic Ocean (IBCAO) Version 3.0, Geophysical Research Letters, 39(12), 1-6, doi: 10.1029/2012GL052219.

Jonas, J., S. Hall, and J. Casey (1991), Gravity anomalies over extinct spreading centers: A test of gravity models of active centers, Journal of Geophysical Research: Solid Earth, 96(B7), 11759-11777, doi:10.1029/91jb00617.

Kegel, J., D. Chaikin, and B. Torry (2016), New insights from 3D data over an extinct spreading ridge and its implications to deepwater offshore exploration, Gulf Coast Association of Geological Societies Transactions, 66, 307–312.

Liu, B., S. Z. Li, S. H. Jiang, Y. H. Suo, L. L. Guo, Y.M. Wang, and H.X. Zhang (2017), Origin and model of transform faults in the Okinawa Trough, Marine Geophysical Research, 38(1-2), 137-147, doi: 10.1007/s11001-017-9306-7.

Macdonald, K., D. Scheirer, S. Carbotte, and P. Fox (1993), It's only topography: Part 2. GSA Today, 3(1), 29-35.

Mammerickx, J., and D. Sandwell (1986), Rifting of old oceanic lithosphere, Journal of Geophysical Research: Solid Earth, 91(B2), 1975-1988, doi:10.1029/jb091ib02p01975.

Mammerickx, J., D. F. Naar, and R. L. Tyce (1988), The mathematician paleoplate, Journal of Geophysical Research: Solid Earth, 93(B4), 3025-3040, 10.1029/jb093ib04p03025.

Marton, G. (1995), Jurassic evolution of the southeastern Gulf of Mexico, Ph.D. Dissertation, University of Texas at Austin, Austin, Texas, 276 p.

Marton, G., and R. Buffler (1994), Comment on Jurassic reconstruction of the Gulf of Mexico Basin, International Geology Review, 36(6), 545–586, doi:10.1080/00206819409465475.

Marton, G., and R. Buffler (1999), Jurassic—Early Cretaceous tectono-paleogeographic evolution of the southeastern Gulf of Mexico basin, Sedimentary Basins of the World, 4, Elsevier, 63-91, doi:10.1016/s1874-5997(99)80037-9.

McHone, J. G. (2003), Volatile emissions from Central Atlantic Magmatic Province basalts: mass assumptions and environmental consequences, Geophysical Monograph-American Geophysical Union 136, 241-254, doi:10.1029/136gm013.

Morris, E., R. Detrick, T. Minshull, J. Mutter, R. White, W. Su, and P. Buhl (1992), Seismic structure of oceanic crust in the western North Atlantic, Journal of Geophysical Research, 98(B8), 13879-13903, doi:10.1029/93jb00557.

Mutter, J., and J. Karson (1992), Structural processes at slow-spreading ridges, Science, 257(5070), 627-634, doi:10.1126/science.257.5070.627.

Müller, R. D., M. Sdrolias, C. Gainaand, and W. R. Roest (2008), Age, spreading rates, and spreading asymmetry of the world's ocean crust, Geochemistry, Geophysics, Geosystems, 9(4), doi:10.1029/2007GC001743.

Nguyen, L., and P. Mann (2016), Gravity and magnetic constraints on the Jurassic opening of the oceanic Gulf of Mexico and the location and tectonic history of the Western Main transform fault along the eastern continental margin of Mexico, Interpretation, 4(1), SC23-SC33, doi:10.1190/int-2015-0110.1.

Osler, J., and K. Louden (1995), Extinct spreading center in the Labrador Sea: Crustal structure from a two-dimensional seismic refraction velocity model, Journal of Geophysical Research: Solid Earth, 100(B2), 2261-2278, doi:10.1029/94jb02890.

Pascoe, R., P. Nuttall, D. Dunbar, and D. Bird (2016), Constraints on the timing of continental rifting and oceanic spreading for the Mesozoic Gulf of Mexico Basin, in Mesozoic of the Gulf Rim and Beyond: New Progress in Science and Exploration of the Gulf of Mexico Basin, 35th Annual Gulf Coast Section SEPM Foundation Perkins-Rosen Research Conference, GCSSEPM Foundation, Houston, TX, USA, 81–122.

Parker, R. (1973), The rapid calculation of potential anomalies, Geophysical Journal International, 31(4), 447-455, doi:10.1111/j.1365-246X.1973.tb06513.x.

Pindell, J., and L. Kennan (2009), Tectonic evolution of the Gulf of Mexico, Caribbean and northern South America in the mantle reference frame: an update: in The Origin and Evolution of the Caribbean Plate, Geological Society Special Publications, edited by K. H. James, M. A. Lorente, and J. L. Pindell, Geological Society, London, 328(1), 1–55, doi:10.1144/SP328.1.

Pindell, J., C.E. Miranda, A. Cerón, and L. Hernandez (2016), Aeromagnetic map constrains Jurassic–Early Cretaceous synrift, break up, and rotational seafloor spreading history in the Gulf of Mexico, Mesozoic of the Gulf Rim and Beyond: New Progress in Science and Exploration of the Gulf of Mexico Basin, edited by C.M. Lowery, J.W. Snedden, and N.C. Rosen, 35th Annual Gulf Coast Section SEPM Foundation Perkins-Rosen Research Conference, GCSSEPM Foundation, Houston, TX, USA, 123–153.

Ranero, C., E. Banda, and P. Buhl (1997a), The crustal structure of the Canary Basin: Accretion processes at slow spreading centers, Journal of Geophysical Research: Solid Earth, 102(B5), 10185-10201, doi:10.1029/97jb00101.

Ranero, C. R., T. J. Reston, I. Belykh, and H. Gribidenko (1997b), Reflective crust formed at a fast-spreading center in the Pacific, Geology, 25(6), 499-502, doi:10.1130/0091-7613(1997)025<0499:rocfaa>2.3.co;2.

Reid, I., and H. Jackson (1981), Oceanic spreading rate and crustal thickness, Marine Geophysical Researches, 5(2), 165-172, doi:10.1029/92gl00161.

Row, L., P. Dunbar, and D. Hastings (1995), TerrainBase: Worldwide digital terrain data, National Geophysical Data Center, Available online at http://www. ngdc. noaa. gov.

Sandwell, D., R. Müller, W. Smith, E. Garcia, and R. Francis (2014), New global marine gravity model from CryoSat-2 and Jason-1 reveals buried tectonic structure, Science, 346(6205), 65–67, doi:10.1126/science.1258213.

Schultz, R., C. Okubo, and S. Wilkins (2006), Displacement-length scaling relations for faults on the terrestrial planets, Journal of Structural Geology, 28(12), 2182-2193, doi:10.1016/j.jsg.2006.03.034.

Snedden, J., D. Eddy, G. Christeson, H. Van Avendonk, H. Olson, P. Ganey-Curry, and I. Norton (2013), A new temporal model for eastern Gulf of Mexico Mesozoic deposition, Gulf Coast Association of Geological Societies Transactions, 63, 609–612.

Snedden, J., I. Norton, G. Christeson, and J. Sanford (2014), Interaction of deepwater deposition and a mid-ocean spreading center, eastern Gulf of Mexico Basin, USA, Gulf Coast Association of Geological Societies Transactions, 64, 371-383.

Steinberger, B. (2000), Plumes in a convecting mantle: Models and observations for individual hotspots, Journal of Geophysical Research: Solid Earth, 105(B5), 11127-11152, doi:10.1029/1999jb900398.

Stephens, B. (2001), Basement controls on hydrocarbon systems, depositional pathways, and exploration plays beyond the Sigsbee Escarpment in the central Gulf of Mexico, Proceedings 21st Annual GCSSEPM Foundation Bob F. Perkins Research Conference, Petroleum Systems of Deep-Water Basins: Global and Gulf of Mexico Experience, 129-157, doi:10.5724/gcs.01.21.0129.

Taylor, B., A. M. Goodliffe, and F. Martinez (1999), How continents break up: Insights from Papua New Guinea, Journal of geophysical research, 104(B4), 7497-7512, doi:10.1029/1998jb900115.

Van Avendonk, H. J., Davis, J. K. Harding, J. L., and L. A. Lawver (2017), Decrease in oceanic crustal thickness since the breakup of Pangaea, Nature Geoscience, 10(1), 58-61, doi:10.1038/ngeo2849.

White, R., R. Detrick, J. Mutter, P. Buhl, T. Minshull, and E. Morris (1990), New seismic images of oceanic crustal structure, Geology, 18(5), 462-465, doi:10.1130/0091-7613(1990)018<0462:nsiooc>2.3.co;2.

White, R., D. McKenzie, and R. O'Nions (1992), Oceanic crustal thickness from seismic measurements and rare earth element inversions, Journal of Geophysical Research: Solid Earth, 97(B13), 19683-19715, doi:10.1029/92jb01749.

Whittaker, J., A. Goncharov, S. Williams, R. Müller, G. Leitchenkov (2013), Global sediment thickness dataset updated for the Australian-Antarctic Southern Ocean, Geochemistry, Geophysics, Geosystems, 14(8), 3297-3305, doi:10.1002/ggge.20181.

Zhao, M., J. Sibuet, E. He, P. Tan, J. Wang, and X. Qiu (2016), The formation of post-spreading volcanic ridges in the South China Sea, In EGU General Assembly Conference Abstracts, 18, 3239.